Université de Montréal

Suivi des changements des utilisations/occupations du sol en milieu urbain par imagerie satellitale de résolution spatiale moyenne: Le cas de la région métropolitaine de Montréal

Par
Feng Mei LANG

Département de Géographie
Faculté des Arts et des Sciences

Mémoire présenté à la Faculté des études supérieures
en vue de l'obtention du grade de Maître ès sciences en géographie

Mai 2012

Ce mémoire intitulé :

Monitoring Land Use/Land Cover Changes in Urban Areas Using Medium Spatial Resolution Satellite Imagery: the Case of the Montreal Metropolitan Area

(Suivi des changements des utilisations/occupations du sol en milieu urbain par imagerie satellitale de résolution spatiale moyenne: le cas de la région métropolitaine de Montréal)

présentée par :

Feng Mei LANG

a été évalué par un jury composé des personnes suivantes :

Oliver SONNENTAG

président-rapporteur

François CAVAYA

directeur de recherche

Yves BAUDOUIN

membre du jury

Abstract

Nowadays land use/land cover maps at regional scale are commonly generated with satellite data of medium spatial resolution (between 10 m and 30m). The National Land Cover Database (NLCD) in the United States and the Coordination of Information on the Environment (CORINE) Land Cover program in Europe, both based on LANDSAT images, are two typical examples. However, these maps become rapidly obsolete, especially in highly dynamic areas such as mega cities and metropolitan areas. In many applications, such as to monitor the water quality affected by the Land use/Land cover (LULC) change, the spread of invasive species, policy making for city managers, annual updating of LULC maps is required. Since 2007, the USGS offers access to ortho-rectified LANDSAT imagery free of charge. Both archived (since 1984) and recently acquired images are available. Without doubt, such data availability will stimulate the research on fast and cost effective methods and techniques for "continuous" regional land cover/use map updating using medium resolution satellite imagery.

The objective of this research was to evaluate the potential of such medium resolution satellite imagery for providing information on changes useful for the continuous updating of LULC maps at a regional scale in the case of the Montreal Metropolitan Community (MMC) area, a typical North American metropolis.

Previous studies have demonstrated that many factors could affect the results of automatic change detection such as: (1) the characteristics of the images (spatial resolution, spectral bands, etc.); (2) the method itself used to automatically detect changes; and (3) the complexity of the landscape. In the study site except for the Central Business District (CBD) and some commercial streets, land uses (industrial, commercial, residential, etc.) are well delimited. Thus this study was focused on the other factors affecting change detection results, namely, the characteristics of the images and the method of change detection. We used 6 spectral bands of LANDSAT TM/ETM+ with 30 m spatial resolution and 3 spectral bands of ASTER-VNIR with 15 m spatial resolution to evaluate the impact of image characteristics on change detection. Concerning the change detection method, we decided to compare two types of automatic techniques: (1) techniques providing information principally on the location of changed areas,

and (2) techniques providing information on both the location of changed areas and the type of changes ("from-to" classes).

The main conclusions of this research are as follows:

Change detection techniques such as image differencing or change vector analysis applied to LANDSAT multi-temporal imagery provide an accurate picture of changed areas in a fast and efficient manner. They can thus be integrated in a continuous monitoring system for a rapid evaluation of the volume of changes. The produced maps could be helpful to guide the acquisition of high spatial resolution imagery if a detailed identification of the type of changes is required.

Change detection techniques such as principal component analysis and post-classification comparison applied to LANDSAT multi-temporal imagery could provide a relatively accurate picture of “from-to” classes but at a very general thematic level (for example, built-up to green space and vice-versa, forest lands to bare soil and vice-versa, etc.). ASTER images with better spatial resolution but with less spectral bands than LANDSAT images do not provide more detailed thematic information (for example forest land to commercial or industrial areas).

The results indicate that future research should be focused on the detection of changes in the vegetation cover as medium resolution imagery is highly sensitive to this type of surface cover. Maps indicating the location and the type of changes in vegetation cover are in itself very useful for various applications, such as environmental monitoring or urban hydrology, and can be used as indicators on land use changes. Techniques such as change vector analysis or vegetation indices could be used to this end.

Keywords: Land Cover/Use, Urban areas, Change Detection, Medium Spatial-Resolution Satellite-Imagery, LANDSAT TM, LANDSAT ETM+, ASTER-VNIR.

Résumé

De nos jours les cartes d'utilisation/occupation du sol (USOS) à une échelle régionale sont habituellement générées à partir d'images satellitales de résolution modérée (entre 10 m et 30 m). Le National Land Cover Database aux États-Unis et le programme CORINE (Coordination of information on the environment) Land Cover en Europe, tous deux fondés sur les images LANDSAT, en sont des exemples représentatifs. Cependant ces cartes deviennent rapidement obsolètes, spécialement en environnement dynamique comme les megacités et les territoires métropolitains. Pour nombre d'applications, une mise à jour de ces cartes sur une base annuelle est requise. Depuis 2007, le USGS donne accès gratuitement à des images LANDSAT ortho-rectifiées. Des images archivées (depuis 1984) et des images acquises récemment sont disponibles. Sans aucun doute, une telle disponibilité d'images stimulera la recherche sur des méthodes et techniques rapides et efficaces pour un monitoring continue des changements des USOS à partir d'images à résolution moyenne.

Cette recherche visait à évaluer le potentiel de telles images satellitales de résolution moyenne pour obtenir de l'information sur les changements des USOS à une échelle régionale dans le cas de la Communauté Métropolitaine de Montréal (CMM), une métropole nord-américaine typique.

Les études précédentes ont démontré que les résultats de détection automatique des changements dépendent de plusieurs facteurs tels : 1) les caractéristiques des images (résolution spatiale, bandes spectrales, etc.); 2) la méthode même utilisée pour la détection automatique des changements; et 3) la complexité du milieu étudié. Dans le cas du milieu étudié, à l'exception du centre-ville et des artères commerciales, les utilisations du sol (industriel, commercial, résidentiel, etc.) sont bien délimitées. Ainsi cette étude s'est concentrée aux autres facteurs pouvant affecter les résultats, nommément, les caractéristiques des images et les méthodes de détection des changements. Nous avons utilisé des images TM/ETM+ de LANDSAT à 30 m de résolution spatiale et avec six bandes spectrales ainsi que des images VNIR-ASTER à 15 m de résolution spatiale et avec trois bandes spectrales afin d'évaluer l'impact des caractéristiques des images sur les résultats de détection des changements. En ce qui a trait à la méthode de détection des changements, nous avons décidé de comparer deux types de techniques automatiques : (1) techniques fournissant des informations principalement sur la localisation des changements et (2)

techniques fournissant des informations à la fois sur la localisation des changements et sur les types de changement (classes « de-à »).

Les principales conclusions de cette recherche sont les suivantes :

Les techniques de détection de changement telles les différences d'image ou l'analyse des vecteurs de changements appliqués aux images multi-temporelles LANDSAT fournissent une image exacte des lieux où un changement est survenu d'une façon rapide et efficace. Elles peuvent donc être intégrées dans un système de monitoring continu à des fins d'évaluation rapide du volume des changements. Les cartes des changements peuvent aussi servir de guide pour l'acquisition d'images de haute résolution spatiale si l'identification détaillée du type de changement est nécessaire.

Les techniques de détection de changement telles l'analyse en composantes principales et la comparaison post-classification appliquées aux images multi-temporelles LANDSAT fournissent une image relativement exacte de classes "de-à" mais à un niveau thématique très général (par exemple, bâti à espace vert et vice-versa, boisés à sol nu et vice-versa, etc.). Les images ASTER-VNIR avec une meilleure résolution spatiale mais avec moins de bandes spectrales que LANDSAT n'offrent pas un niveau thématique plus détaillé (par exemple, boisés à espace commercial ou industriel).

Les résultats indiquent que la recherche future sur la détection des changements en milieu urbain devrait se concentrer aux changements du couvert végétal puisque les images à résolution moyenne sont très sensibles aux changements de ce type de couvert. Les cartes indiquant la localisation et le type des changements du couvert végétal sont en soi très utiles pour des applications comme le monitoring environnemental ou l'hydrologie urbaine. Elles peuvent aussi servir comme des indicateurs des changements de l'utilisation du sol. De techniques telles l'analyse des vecteurs de changement ou les indices de végétation son employées à cette fin.

Mots-clés : Occupations/utilisations du sol, milieux urbains, détection des changements, ETM+/TM LANDSAT, VNIR-ASTER.

Table of Contents

List of Tables

List of Figures

List of abbreviations

ASTER	Advanced Space-borne Thermal Emission and Reflection Radiometer
CBD	Central Business District
CLC	CORINE Land Cover
CORINE	Coordination of information on the environment
CVA	Change Vector Analysis
DN	Digital Number
EROS	Earth Resource Observation Science
GIS	Geographic Information System
GLS2005	Global Land Surveys
GRS80	Geodetic Reference System
ETM+	Enhanced Thematic Mapper Plus
IFOV	Instantaneous Field Of View
LULC	Land Use/Land Cover
MMC	Montreal Metropolitan Community
MSS	Multiple Spectral Scanner
NAD83	North American Datum 1983
NASA	National Aeronautics and Space Administration
NDBI	Normalized Difference Built-up Index
NDVI	Normalized Difference Vegetation Index
NIR	Near infrared reflectance
NLCD	National Land Cover Dataset
PCA	Principle Component Analysis

PCC	Post Classification Comparison
SWIR	Short Wave Infrared
TM	Thematic Mapper
USGS	United States Geological Survey
UTM	Universal Transverse Mercator
VNIR	Visible Near-Infrared

Dedications

To my father, who taught me to never give up and this will stay in me forever.

To my family members, who helped and encouraged me to complete this thesis.

I want to offer you my gratitude for all your support and I love you all.

Without your support, this thesis would be impossible to materialize.

Acknowledgements

I want to thank my supervisor, Dr. Francois Cavayas, for his endless support in every step of this study. His advice and encouragement made it possible for me go through all the difficulties during the study. Specially, his sense of humor cheered me up when I was really down periodically.

Also, I would like to take this opportunity to offer my gratitude to my colleges, Dr. Robert Cissoko and Dr. Robert Fiset, for their support. Moreover, I would also like to express my gratitude to my employer Mr. Dick Johnsson for providing me a flexible work schedule enabling me to do my study.

This thesis would not be complete without data, which was provided by the LP DAAC (Land Processes Distributed Active Archive Centre) and USGS (United States Geological Survey) for the ASTER and LANDSAT satellite imagery data.

Chapter 1 Introduction

1.1 Land Use/Land Cover Change Monitoring in Urban Territories: Problem Statement

Land Use/Land Cover (LULC) inventories and maps in urban territories provide basic information to various application fields including: territorial management and planning, traffic studies, modeling and planning of public transportation, studies in environmental quality, urban climatology and urban hydrology. According to Jensen (2005), land use refers to what people do on the land surface, such as agriculture, commercial, residential, and transportation whereas land cover is the type of material present in the landscape such as water, vegetation, soil, and man-made materials. Taxonomy systems used for mapping purposes are hierarchical in nature with the most generalized level, a blend of land cover and land use categories such as built-up and urban areas, agriculture, forests, and rangeland. Such thematic levels are depicted on small scale maps (e.g. 1:250 000 or smaller) and are often used for studies at the national level. At more detailed levels, land use categories are almost exclusively defined. In built-up and urban areas categories such as single- or multi-family residential areas, chemical industries, and shopping centers are specified. These categories are depicted on medium and high scale maps helpful for studies at regional and local levels (Anderson *et al.* 1976). Thus, in general, taxonomy systems and corresponding maps are usually termed as LULC taxonomy systems and maps.

Change detection is defined as the process of identifying differences in the state of an object or phenomenon by observing it at different times (Singh, 1989). In the context of LULC mapping, change detection is applied principally for the updating of LULC maps. In fact, these maps can become rapidly obsolete especially in urban territories due to the densification of the built-up area and the urban sprawl.

Remotely sensed images, either space-borne or airborne, play an important role in mapping land use patterns and updating LULC maps. Ortho-photography and digital aerial or satellite imagery of high spatial resolution are used for mapping LULC at large scales, mostly by visual interpretation, while space-borne imagery of medium (10m~50m) spatial resolution is

used for mapping LULC at regional and national scales, mostly by digital analysis and classification.

Based on medium (10-50m) resolution imagery provided by various satellite missions (LANDSAT, SPOT, IRS, etc.), programs of systematic LULC mapping at regional scales and map updating come into being worldwide. In the United States, for example, two generations of the National Land Cover Dataset (NLCD), a component of the USGS Land Cover Characterization Program, has been released covering the United States. The first generation, NLCD 1992, was produced for the conterminous United States on the basis of 1992 LANDSAT Thematic Mapper (TM) imagery and supplemental data by the U.S. Geological Survey (USGS), in cooperation with the U.S. Environmental Protection Agency. The second generation, NLCD 2001, was released on 2007. It is produced on the basis of LANDSAT Enhanced Thematic Mapper (ETM+) imagery covering the entire U. S. A., including Hawaii, Alaska, and Puerto Rico. A third generation, NLCD 2006, is underway based on LANDSAT images of 2006. The method used to generate the NLCD 2006 dataset is to detect changed areas between 2001 and 2006, classify them and integrate the results into the NLCD 2001 dataset. The NLCD datasets are distributed in 30m resolution.

CORINE (Coordination of Information on the Environment) Land Cover (CLC) Data is another important application of LANDSAT satellite imagery. Two generations have been released in resolution of 100m. The first generation, CLC 1990, has been produced in 1996 for most of the European countries based on the 1990 LANDSAT TM. The second generation, CLC 2000, has been produced in 2007 based on 2000 LANDSAT 7 ETM+. The method to generate CLC 2000 is to detect the changes between the images acquired in 2000 and in 1990, similar to the method used by the USGS for NLCD 2006. The detected changes are then classified and integrated to the dataset CLC 1990 to create the dataset CLC 2000.

In Canada, LULC maps for the entire country are not available at scales similar to the above mentioned map series. Two governmental programs of the Ministry of Environment intended to systematically mapping LULC in rural and urbanized areas with provision to actualize them in regular intervals, the Canada Land Inventory and the Canada Land Use Monitoring Program (CLUMP), are abandoned since many years. Only some land cover datasets

are presently available to the public, such as the Circa-2000 Northern Land Cover of Canada at 30 m resolution, covering the North Provinces derived from LANDSAT 5 TM and LANDSAT-7 ETM+ between the years of 1999-2001 (Olthof *et al.*, 2009), and the Ontario Land Cover data derived from LANDSAT TM imagery from the early 1990s. Local governmental agencies in urban communities and municipalities maintain LULC mapping activities and update their maps more or less at regular intervals, usually every 5 years or even more. However, such an updating rate, although responding relatively well to the needs of territorial managers and planners, is not adequate to support studies related to other application fields such as transportation modeling, environmental quality monitoring, etc. For these applications, especially in highly dynamic areas such as Metropolitan communities and mega-cities, a continuous monitoring of changes is the optimum. To illustrate this we present as an example the situation in the Montreal Metropolitan Community (MMC) area, our study site. The MMC, like other metropolitan areas of the world, shows rapid changes in land use/land cover, especially from the late nineties. The value of building permits is a good indicator of the rapidity of changes. According to Statistics Canada, this value from less than 2 billion dollars in 1995 peaks over 6.5 billion dollars in 2007. Even though there is a slight decrease in 2008, the value is still up to 6.4 billion CAD. Detailed information is listed in Table 1. Many new constructions have been developed in vacant lands and even some industrial or recreation lands, converted to residential areas. According to a recent study by Cavayas and Baudouin (2008) within the urban perimeter of the MMC area, vacant lands are built-up in at a rate of about 7 km^2 per year. This development has an important effect especially in the forest land cover. Only in the Montreal Island in the period between 1999 and 2005, 18% of the forest lands (private sector) were lost converted mostly to residences (Cavayas and Baudouin, 2008). This phenomenon has therefore been causing increased land consumption and the continuous modification in the status of land use/land cover over time. An evaluation of the nature of these changes at an annual rate is thus important for the pre-mentioned applications.

Since 2007, USGS offers free of charge access to ortho-rectified LANDSAT imagery (from 1984 to present) as well as to other imagery types of medium spatial resolution (ASTER imagery data covering U.S.A.). Every year at least one cloud-free LANDSAT image could be found covering any part of the world. It is thus interesting to examine if this type of imagery

could constitute the basis for a continuous monitoring of changes in LULC in metropolitan areas such as the Montreal one.

Table 1: Building permits in Montreal region from 1995-2008

Year	Total residential and non-residential (dollars - thousands)	Total residential (dollars - thousands)	Residential percent of the total building permits	Total built permits dollar _Percent Change (year-to-year)	Residential permits dollar_ Percent Change (year-to-year)
1995	1,933,651	860,466	44%	----	----
1996	1,954,863	965,938	49%	1.1	12.3
1997	2,414,381	1,216,638	50%	23.5	26
1998	2,781,922	1,310,796	47%	15.2	7.7
1999	2,935,141	1,536,451	52%	5.5	17.2
2000	3,239,861	1,637,948	51%	10.4	6.6
2001	4,218,111	1,892,141	45%	30.2	15.5
2002	4,604,357	2,731,273	59%	9.2	44.3
2003	5,278,343	3,453,246	65%	14.6	26.4
2004	6,232,700	4,356,745	70%	18.1	26.2
2005	5,800,395	4,094,856	71%	-6.9	-6
2006	6,034,021	3,955,144	66%	4	-3.4
2007	6,506,449	4,062,093	62%	7.8	2.7
2008	6,442,007	4,252,441	66%	-1	4.7

(Source: Statistics Canada 2009. CANSIM table 026-0006. Retrieved from http://www.statcan.gc.ca/datawarehouse/paiement/paiement.cgi?demande_id=2009101515500855613 (October 15 2009))

1.2 Study objectives and hypotheses

Automatic change detection methods, usually applied with medium resolution imagery, imply the comparison of geometrically compatible multi-temporal images on a pixel by pixel basis. These methods could be divided into two broad categories (Lu *et al.,* 2003): (i) methods indicating only the location of changed areas and (ii) methods providing both the location and the type of changes ("from-to" classes). Methods of the first category are based on spectral signatures comparison and could be used to provide information on material cover changes such as vegetation lost (or gained). Such information is valuable for studies related especially to

environmental quality evaluation (Cavayas and Baudouin, 2008). On the other hand, these maps could be used as a basis for obtaining higher resolution imagery covering areas that have major changes. Methods of the secondary category are based on different classification algorithms and could provide information useful for studies seeking to understand the trends in the development of urban areas for modeling or territorial planning purposes. As demonstrated by many previous studies with medium resolution imagery of the LANDSAT type (30 m spatial resolution) in urban areas only general classes of LULC could be extracted with sufficient accuracy such as built-up, forest lands, grasslands and water (e.g., Cavayas and Baudouin, 2008). Under some particular circumstances, depending mostly on the structure of the urban territory, more detailed categories can be extracted such as residential and commercial/industrial, especially in the outskirts and in the urban fringe. Such detailed categories are more easily extracted with imagery of relatively finer resolution (10-20 m).

Few attempts have been made to evaluate the potential of both approaches for the multi-temporal analysis of medium resolution multispectral images for LULC change monitoring in the Montreal region. The most recent study was done by Cavayas and Baudouin (2008) in the context of the "Biotope" project. This project was aiming at the examination of the correlation between LULC and changes in the thermal environment in the Montreal Metropolitan Community Area for the period 1984-2005. However, the approach employed for change detection was the so-called "map guided" change detection. In this approach the existing LULC map is compared to a recently acquired image and as that this method is more oriented to LULC map updating rather than change monitoring.

For all these reasons we decided to confine the following objectives of our study:

(a) Examine the possibilities of LANDSAT multispectral images to provide accurate information on the location of changed areas using comparison methods based solely on spectral signatures. Given the number of available spectral bands and their location in the solar spectrum spanning blue, green, red, near infrared, and short wave infrared wavelength ranges. We hypothesize that these images could effectively provide such information being sensitive especially to vegetation cover changes.

(b) Study the possibilities of LANDSAT multispectral images to provide accurate information on the type of changes specifically applied to the Montreal Metropolitan Community area. Regarding the level of detail on LULC extractible from these images in the Montreal area, only limited evidence exists in the literature provided by a study of Desjardins and Cavayas (1991). The authors using a LANDSAT TM image and visual interpretation criteria found that it was possible to identify within the built-up area without particular difficulties only the residential and some industrial areas. Categories characterized by vegetation cover such as parks, golf courses and forested areas, were easily identified. Thus we hypothesize that using classification algorithms based on spectral signature of objects, only general LULC categories should be extractible from LANDSAT images with sufficient accuracy even in the case of the Montreal urban environment.

(c) Compare the performance of other types of images of better spatial resolution available from the USGS to that of LANDSAT images concerning the identification of the type of changes. Among the available images, only these 15 m resolution VNIR images which provided by the ASTER sensor onboard of the experimental TERRA satellite present a particular interest in the context of change monitoring. However, the spatial coverage of one VNIR image is only about 10% of LANDSAT coverage and much less relatively frequent covering of the Montreal area (from 2000 to present). To the best of our knowledge, no studies of the Montreal area using this type of imagery exist. We hypothesize that the change in resolution from 30 m to 15 m should have an impact on the minimum size of detected areas of change. This is important in the case of existing sparsely built-up areas. It is less important in the case of newly developed areas mainly in the outskirts of urban areas. Concerning the level of detail, we expect that the identification of some categories within the built-up area should be easier than with LANDSAT images.

1.3 Structure of the thesis

This thesis is organized into seven chapters. The first chapter provides background and rationale for the study and research objectives. The second and third chapters are literature reviews and outline the results of previous studies on LULC mapping using medium spatial resolution imagery and on the automatic change detection techniques, respectively. Chapter four describes the framework of this study, including the study site, the images used in this study and the pre-processing as well as the methodological approaches. Chapter five explains how the data have been processed for detecting the LULC changes in the case of LANDSAT images. Chapter six compares the results of change detection obtained with ASTER-VNIR and LANDSAT imageries. Finally, chapter seven presents the main conclusions of this study.

Chapter 2 Mapping LULC from Medium Resolution Multi-spectral Imagery

2.1 Introduction

The aim of our study is to examine the potential of medium resolution imagery for LULC change to monitor in urban areas. Thus first of all we have to define the topology of LULC extractible from this imagery. The next section is a brief review of the classification schemes used in LULC mapping. As also mentioned we would like to study the possibilities of various types of medium resolution imagery readily available free from the USGS services. More specifically we are interested in LANDSAT imagery (TM or ETM+) and to ASTER -VNIR imagery. The former is a multispectral imagery with six bands covering almost the entire solar spectrum (visible, near- and shortwave-infrared) with 30 m spatial resolution while the latter is a multispectral imagery with three spectral bands (green, red and near-infrared) of finer resolution (15 m) than the LANDSAT images. So the question addressed in this study is how the interpretation of spatial and spectral resolution affects the change-detection results. Section 2.3 presents a review of studies addressing this particular question.

2.2 LULC Classification Schemes

The best way to ensure that useful information on urban LULC is derived from remotely-sensed data is to base our work on a standardized LULC scheme (Chen and Stow, 2003). Many LULC classification schemas have been developed, such as: (a) the Land-Base Classification Standard (LBCS) developed by the American Planning Association (2006); (b) the CORINE (Coordination of information on the environment) in Europe; (c) the PELCOM (Pan-European Land Cover Monitoring) and (d) the USGS LULC classification system for use of remotely-sensed data. In North America and in the context of remote sensing image analysis, the standard LULC classification system is the USGS (Anderson *et al.,* 1976), even though each city or urban community may have a slightly different system. This last scheme (d) was adopted since our study area was the Montreal Metropolitan territory.

USGS LULC classification system is a four level hierarchical taxonomy system. Table 2 shows the first two levels accessible, in principle, from medium resolution imagery (Jensen 2007): Level I (9 classes) and Level II (37 classes).

Table 2: Land use and land cover classification system for use with remotely sensed images

Level I	**Level II**
1 Urban or Built-up Land	11 Residential
	12 Commercial and Services
	13 Industrial
	14 Transportation, Communications, and Utilities
	15 Industrial and Commercial Complexes
	16 Mixed Urban or Built-up Land
	17 Other Urban or Built-up Land
2 Agricultural Land	21 Cropland and Pasture
	22 Orchards, Groves, Vineyards, Nurseries, and Ornamental Horticultural Areas
	23 Confined Feeding Operations
	24 Other Agricultural Land
3 Rangeland (Grass)	31 Herbaceous Rangeland
	32 Shrub and Brush Rangeland
	33 Mixed Rangeland
4 Forest Land	41 Deciduous Forest Land
	42 Evergreen Forest Land
	43 Mixed Forest Land
5 Water	51 Streams and Canals
	52 Lakes
	53 Reservoirs
	54 Bays and Estuaries
6 Wetland	61 Forested Wetland
	62 Non-forested Wetland
7 Barren Land	71 Dry Salt Flats
	72 Beaches
	73 Sandy Areas other than Beaches
	74 Bare Exposed Rock
	75 Strip Mines Quarries, and Gravel Pits
	76 Transitional Areas
	77 Mixed Barren Land
8 Tundra	81 Shrub and Brush Tundra
	82 Herbaceous Tundra
	83 Bare Ground Tundra
	84 Wet Tundra
	85 Mixed Tundra
9 Perennial Snow or Ice	91 Perennial Snowfields
	92 Glaciers

(Adopted from Jensen, 2007)

2.3 Spatial Resolution vs. Spectral Resolution

2.3.1 Definitions

Spatial resolution refers to the size of the smallest feature depicted on a map or visible on an image. Two major factors are affecting the spatial resolution of the images: the size of the resolution cell and the contrast between the object and the surrounding ground. The resolution cell is defined by the instantaneous-field-of-view (IFOV) and the height of the sensor (Figure 1). In practice, when speaking about spatial resolution we refer to the size of the resolution cell by ignoring the impact of the contrast. In fact, as one sole radiance measurement of the sensor corresponds to the entire resolution cell, the size of the object has to be at least equivalent to the size of the resolution cell to de distinguishable on the image. However this is not always the case, since an object of the size of a resolution cell could be "undetectable" if it presents a low contrast with its surrounding ground. On the contrary, some high contrast features such as narrow rivers and canals or roads are visible even if their width is less than the sensor's resolution cell. Many practitioners use as a rule of thumb that an object to be not only detected but also identified has to have a size at least 4 times the resolution cell of the sensor (Colwell, 1983).

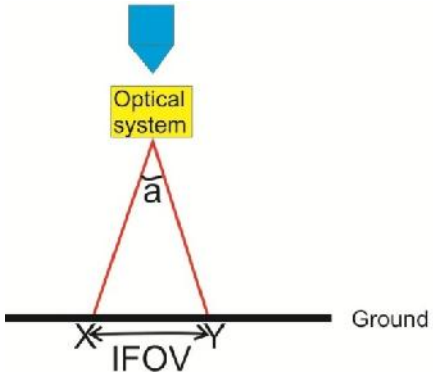

Figure 1: Angular IFOV and height above ground of the sensors define the size of the resolution cell.

(Adopted from Colwell, 1983)

Spectral resolution, on the other hand, is the number and width of specific wavelength interval (bands/channels) in the electromagnetic spectrum to which a remote sensing instrument is sensitive. Bands/channels refer to recorded radiances by the sensor in different portions of the electromagnetic spectrum for the same material on the ground. As indicated by Colwell (1983), the surface of the Earth is illuminated by the sun's radiation covering a large spectrum of wavelengths. Different materials have different characteristic absorption when solar radiation impinges on them. For instance, vegetation has a relatively strong absorption around the red wavelength. What is not absorbed by an object is reflected into space and is partially captured by the sensor. The reflection capacity of a material through the solar spectrum is described by its spectral signature (Figure 2). These signatures are often used in remote sensing as a means to identify LULC classes. Thus a multispectral sensor with fine spectral resolution offers a higher discrimination potential of ground features than another with few spectral bands (Colwell (1983).

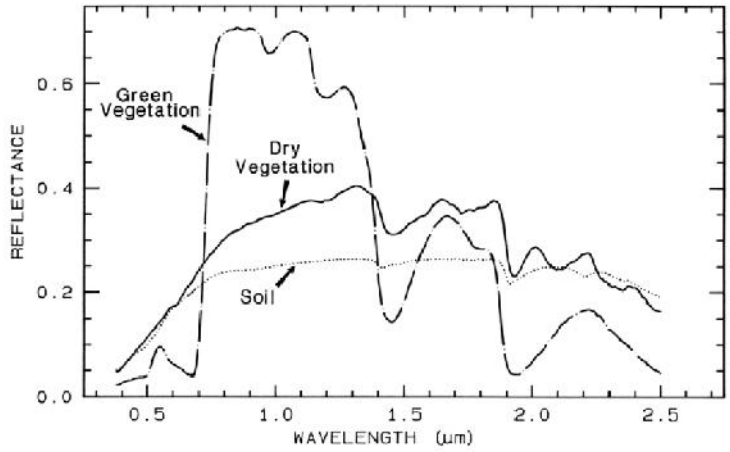

Figure 2: Typical spectral signature for soil, green vegetation and dry vegetation.

(Adopted from Rencz, 1999)

2.3.2 Previous findings

Very few studies addressed the question of how both spectral and spatial resolutions affect the discrimination capacity of LULC on medium-resolution satellite images especially in urban environments. Concerning the spatial resolution we have to go back in the 1980's and the study of Welch (1985). The author compared two types of satellite images over an urban

environment of Athens in Greece, LANDSAT TM (30 m) and merged panchromatic and multispectral SPOT HRV imagery (10 and 20 m respectively), simulated from airborne images. Enhanced false color composites created from these images were then visually interpreted. Figure 3 reproduces the principal results of this study. Figure 3-b shows that the taxonomy system used in their study included Level II and III categories of the USGS system. The impact of change in image resolution from 30 m to 10 m is obvious comparing the obtained LULC maps (figure 3-a). The accuracies per LULC category was about 80% and even better with simulated SPOT images. Whereas in the case of simulated TM images the accuracy is about 60% (figure3-c). The authors note also that the application of automatic classification techniques was not successful to give thematic detail at the Level II and III categories.

Figure 4 shows an example of the impact on the visual appearance of an urban environment by choosing the resolution of the imageries from 30m to 15m used in this study (chapter 4). According to the results of Welch (1985) and given the fact that our study is based entirely on digital image analysis, it is expected that the application of ASTER will provide higher accuracy in classifying our images at least at the Level II of the USGS. A study for Phoenix metropolitan area by Waler and Blaschke (2008) using the method of object-oriented LULC classification to analyze the image in 0.61 m resolution acquired by a sensor called Landiscor with 3 bands (RGB). The overall accuracy is about 80% in Level II categories with 5 classes: soil, grass, woody, building and impervious. The major confusion for this study is caused by the big shadows of objects and to find the ‘best’ segmentation for a classification of many land-cover types with different sizes, shapes, and spectral characteristics. Based on this study, it shows that only the improvement of the resolution of spatial resolution will not able to derive more accurate classification result. The object-oriented classification technique is different with the techniques based on spectral per pixel (more in chapter 3). It is first introduced in the 1970s (de Kok *et al*. 1999). However, the method was limited by hardware, software, poor resolution of images and interpretation theories (Flanders *et al*. 2003). With an increase in hardware capability and availability of high spatial resolution images, specially, after the first commercial IKONOS 4 m MMS images available, the demand for object-oriented analysis has also increased (de Kok *et al*. 1999) because the techniques of "per-pixel" are no longer adequate for high resolution (less than 10 m) images. Due to the high cost of purchasing the high

resolution imageries, this study are only focus on these medium resolution images with free access from USGS.

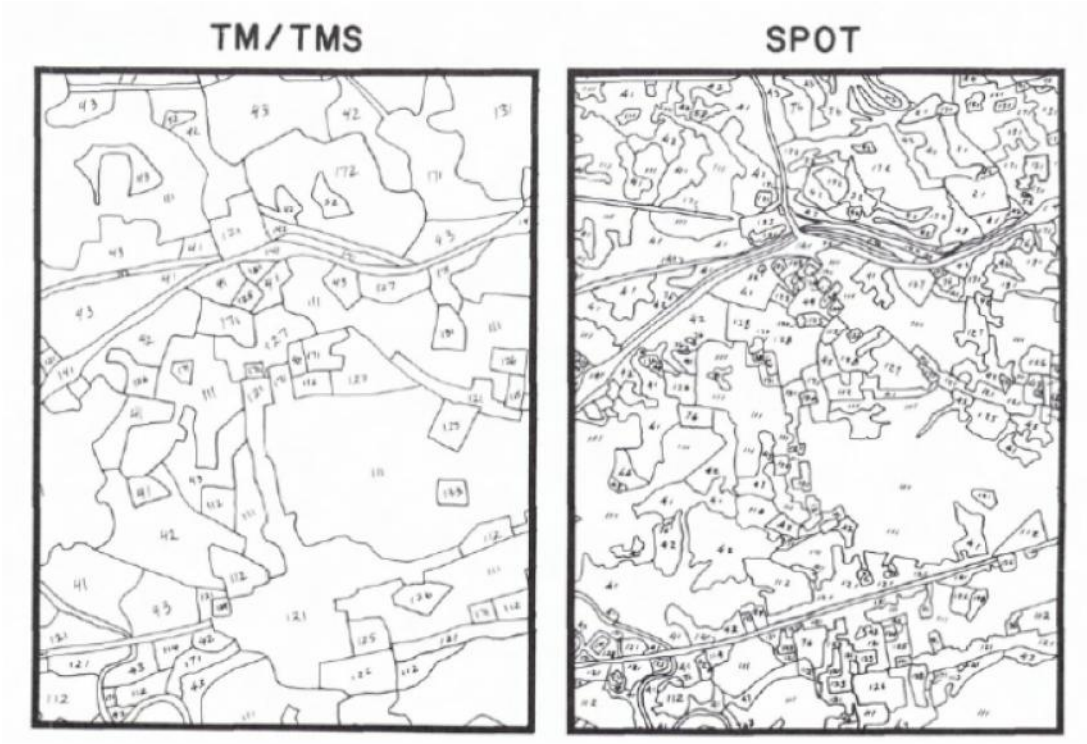

a

URBAN OR BUILT-UP (1)
11 Residential
111 Single Family Housing
112 Multiple Family Housing
12 Commercial and Services
121 Commercial
122 Institutional
13 Industrial
14 Transportation and Utilities
141 Road, Highway, Railroad
142 Utilities
17 Other Urban or Built-up Land
171 Urban Grassland
172 Golf Course
AGRICULTURAL LAND (2)
21 Cropland and Pasture
FOREST LAND (4)
41 Deciduous Forest Land
42 Evergreen Forest Land
43 Deciduous and Evergreen Forest Land
44 Scrub and Woodland
WATER (5)
51 Rivers, Streams, and Ponds
WETLANDS (6)
61 Forested Wetland
BARREN LAND (7)
76 Barren Transitional Areas

b

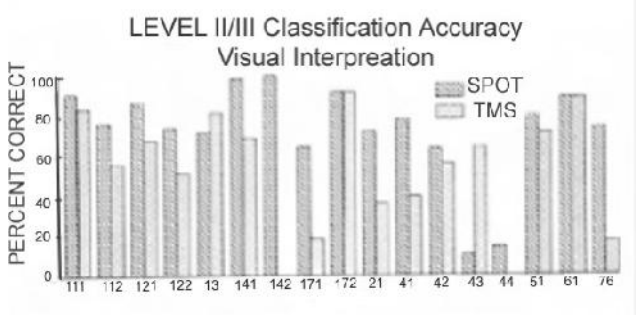

c

Figure 3: Comparative results obtained with two types of medium spatial resolution images (Adopted from Welch, 1985)

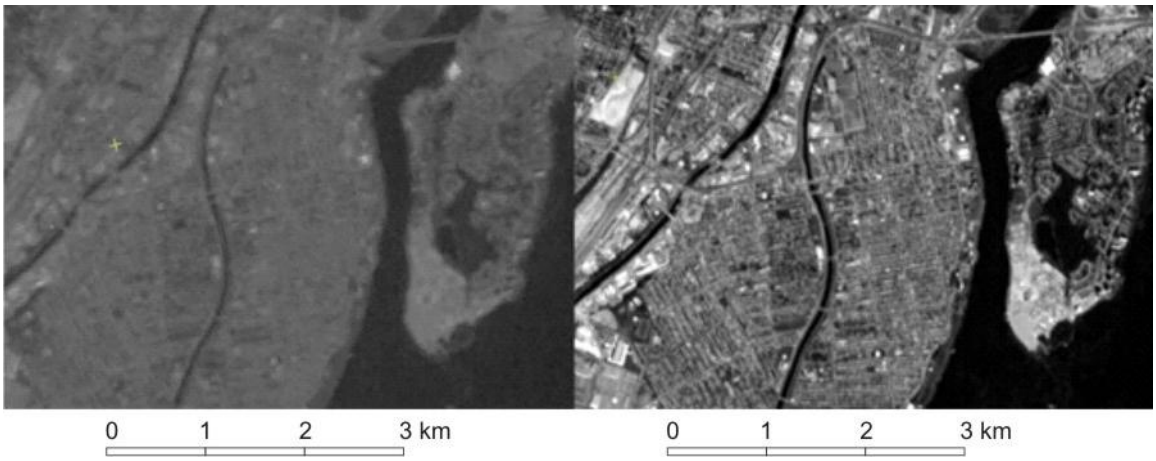

Figure 4: One example for difference in spatial resolution between LANDSAT 30m data and ASTER 15m data in same spectral band: band 2

A study by Herold *et al.* (2003) indicates, however, that these expectations have to be lowered since ASTER-VNIR images are poorer in terms of spectral resolution (Table 4) compared to LANDSAT images (Table 3). Even if this study concerns the classification of surface materials (asphalt, metal roof, water, vegetation, etc.), it provides interesting cues to understand the impact of spectral resolution alone. The authors using standard spectral signatures first established 14 narrow spectral bands in the solar spectrum useful for recognizing 25 different materials common in urban environments. A hyperspectral airborne image (224 spectral bands) was then used as a basis to simulate the signal which would be measured with the far more large spectral bands of two multispectral sensors while maintaining the spatial resolution fixed. The first simulated sensor is the IKONOS having four spectral bands (blue, green, red and NIR) while the second was the LANDSAT TM with six spectral bands (Table 3) in the solar spectrum. The hyper-spectral image and the two multispectral simulated images were then classified and the classification results quantitatively assessed. As expected, the best classification results of the 25 materials were obtained with the hyperspectral imageries. The accuracy is about 70%. Classification using the simulated IKONOS images produced a score 30% lower than those using the hyper spectral imageries, while the classification of the simulated TM image was only 13% lower. This higher performance of the TM image is explained by the presence of the two bands in the SWIR not available in the case of the IKONOS image. However, as the authors stress many misinterpretations exist between materials having

similar spectral signatures, such as the soil of bare land the concrete of built-up. Thus even if the hyperspectral imagery includes the 14 optimal bands global classification accuracy is lower than 70%.

In conclusion, the impact of both spatial and spectral resolution in the quality of LULC mapping and change detection is largely unexplored and in this sense, our study will contribute to find an answer to the question addressed in this section.

Table 3: Spectral bands of LANDSAT 5/7 TM/ETM+ sensors in the solar spectrum

LANDSAT TM/ETM+	Spectral Sensitivity (µm)	Nominal Spectral Location
Band 1	0.45-052	Blue
Band 2	0.52-0.6	Green
Band 3	0.63-0.69	Red
Band 4	0.76-0.9	Near-IR
Band 5	1.55-1.75	Shortwave-IR
Band 7	2.08-2.35	Shortwave-IR

(Source: adopted from USGS, retrieved from http://LANDSAT.usgs.gov/about_mission_history.php)

Table 4: Spectral bands of ASTER VNIR sensor in the solar spectrum

ASTER_VNIR	Spectral Sensitivity (µm)	Nominal Spectral Location
Band 1	0.52-0.60	Green
Band 2	0.63-0.69	Red
Band 3N	0.78-0.86	Near-IR

(Source: adopted from USGS, retrieved from https://lpdaac.usgs.gov/products/ASTER_overview)

Chapter 3 Methods for LULC change detection based on medium resolution multitemporal imagery

3.1 Basic Concepts

According to Green *et al.* (1994) change detection implies the comparison of the spatial representation of the same area in two different times and the measure of differences in the variables of interest while controlling differences caused by variables that are not of interest. In the case of comparison of multi-temporal remotely-sensed images the variable of interest is usually the spectral signature of objects included in the same area. A significant difference in spectral signatures means a change in the land cover. However as measured radiances are influenced by many other factors such as solar illumination conditions and atmospheric conditions during image acquisition, the direct comparison of images could lead to erroneous results. In order to obtain optimal results specific spatial, temporal, spectral and radiometric data issues have to be addressed. A typical list of criteria would include the following issues (Coppin *et al.,* 2004; Jensen *et al.,* 1997; Lunetta and Elvidge, 1998; Millward *et al.,* 2006):

- The sensors should have similar sensitivity imaging - ideally, the data from the same sensor has to be used to minimize spectral, radiometric and spatial resolution differences;
- The images should be from the same time of year or season to minimize solar illumination angle effects and differences in seasonal vegetation cover;
- The images should be co-registered to better than one half pixel accuracy to minimize spatial offset and distortion,
- Radiometric normalization may be necessary in order to remove atmospheric effects – differences caused by scattering and absorption by atmospheric constituents, and by differing solar zenith angles.

In the past four decades, there have been many studies proposing various algorithms for obtaining LULC change information using a wide variety of remotely sensed data. Lu *et al.* (2003) provides an extensive review of these studies. According to these authors the proposed algorithms for change detection can be categorized into two main categories. The first category

includes methods focused on the detection of detailed change trajectories (“from-to” classes), and the second focuses on detection of binary change and non-change features. Post-classification comparison is the most often used approach to detect detailed "from-to" change trajectory; while image differencing, image rationing, vegetation index differencing, and principal component analysis (PCA) are often used to detect binary change and non-change information. The adopted methods in this study in both categories are presented in the next section.

3.2 Adopted Automated Change Detection Techniques

Few studies present comparative results of the various change detection approaches. The most relevant ones are briefly summarized here. Civco *et al. (*2002) used five LULC change detection methods - post–classification cross tabulation, cross correlation analysis, neural networks, knowledge–based expert systems, and object–oriented classification. Nine land use/cover classes were selected for analysis. It was observed that there were merits to each of the five examined methods, and no single approach can solve the land use change detection problem. Mas (1997) tested 6 change detection techniques using LANDSAT Multi-Spectral Scanner (MSS) images for detecting areas of changes in the region of the Terminos Lagoon, Mexico. The change detection techniques considered were image differencing, vegetation index differencing, principal components analysis (PCA), direct multi-date unsupervised classification, post-classification change differencing and combination of image enhancement and post-classification comparison. The accuracy of the results was evaluated by comparison with aerial photographs through Kappa coefficient calculation. Besides providing information on the nature of changes, post-classification comparison was found to be the most accurate procedure. The author also pointed out that methods based on classification were found to be less sensitive to spectral variations and more robust when dealing with data captured at different times of the year. Yuan *et al.* (2005) found also that the post classification comparison method provides good-accuracy results (between 80% and 90%) when applied to LANDSAT images of the Twin Cities (Minnesota) Metropolitan Area. In his particular study the emphasis was put on the generation of transition matrix (“from-to” classes).

Based on the merits and complexity of the studies cited earlier, we decided to compare four automated change detection techniques in the case of our study area: (1) image differencing,

(2) change vector analysis, (3) principal components analysis, and (4) post-classification comparison. Table 5 summarizes the advantage and disadvantages of these four methods.

Table 5: Summary of Change Detection Techniques as outlined in Singh (1989), Coppin and Bauer (1996), Lunetta and Elvidge (1998), Coppin *et al.* (2004), and Lu *et al.* (2003)

Technique	Method	Advantage	Disadvantage
Image differencing	Subtraction of multi temporal imagery on a spectral band basis-original or transformed data	Simple and easy to interpret	Cannot provide transition matrix ("from-to" classes) and requires the definition of a threshold
Change Vector analysis	Multivariate change detection that exploits the full dimensionality of the image data; Produce two outputs: change magnitude and change direction	Ability to process any number of spectral bands desired and to provide detailed change information	Difficult to identify land cover change trajectories
Principal component analysis (PCA)	Applied to two-date imagery to produce uncorrelated data; variations in land-covers are usually appear in specific principal components	Reduces data redundancy between bands and emphasizes different information in the derived components	Requires comprehensive knowledge of the study area; the changes are often difficult to interpret and to label because of PCA depending on the input data statistics; it cannot provide a complete matrix of change classes and need to determine the thresholds to identify the changed areas
Post classification comparison	Spectral classification of each image in the multi-temporal set; comparison of the classified images on pixel-by-pixel basis	Minimizes impacts of differences caused by atmosphere, sensor and environment between multi-temporal images; provides a complete matrix of change information	Requires comprehensive knowledge of the study area; time consuming; final accuracy depends on the result of classification of each date

.

3.2.1 Image Differencing

Image differencing is a commonly used technique to rapidly locate changed areas by subtracting pixel values in a specific spectral band of two or more images of the same area acquired at different times (Coppin and Bauer 1996; Lunetta and Elvidge 1998, Coppin *et al.* 2004). To use this technique effectively, it requires a process of rigorous normalization of the data to the same geometric and radiometric referential. In the case of rugged terrain this normalization is far more complicated than in the case of a low relief terrain. In fact, even with medium-resolution imagery, ortho-rectification has to be applied for geometric normalization. When applying the radiometric normalization one has to take into account not only atmospheric effects but also topographic effects on image radiometry (Bouroubi *et al*., 2006). Assuming that such rigorous normalization has been done, application of this technique is simple and straight forward and the result is easy to interpret (Lu *et al.*, 2003). The operation results in either positive or negative values where a change has occurred. Values close to zero indicate unchanged areas. However, proper choice of spectral bands and thresholds are crucial for providing accurate results. In practice, spectral bands offering a high contrast between vegetation cover and other land covers (such as the red band) are chosen for detecting urban development (Jensen and Toll, 1982), while the infrared bands are used for detecting changes within agricultural and forested terrains. In many cases, the shortwave infrared band (around 2.5 μm) is used for forest regeneration and deforestation monitoring. Concerning the thresholds, one has to decide on the minimum absolute difference value representing a change on the land cover of each pixel. Such threshold is usually empirically defined by observing areas of a priori known changes. As indicated in Table 5, the most important weakness of this method is that it can provide only a binary image of changes.

3.2.2 Change Vector Analysis (CVA)

Change Vector Analysis can be thought as an extension of the previous technique in a multi-dimensional spectral space. The difference in location of a given pixel in this spectral space in two (or more) moments in time provides the necessary information to measure the degree of changes (distance) as well as the direction of changes (for example for low values to high values in all bands) (Michalek *et al.,* 1993). Assuming a pixel with grey-level values in two

images on dates t1, t2 given by A = $[a_1, a_2, a_3,..., a_n]^T$ and B = $[b_1, b_2, b_3,..., b_n]^T$, respectively, where n is the number of bands, a change vector is defined as follows:

$$\Delta G = A - B = \begin{pmatrix} a_1 - b_1 \\ a_2 - b_2 \\ a_3 - b_3 \\ \text{- - - -} \\ a_n - b_n \end{pmatrix} \qquad \text{Equation (1)}$$

The change magnitude ΔG for that particular pixel is the Euclidean distance in multidimensional space:

$$\Delta G = \sqrt{(a_1 - b_1)^2 + (a_2 - b_2)^2 + (a_3 - b_3)^2 ... + (a_n - b_n)^2} \qquad \text{Equation (2)}$$

Whereas its direction with reference to a particular axis (spectral band) is given by:

$$\theta = \cos^{-1}\left(\frac{a_i - b_i}{\Delta G}\right) \qquad \text{Equation (3)}$$

Although this method has the advantage of being able to treat any number of spectral bands and to produce detailed change detection information, it is difficult to identify land cover change trajectories, especially when the number of bands is high (Lu *et al*., 2003). Michalek *et al.* (1993) have tested the CVA method for a coastal zone and concluded that it is a valuable tool for costal resource surveys and monitoring. Lambin and Strahler (1994) also used CVA combined with PCA (see below) and found that it was effective in detecting and categorizing inter-annual changes. As previously, this method to be effective, rigorous normalization in both geometry and radiometry is necessary.

3.2.3 Principal Components Analysis (PCA)

PCA is a linear transformation which rotates the axes of image space along lines of maximum variance. The rotation is based on the orthogonal eigenvectors of the covariance matrix (non-standardized data) or of the correlation matrix (standardized principal components) generated from a sample of image data from the input layers. The output from this transformation is a new set of image layers. In the case of multi-temporal analysis the eigenvectors are computed using all the available spectral bands of two (or more) multi-temporal

images. Alternatively, PCA is applied separately to reduce data dimensionality and then one of the previous methods can be applied in order to detect changes. However, as pointed out by Fung and LeDrew (1987), for land cover change detection, it is best to derive the eigen-structure from the entire data set. Li and Yeh (1998) classified the stacked components of PCA using interactive editing method to detect the changes and derived the change land cover nature of "from-to". It reported that the accuracy is about 86% and that their approach reduces the over-estimation of changed areas observed with the post-classification comparison approach (see next section).

An alternative method to the PCA is the "tasseled cap" transformation. This method uses a different algorithm to process the available spectral bands. It is customized for LANDSAT data. Contrary to the PCA, where the orientation of the new orthogonal axes of data representation is defined statistically, the tasseled cap transformation is operated using fixed a priori orthogonal axes. Also PCA generates a new representation space of dimension equal to the dimension of the original space whereas tasseled cap transformation generates a new space of only three axes termed in the case of LANDSAT images: brightness, greenness and wetness. The tasseled cap transformation rotates the LANDSAT data such that 95% or more of the total variability is expressed in the first two bands: brightness and greenness (Lillesand and Kiefer, 2004). Brightness is defined in the direction of the principal variation in soil reflectance and greenness is strongly related to the amount of green vegetation present in the scene. Fung (1990) compared the PCA and Tasseled Cap transformations and found that both techniques were not able to detect all types of land cover changes over the Waterloo area, Ontario, Canada.

As previously, all these methods require a rigorous normalization in both geometry and radiometry to minimize false change detections.

3.2.4 Post Classification Comparison (PCC)

Post classification comparison is carried out by overlaying two independently classified multi-temporal images, and then comparing the classes on pixel by pixel basis. A complete matrix of change information is thus provided. The resulting thematic map shows both the nature of change as well as the amount of change. In this method, errors due to atmospheric, sensor and environmental differences between multi-temporal images are minimized. However,

errors in the individual data classification map would remain in the final change detection map. Hence, the result depends on the quality of the classified image of each date.

Post-classification comparison is a common approach used for change detection in practice, but the difficulty in classifying historical image data can seriously affect the change detection results (Lu *et al.* 2003). As mentioned, Mas (1997) identified the post-classification comparison as the most effective change detection technique. He pointed out that this method has the advantage of indicating the nature of the change and should be used as the reference for evaluating other change detection methods. Yuan *et al.* (2005) used post-classification comparison method and successfully analyzed changes in Twin Cities (Minnesota) Metropolitan area over a period from 1986 to 2002. The accuracy was between 80 to 90% for over a 16 years period. Foody (2001) found that post-classification comparison underestimated the areas of land-cover change, but where the change was detected, it typically overestimated. Petit *et al.* (2001) used the combination of image differencing and post classification to detect detailed 'from–to' land-cover changes in south-eastern Zambia and such a hybrid change detection method was considered as better than using only post-classification comparison.

Chapter 4 Framework of the study

4.1 Study Area and Data Sets

Our study area is the Montreal Metropolitan Community (MMC) territory. This territory, encompassing 82 municipalities including the city of Montreal, covers about 4,500 km^2 and has a population of more than 3.5 million. 10% of the MMC area is covered by water (mostly a portion of the Saint-Lawrence River), about 40% is allocated to urban activities and 50% are protected agricultural land under law. All the tests described in this study were undertaken within the urban perimeter where the changes in land cover are the most important. According to a land cover map published circa 1995 by the Ministry of Municipal Affairs, Quebec, the urbanized area was reserved to residences (40.6%), commercial/industrial uses (14.7%), institutional use (9.7%), green spaces and major highways (10.1%), while 26.5% were unoccupied (vacant areas).

Among the archived LANDSAT and ASTER images available from the USGS we selected the set indicated in Table 6 for the following reasons. The year of 1994 has been chosen as the basis for comparison with the present situation because of the availability of many publications (ortho-photographies, forestry maps, topographic maps, etc.) very useful invalidating the results of our analysis. For that year only LANDSAT-5 TM was in operation. A cloud free image covering almost the entire urbanized area acquired in August of 1994 was available. LANDSAT-7 ETM+ is in operation since 1999, however after 2003 the generated images have blank stripes over the terrain without data due to a mechanical problem. For that reason a LANDSAT-5 TM image has been selected for this study. The selected image has been acquired in August of 2008 in order to minimize seasonal variations between the two images. The image is also cloud free and covers almost the same area as the 1994 image. Figure 4 shows as an example the portion of the urbanized area of the MMC covered by a LANDSAT TM image. The area shown in this figure constitutes our experimental site for change detection (period 1994-2008) using LANDSAT images. ASTER is in operation since 1999 but the coverage of a particular area is far less frequent than in the case of LANDSAT (same revisit time as LANDSAT, but only 10% of LANDSAT coverage. Also, because of a limited duty cycle (about 750 scenes per day), ASTER was scheduled to selectively obtain images based on requests from researchers or specific missions). Two ASTER-VNIR images covering partially

the MMC territory have been found, the one acquired in 2001 (early summer) and the second in 2007 (early fall). The two LANDSAT images acquired in 2001 and 2007 indicated in Table 6 were used in order to evaluate the effects of spatial resolution (30 m vs. 15 m) on the quality of change detection. Coincidentally, in 2001 the LANDSAT-7 ETM+ was collected at the same day only half an hour after the ASTER image acquisition. This pair of images will eliminate atmospheric effects. The common portion of these 4 images is indicated as site II in figure 5. Figure 6 presents as an example the portion of a LANDSAT image covering this second experimental site.

Table 6: Image set used in this study

Data source	Acquisition date	Spatial resolution	Processing Level	Source
LANDSAT 5 TM (1994)	8/16/1994	30m	L1T	USGS
LANDSAT 7 TM (2001)	6/15/2001	30m	L1T	USGS
LANDSAT 5 TM (2007)	9/05/2007	30m	L1T	USGS
LANDSAT 5 TM (2008)	8/22/2008	30m	L1T	USGS
ASTER VNIR (2001)	6/15/2001	15m	1B	USGS
ASTER VNIR (2007)	9/04/2007	15m	1A	USGS

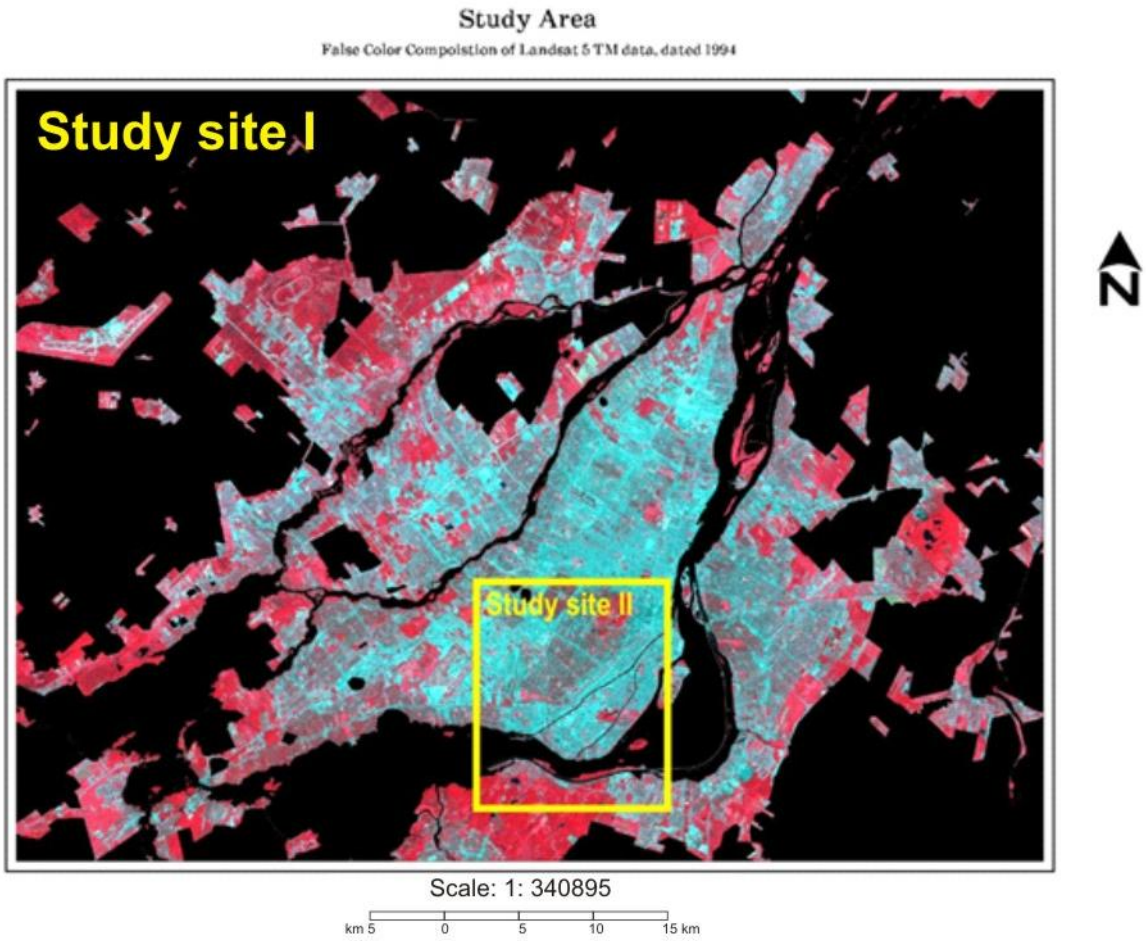

Figure 5: Study sites: site I is the entire ubanized portion of the Montreal Metropolitan Community area ; site II is the area indcated by the yellowrectangle (see Figure 6)

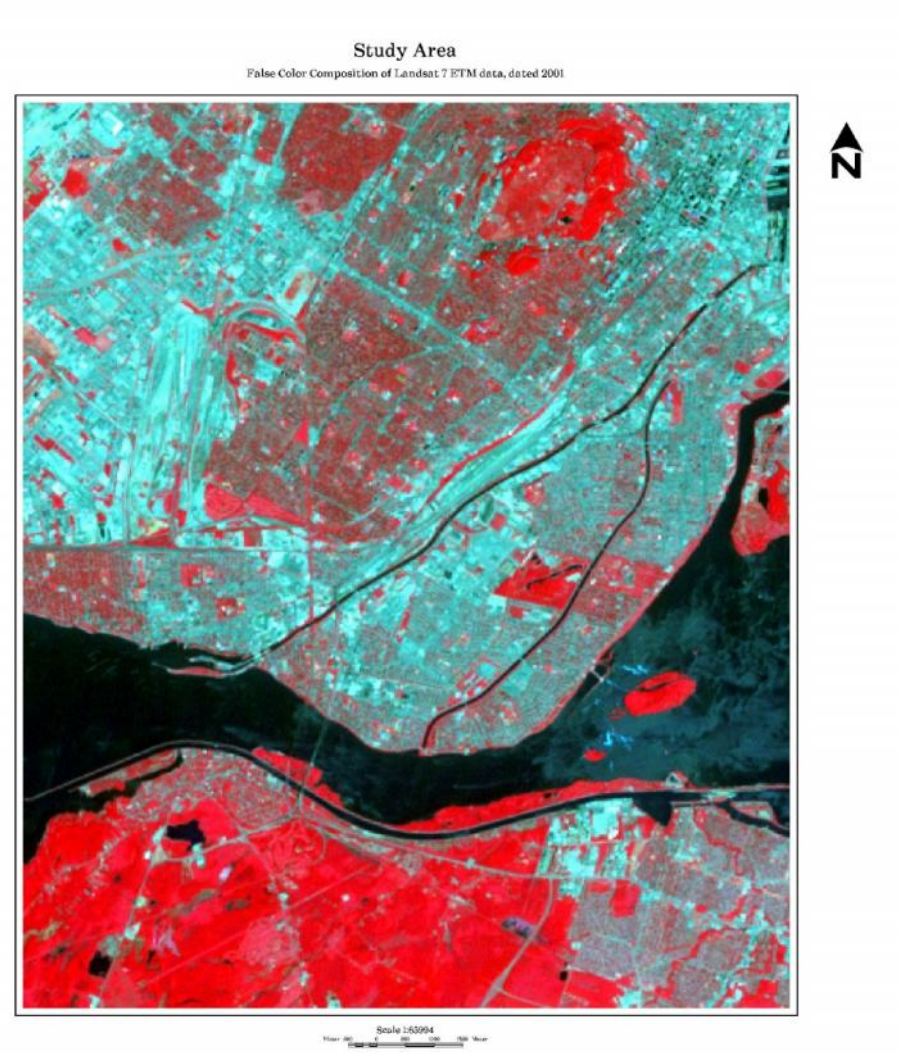

Figure 6: Study site – II (False color composite of 1994 LANDSAT data : red-band4, green-band 3 and blue-band 2)

Other data used in this study included the following:

1. Digital ortho-photographies (1 m spatial resolution) acquired in April, 1994. This data set was used for the evaluation the 1994 image analysis results.
2. A QUICKBIRD image (1 m resolution images) presented on Google Earth acquired in August 26th, 2008 used as the "ground truth" (as reference) data for evaluating the 2008 image analysis results.

3. Road network database over Montreal region at scale 1: 10 000 from the government of Canada. This set of data was updated in 2003 and used to locate tie points for geo-referencing the ASTER images.

4. Digital Elevation Model (DEM) for Montreal region in 30 m resolution downloaded from government of Canada at www.geobase.com used for the ortho-rectification of the ASTER images.

4.2 Methodological approach

The first two objectives of this study concern LANDSAT imagery and its potential for providing information on the location of changed areas as well as on the types of changes. Four change-detection techniques are examined: image differencing, CVA, PCA, and PCC. The third objective is to evaluate the impact of a finer spatial resolution (ASTER images) to the results. In order to obtain the objectives of this study, our methodological approach includes the following steps:

1. Selection of a land cover classification scheme;

2. Data preparation

3. Application of the selected change detection techniques on the LANDSAT images and accuracy assessment

4. Comparison of LANDSAT and ASTER images using the standard approach of post-classification comparison and conclusions on the impact of spatial resolution on the results

These four steps are described in more details in the following paragraphs and the major procedures of this study are shown as figure 7.

.

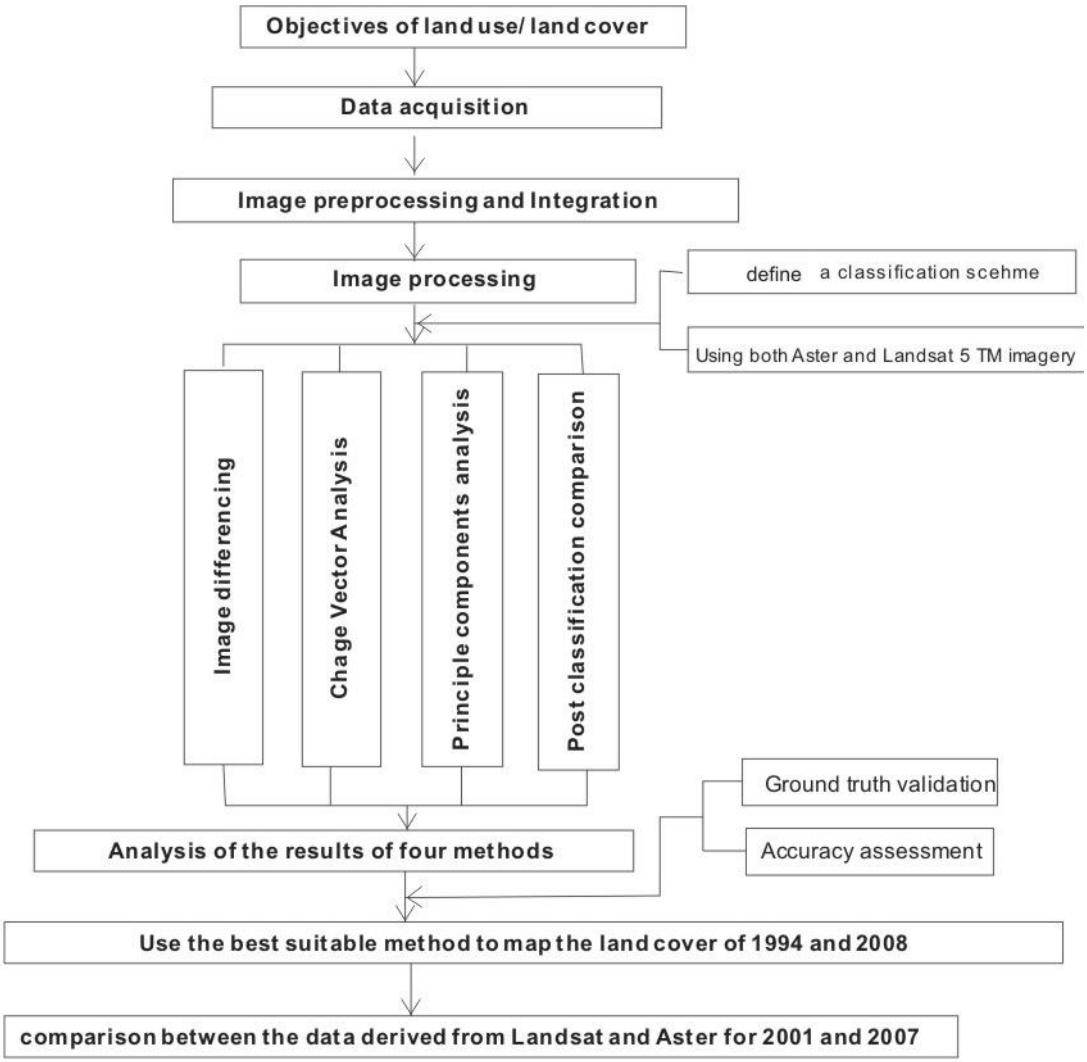

Figure 7: Procedures of the study

4.2.1 Land use / land cover classification scheme

There is no a simple classification scheme of LULC which could be used with all types of imagery and all scales. As mentioned in Chapter 2 in this study the USGS scheme was chosen. Among the 9 classes of Level I (see Table 2), the following are applicable in our case: 1) Urban or Built-up Land; 2) Agriculture; 3) Rangeland; 4) Forest Land; 5) Water; 6) Wetland; and 7) Barren Land. Since only changes within the urbanized area are studied, the class "Agriculture"

is excluded and the rangeland was replaced by a grassland class. The water class here refers only to some ponds and lakes present within the urbanized area.

Upon the examination of the image over the Montreal region, the green space is made up by parks, golf courses, and forest lands, as well as few wetlands. Wetlands occupy only a small portion of the green space and eventual changes of this type of land cover will be difficult to detect due to their relatively small size. In addition, the images used are all acquired during the summer time; the wetland is usually fully covered by vegetation. Without using multi-temporal images from different growing seasons the separation of wetlands from other type of vegetation will be difficult and likely inaccurate.

Furthermore, the barren land could be confused with built up areas as the spectral signature of bare soil is too similar to covering materials of build-up areas, such as concrete or some roofing materials.

Attempts have been made also to study changes with more detailed thematic categories such residential and commercial/industrial, categories belonging to Level II of the USGS classification scheme.

4.2.2 Data preparation

The image set consists of different levels of processing, such as the ASTER image (Table 6). Pre-processing is thus required in order to get a cartographic uniformity and also to reduce the effects caused by the instrument (e.g. striping, atmospheric effects). As the LANDSAT images are already ortho-rectified by the USGS, only atmospheric corrections were applied in each image in order to normalize the multi-temporal set of LANDSAT images to the same radiometric referential. These corrections are described in section 4.3. When using the ASTER images a lot of preprocessing work has to done including: a) de-stripping, b) geometric corrections and c) atmospheric corrections. These operations are described in section 4.4.

4.2.3 LANDSATimage comparison

Four change detection techniques were applied to LANDSAT images of 1994 and 2008 covering the entire study site (Figure 5) and their results were compared using auxiliary data (orthophotos, high resolution images) depicting the past and present situations. All these experiments are descibed in chapter 5.

4.2.4 LANDSAT vs. ASTER

This experiment concerns only the site-II area (Figure 6) and involes the set of ASTER and LANDSAT images acquired in 2001 and 2008. Very few studies addressed the question of the spatial/spectral resolution on change detection with medium spatial resolution images. ASTER images are known to have higher resolution (15 m). In anticipation of higher accuracy using the ASTER images, the experiment with these images is descibed in chapter 6 in detail.

4.3 LANDSATimage preprocessing

The LANDSAT L1T data provided from the USGS are already ortho-rectified (UTM projection, NAD83). USGS used over 200 control points to do the geometric registration and 50 points over the study area zone I. From the header file of each image, the residual in *x* and *y* of each control points is less than +/- 7m and the root mean square (RMS) is less than 0.5 pixel.

The images were radio-metrically normalized in ground reflectance units using the software package "REFLECT" developed at our laboratory (Bouroubi *et al.,* 2006). The conversion of digital values into ground reflectance is a four step procedure:

1) Conversion of digital values into top of the atmosphere (TOA) radiances ;
2) Conversion of TOA radiances to TOA (planetary) reflectance;
3) Estimation of the additive and multiplicative atmospheric effects on TOA reflectance
4) Conversion of TOA reflectance into ground reflectance using the results of the previous step.

The first step is accomplished using the calibration coefficients provided in the metadata file of each scene as follows:

$$L_\lambda = \left(\frac{\mathrm{LMAX}_\lambda - \mathrm{LMIN}_\lambda}{Q_{\mathrm{calmax}} - Q_{\mathrm{calmin}}} \right) \left(Q_{cal} - Q_{\mathrm{calmin}} \right) + \mathrm{LMIN}_\lambda \qquad \text{Equation (4)}$$

where:

λ: TM band number

L_λ: TOA spectral radiance (Spectral radiance measured by the TM or ETM+ sensors),

Q_{calmax}: Maximum quantized calibrated pixel value (DN = 255) corresponding to $LMAX_\lambda$.

Q_{calmin}: Minimum quantized calibrated pixel value (DN = 0) corresponding to $LMIN_\lambda$.

Q_{cal}: Quantized calibrated pixel value (DN), it is 8-bit integer scaled radiance output value (DN),

$LMIN_\lambda$ Spectral radiance that is scaled to Q_{calmin}[W/(m^2· sr·μm)],

$LMAX_\lambda$ Spectral radiance that is scaled to Q_{calmax}[W/(m^2·sr·μm)].

Q_{cal} values and corresponding radiance values are obtained from the header file.

Conversion of TOA radiances to TOA reflectance uses the following equation:

$$\rho^{sat} = \frac{\pi * L_\lambda * d^2}{ESUN_\lambda * \sin(\theta)} \qquad \text{Equation (5)}$$

where

λ: TM band number

L_λ: TOA spectral radiance

ρ^{sat}: TOA reflectance

$ESUN_\lambda$: mean solar exo-atmospheric irradiance (see Table 7)

θ: sun elevation angle, obtained from the header file

d: the earth-sun distance (in astronomical units), which can be calculated using the following equation based on Eva *et al*. (1998)

$$d = 1 - 0.01672 * \cos\left(radians(0.9856 \times (Julian\_Day - 4))\right) \qquad \text{Equation(6)}$$

Table 7: Solar exo-atmospheric spectral irradiance (ESUN; in W/(m^2 . μm) for LANDSAT 5 TM and LANDSAT 7 ETM+

Band	TM	ETM+
1	1957	1997
2	1826	1812
3	1554	1533
4	1036	1039
5	215	230.8
7	80.67	84.90

(Source for TM: Hanscom, 1998; for ETM+: LANDSAT Handbook, retrieved from http://LANDSAThandbook.gsfc.nasa.gov/handbook/handbook_htmls/chapter11/chapter11.html)

For the estimation of the atmospheric effects during the satellite passage REFLECT makes use of the atmospheric code 6S (Vermote *et al.,* 1997). The code is able to simulate the atmospheric effects at the satellite level and a specific spectral band provided that a number of parameters are fixed by the user. These parameters are:

a) The temperature and pressure vertical profile of the atmosphere for gaseous absorption and molecular scattering calculations. Various standard profiles are proposed. In the present study the standard mid-latitude summer was used.

b) The total ozone and water vapor content of the atmosphere as well as their vertical distribution for radiation absorption calculations from these particular gases; for the other gases total content and profiles are fixed a priori. REFLECT proposes either a standard model for these two gases or the possibility to adjust the chosen default model (here mid-latitude) according to user defined values of the total ozone content and/or of the water vapor. In the present study the standard model was used for the ozone while for the water vapor, the total content was evaluated using an empirical formula proposed by RFLECT. This formula uses the air temperature and relative humidity. These parameters could be taken from the archives of a meteorological station near the examined scene. In our case we took the values recorded at the Montreal International airport close to the time of satellite passage (Table 8).

Table 8: The temperature and humidity of the time (hour) image acquired

Image	Date	Time (GMT)	Temperature(^{o}C)	Relative Humidity (%)
1994 LANDSAT 5	August 16 1994	15:30	19	64
2001 LANDSAT 7	June 15 2001	15:30	29.5	56
2007 LANDSAT 5	September 05 2007	15:30	14.9	50
2008 LANDSAT 5	August 22 2008	15:30	22.9	54
2007 ASTER	September 04 2007	16:00	17.8	51
2001 ASTER	June 15 2001	11.10	29.5	56

(Source: retrieved from http://www.climate.weatheroffice.ec.gc.ca/climateData/hourlydata_e.html?timeframe=1&Prov=QC&StationID=5415&Year=2001&Month=7&Day=2)

c) The total aerosol content and its vertical distribution, its composition and optical characteristics, the aerosol optical depth (AOD) being the most crucial parameter. In the present study the default urban model was specified concerning the composition of the aerosol. Using this model 6S computes the aerosol properties, while a standard vertical distribution is assumed. The sole unknown is the AOD. REFLECT proposes the so-called dark target method for the estimation of this parameter. Dark targets are visible features on the images of very low reflectance such as water plans (in the entire solar spectrum) or dense vegetation canopies (in the blue and red bands). Due to this property, the signal observed over these dark targets could be considered as the result of the additive effects of the atmosphere (scattering). It is then possible to estimate the AOD of the aerosol giving rise to the signal observed over these targets. In our case we located a number of lakes and dense vegetation canopies on the images using the method proposed by REFLECT and then calculated the various parameters needed to compute the atmospheric effects as it will be explained in the next paragraphs.

For the final conversion to ground reflectance one has to assume the reflection properties of the surfaces. In the present study and in order to simplify the computations we assumed that the surfaces behave as isotropic (lambertian) reflectors extended to the infinity (the reflection of one pixel does not affect the reflection of its surrounding pixels). In that case the conversion of TOA reflectance to ground reflectance uses the following equation (Bouroubi *et al*. 2006):

$$\rho^{sat} = T_{gaz}\left(\rho_{atm} + \frac{T^{\downarrow}T^{\uparrow}\ \rho_{sol}}{1 - S_{alb}\rho_{sol}}\right) \qquad \text{Equation (7)}$$

where:

ρ^{sat}: TOA reflectance

ρ_{sol}: surface reflectance

ρ_{atm} : atmospheric reflectance due to aerosol and molecule scattering (calculated in step 3)

T_{gas} : total gaseous transmittance –ascending and descending path (calculated in step 3)

$T^{\downarrow}$: total (descending path) atmospheric transmittance due to scattering (calculated in step 3)

$T^{\uparrow}$: total (ascending path) atmospheric transmittance due to scattering (calculated in step 3)

S_{alb}: spherical albedo of the atmosphere (calculated in step 3)

The results of this operation are illustrated with the 2008 LANDSAT image in Figure 8 and 9. The quality of the processed image is clearer with higher contrasts than before pre-processing.

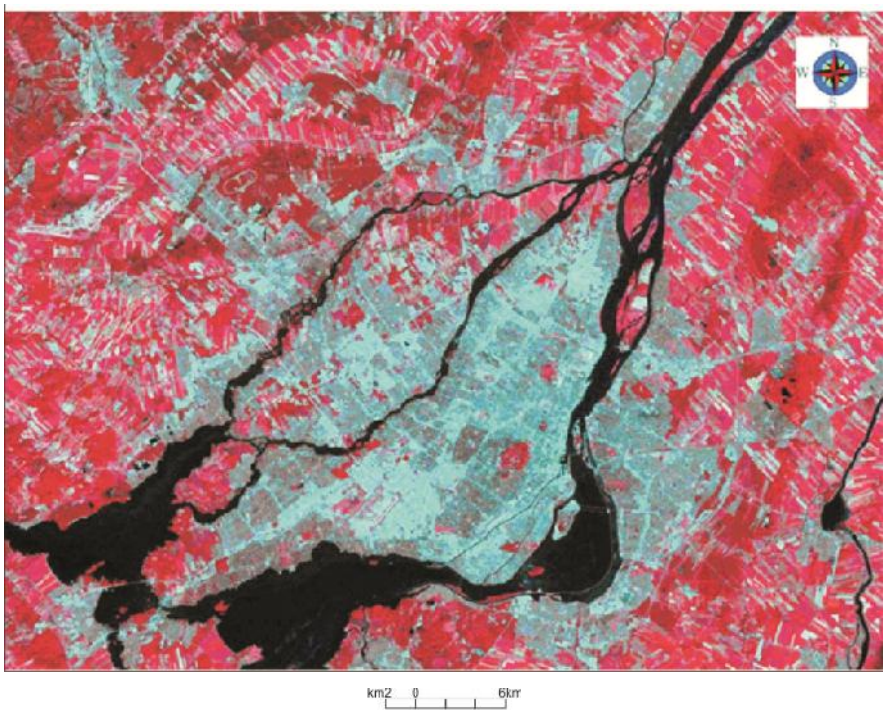

Figure 8: False color composition (R: band 4, G: band 3, B: band 2) of the LANDSAT TM 2008 image before the pre-processing

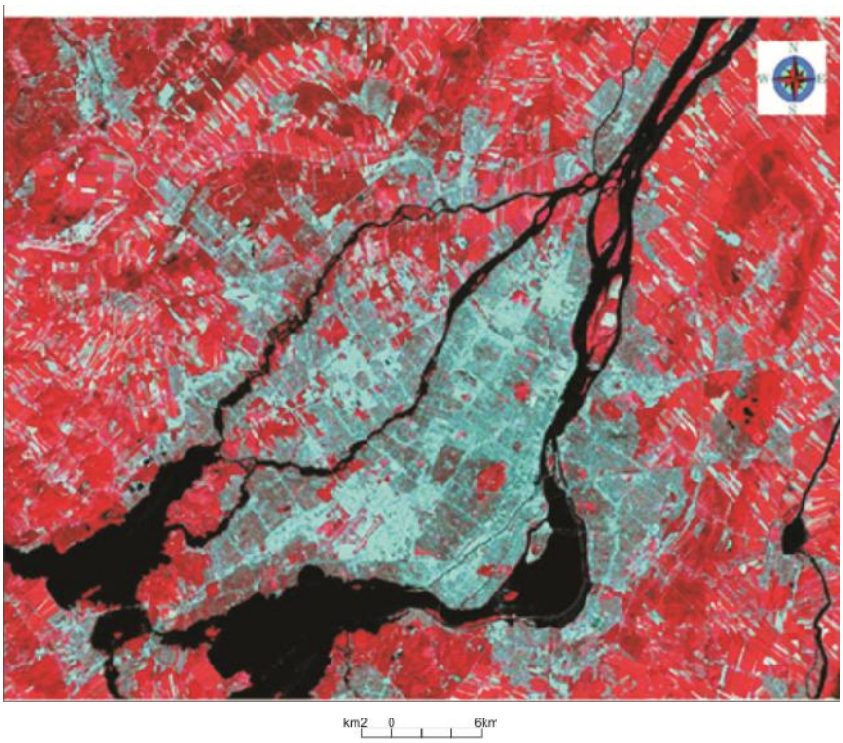

Figure 9: False color composition (R: band 4, G: band 3, B: band 2) of the LANDSAT TM 2008 image after the pre-processing (atmospheric effects removed)

4.4 ASTER image preprocessing

As indicated in section 4.2.2, preprocessing of ASTER data included: a) de-stripping, b) geometric corrections and c) atmospheric corrections.

The striping radiometric noise in CCD array sensors such as the ASTER VNIR is due to particular detectors within the array having a completely different sensitivity to the EM radiation compared to the majority of the detectors in the array. In the geometrically uncorrected image these differences are manifested as stripes in the vertical direction (parallel to the satellite ground track) with a radiometric content different from their surrounding pixels. After visual inspection only the 2007 ASTER image presented an evident stripping radiometric noise which has to be corrected before any data analysis. GEOMATICA proposes a “de-stripping” algorithm DSTRIP based on the location of these stripes on the image and the replacement of the pixel values in the stripes by the average of the values of the surrounding pixels not lain on the stripe. However, this algorithm is adapted to optical-mechanical sensors dotted with a vertical array of detectors such as the LANDSAT TM/ETM where each detector is used to scan an entire scanning line. Thus aberrations in the sensitivity of a particular detector in the array are manifested as strips in the horizontal direction (perpendicular to the satellite ground track). To correct our data with this algorithm we have thus to rotate first our image so the stripes are appearing in the horizontal direction and not in the vertical direction. After de-stripping, the image has to be reoriented in order to proceed with the geometric corrections. Figure 11 shows the result after removing these stripes.

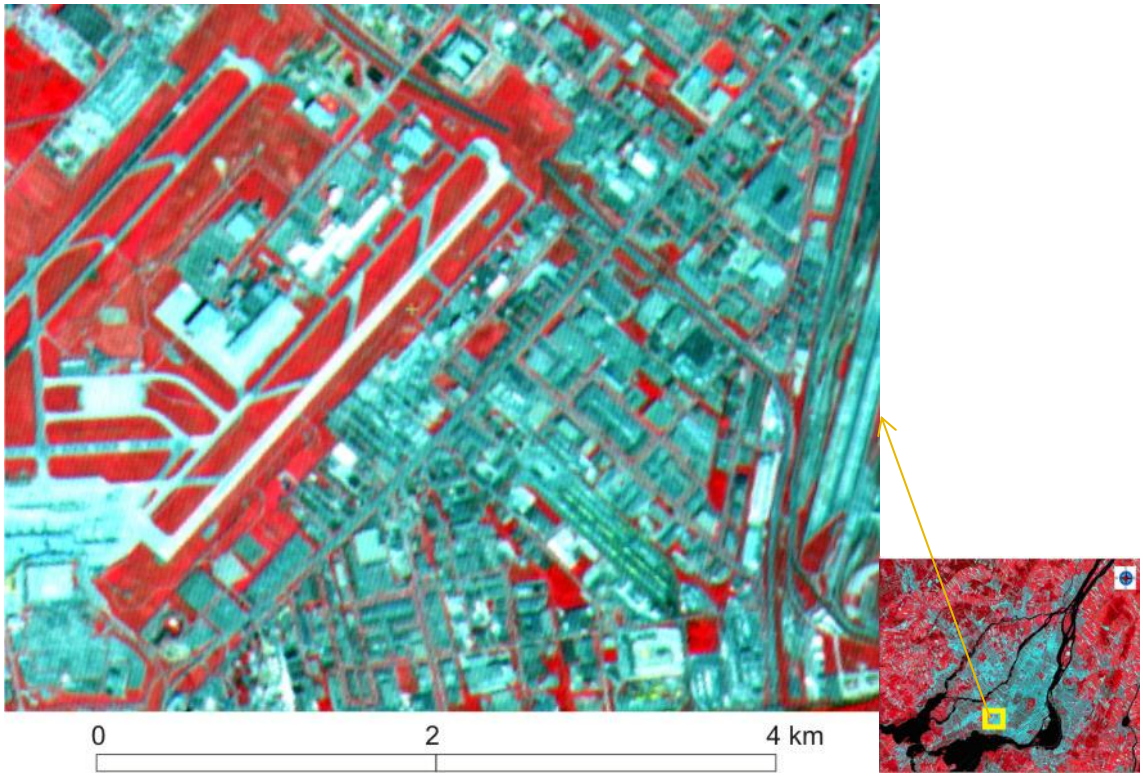

Figure 10: ASTER image (2007) before de-stripping

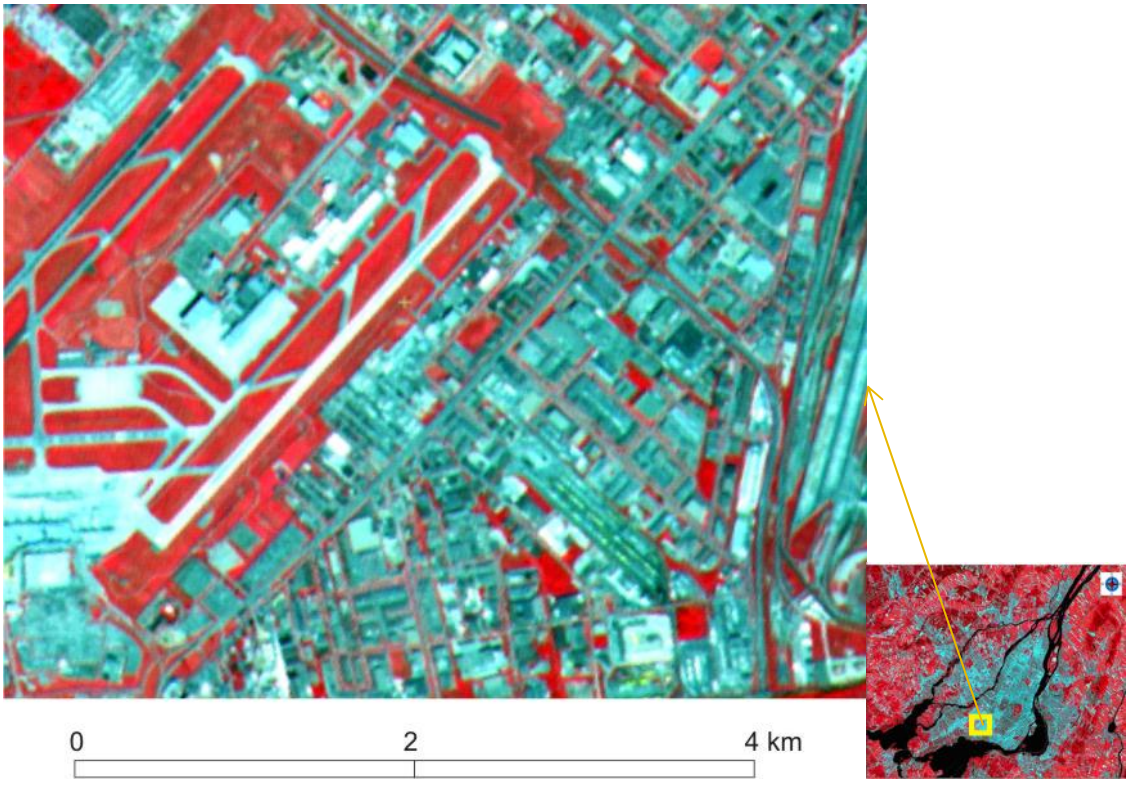

Figure 11: ASTER image (figure 10) after destripping

To geometrically correct the ASTER images, the ortho-rectification procedure available in the GEOMATICA (PCI Inc.) Ortho-Engine module was applied. This procedure uses a model of the satellite orbital path and a DEM of the area of interest to eliminate distortions due to the surface topography and to reference the image to a specific projection (Toutin, 1995). In our case we used the DEM of the region (30 m spatial resolution) and 50 tie points extracted from the road network data at scale of 1: 10 000. The root mean square error was less than 0.50 pixel (one pixel is 15 m X 15 m). The projection is the same as the one used for LANDSAT data - UTM Zone 18 with NAD83 datum based on the GRS80 (Geodetic Reference System) ellipsoid.

Regarding the atmospheric correction, the same approach as before with LANDSAT data was followed. It is to be noted that there are differences in the way to convert digital counts to TOA radiances. ASTER 1-A data has to be converted to scaled radiances using calibration data provided with the image file while ASTER-1B data are already linearly scaled radiance values. The scaled radiances are then converted to TOA radiances (in physical units) using only one coefficient using the following equation:

$$Radiance = (DN\ value - 1) * conversion\ coefficient \qquad \text{Equation (8)}$$

where:

Radiance: the TOA spectral radiance

DN value: the Quantized calibrated pixel value, 8 bit integer scaled radiance output value

Conversion coefficient: radiance per 1DN (Table 9; the gain is indicated in the header file).

Also, another difference compared to LANDSAT data is the value of $ESUN_{\lambda}$ (Table 9).

Table 9: Unit conversion coefficient and solar exo-atmospheric spectral irradiances
(Note: the band 3B is not used in the present study)

Band	Coefficient ($W/m^2*sr*um$)/DN)			*$ESUN_i$
	High Gain	Normal	Low Gain 1	
1	0.676	1.688	2.25	1847
2	0.708	1.415	1.89	1553
3N	0.423	0.862	1.15	1118
3B	0.423	0.862	1.15	

(Source: Thome, 2001)

As an example, the ASTER 2007 images before and after processing are shown in Figure 12 and 13, respectively.

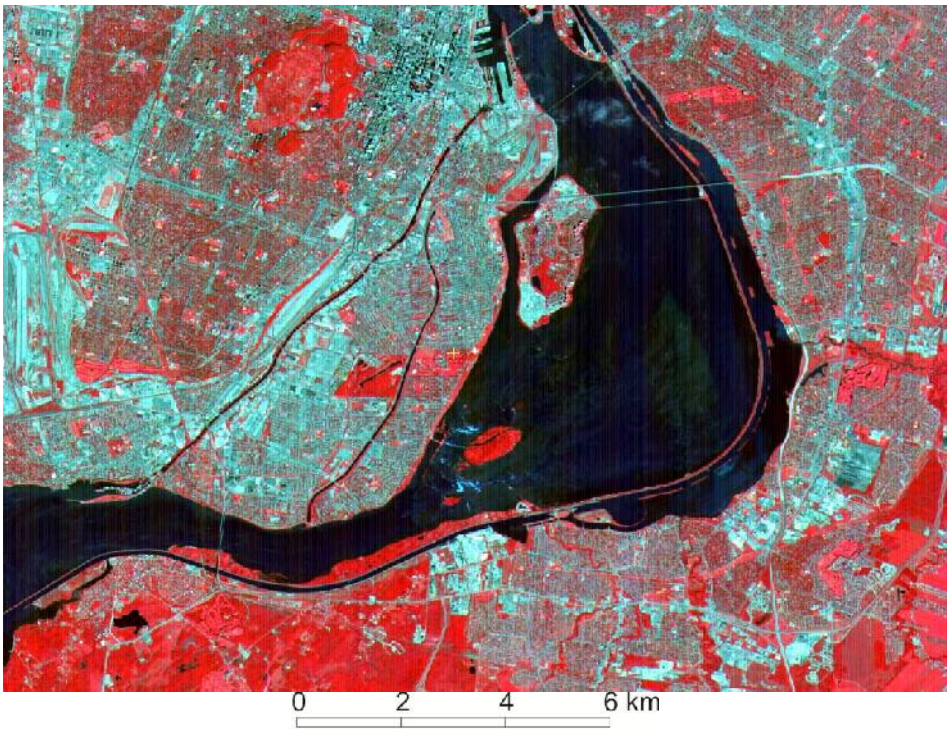

Figure 12: ASTER 2007 data before pre-processing (false color composition: R: band 3, G: band 2, B: band 1)

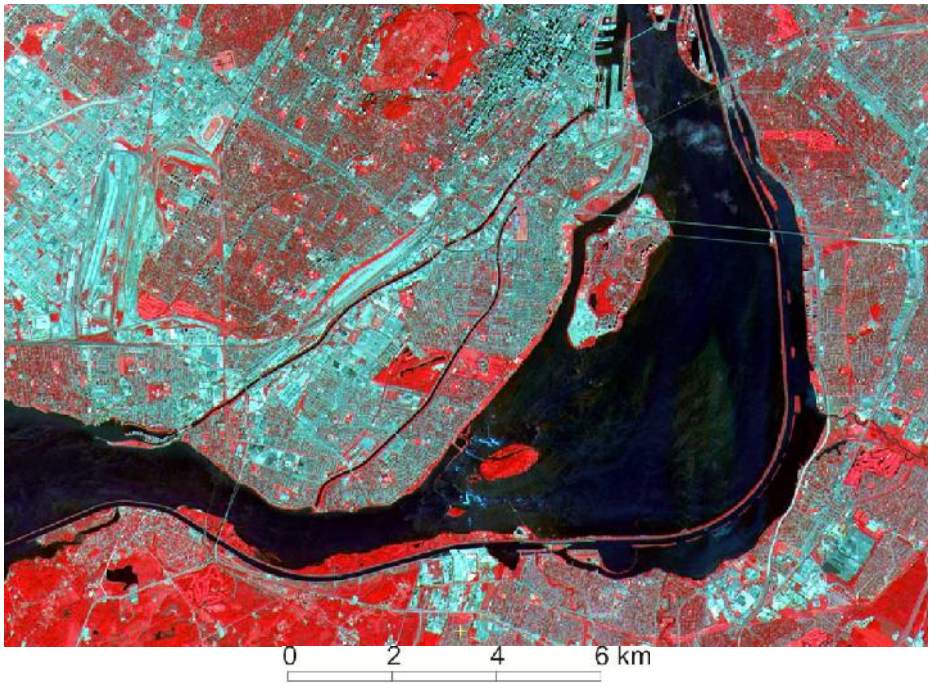

Figure 13: ASTER 2007 data after pre-processing (false color composition: R: band 3, G: band 2, B: band 1)

Chapter 5 Monitoring changes using LANDSAT images: Results and Analysis

5.1 Introduction

The aim of this chapter is to describe the main results obtained by comparing LANDSAT TM images of 1994 and 2008. The material is divided into two parts. The first part presents the results describing the detection of changed areas using the image differencing and CVA approaches. We introduce briefly two other methods after the discussions of image differencing and CVA. They are *NDVI* and *NDBI* which are for detection of locations only. The second part discusses the two methods (PCA and PCC) used to detect types of change.

5.2 Detectection of locations with significant changed areas

In the following discussions we are dealing with the methods of detection of locations that have gone through significant change.

5.2.1 Image differencing

Only the red band (band 3 of LANDSAT 5 TM imagery) has been used for image differencing. As pointed out in chapter 3, this band provides the greatest contrast between vegetation and other land covers and is considered to be superior to other bands for change detection in urban areas. The following equation was applied with our LANDSAT data of 2008 and 1994:

$$Change\ (i,j) = \left(V_{ij}(2008) - V_{ij}(1994) + 1\right) * 100 \qquad \text{Equation (9)}$$

where

Change (*i, j*) is the change in pixel (*i, j*) reflectance (pixel size is 30m by 30m)

Vij(2008) is the reflectance value of TM band 3 in 2008

Vij(1994) is the reflectance value of TM band 3 in 1994

The constant 1 was added in order to avoid negative values, since the change can be positive or negative. The multiplication by 100 provides easier interpretable results. The image

change $Change\ (i,j)$ has a mean value of 99.91with a standard deviation of 1.38. This image has been thresholded and the final binary image of changes is generated.

Singh (1989) suggested that the selection of thresholds can be based on the standard deviation from the mean value of the change image. Analysis of difference values in areas where changes were confirmed by interpreting the available documents indicated us that a threshold equivalent to ±2 standard deviations (one standard deviation is 1.38) from the difference image mean (99.91) effectively portrayed almost all areas of potential change. The numeric range of the change categories were labeled as follows:

Less than 97.15= greenness gain (land covers other than vegetation to vegetation cover)

97.15-102.68 = no change

Greater than 102.68 = greenness loss (vegetation cover to other land covers)

The definition of these change categories makes reference to the reflectance properties of the Earth's surface as captured by the LANDSAT TM sensor. Areas classified as greenness gain are generally characterized by negative values as compared to areas classified as greenness loss which are generally positive. The final difference map was filtered by a 3 by 3 sieve filter in order to remove all areas of change less than the minimum mapping unit of 100mx100m. The resulting LULC change map between1994 and 2008 is shown in Figure 14. From this map, the development of Montreal region is mostly located on the periphery of the city. Notably, there are significant changes occurred during the period 1994-2008 near the P.E Trudeau airport region. The small greenness gain areas could be interpreted as the result of canopies grown in 14 years. The statistics concerning the areas occupied by each category provided by this map are shown in Table 10.

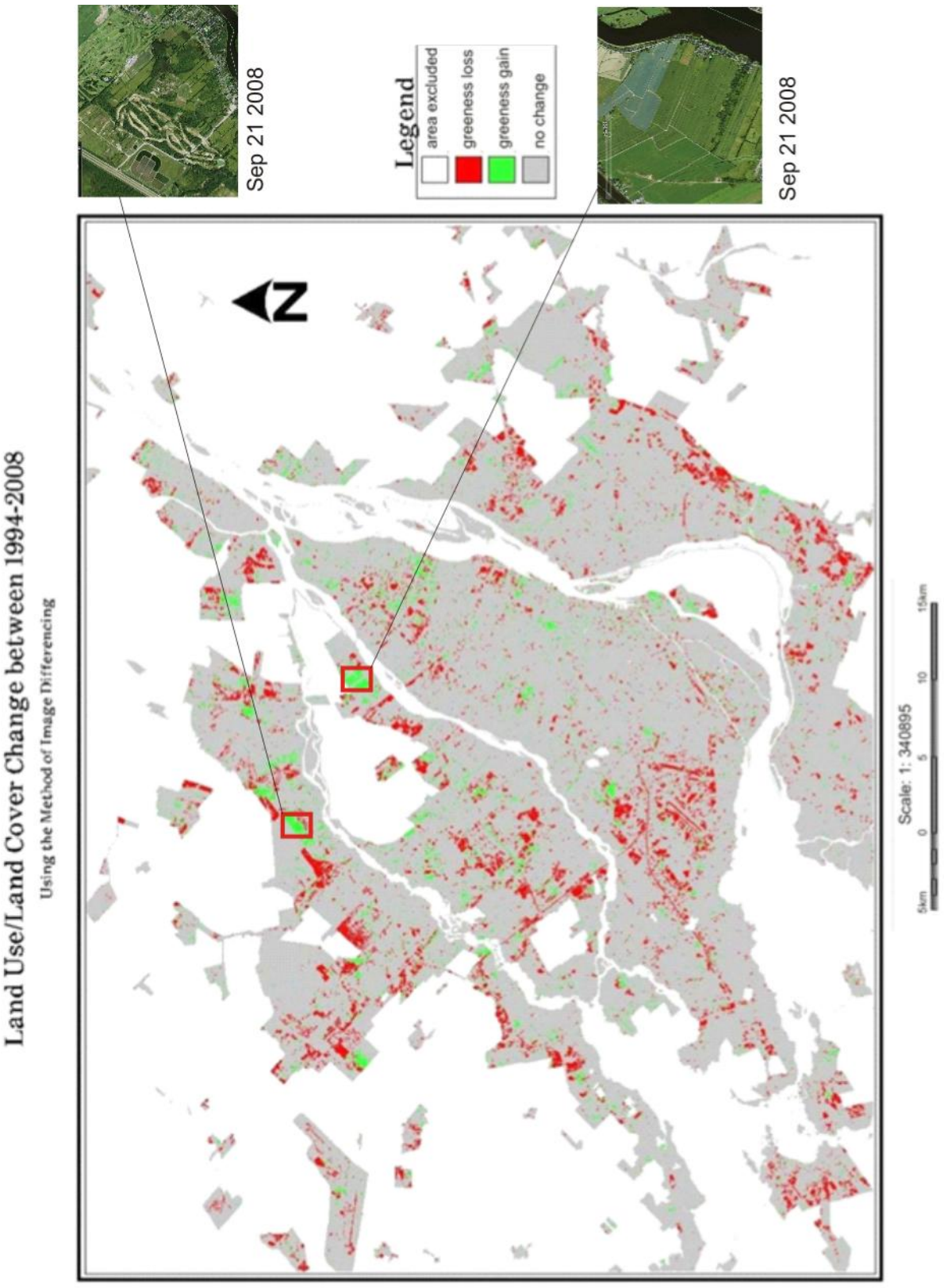

Figure 14: LULC hange map between 1994 to 2008 using image differencing method

Table 10: Areas of LULC cover change between 1994-2008 using the image-differencing method.

Category	Area (in km^2)
Greenness gain	46.76
Greenness loss	106.35
No change	1339.73
Area excluded	2116.82
Total area	3609.66

From table 10, the net greenness loss per year can be calculated as:

Annual net loss per year = total loss (km^2)/ year Equation (10)

So the annual net greenness lost rate per year based on image differencing method should be 106.35 /14=7.59 km^2 per year.

5.2.2 Change Vector Analysis (CVA)

In this study, CVA was applied with LANDSAT images transformed using the tasseled cap transformation. As explained in chapter 3, this is a linear transformation of the original spectral bands into three components: brightness, greenness, and wetness. Besides reducing the data dimensionality, this transformation enhances the contrast between vegetation and no-vegetation covered areas. Each component is calculated using the following:

C1*(TM1)+ C2*(TM2)+C3*(TM3)+C4*(TM4)+C5*(TM5)+C7*(TM7)

Where C*i* is a fixed priori coefficients (see table 11).

The algorithm "TASSEL" (tasseled cap transformation for LANDSAT TM data) included in the GEOMATICS (PCI Inc.). The algorithm is based on the application of the coefficients to the LANDSAT images expressed in the original gray-level scale (8 bit data). This is not suitable to this study because the image data have been transformed to ground reflectance data. Thus, the coefficients in the table 11 proposed by Crist (1985) for TM data expressed in reflectance units were used. The images obtained after this transformation are shown in Figures 15 and 16 - areas where the red hue dominates mean less vegetation.

Table 11: Coefficients used in Tassled Cap transformation

Components	C1	C2	C3	C4	C5	C7
Brightness	0.2043	0.4158	0.5524	0.5741	0.3124	0.2303
Greenness	-0.1603	-0.2819	-0.4934	0.7940	-0.0002	-0.1446
Wetness	0.0315	0.2021	0.3102	0.1594	-0.6806	-0.6109

(Source: reprinted from Crist, 1985.)

The next step in applying the CVA technique is to calculate the magnitude and direction of the difference of the two transformed images. First, change magnitude is measured as the Euclidean distance or length of the change vector from a pixel measurement at time 1 (t1) to the corresponding pixel measurement at time 2 (t2). The magnitude of the vectors could be calculated from the determined difference using the following equation:

$$\Delta G = \sqrt{(\text{brightness} - \text{difference})^2 + (\text{greeness} - \text{difference})^2} \qquad \text{Equation (11)}$$

Thresholds were determined for the magnitude image to separate changed from unchanged pixels. Conventionally, the threshold of the change magnitude is empirically determined. After examining the histogram and statistical values of the magnitude image, change and no-change thresholds were considered as two standard deviations from the mean.

The direction (the angle of change) in reference to the brightness axis was determined as follows:

$$\cos\theta = \frac{\text{brightness} - \text{difference}}{\Delta G} \qquad \text{Equation (12)}$$

$$\theta = \cos^{-1}\left(\frac{\text{brightness} - \text{difference}}{\Delta G}\right) \qquad \text{Equation (13)}$$

The directional images facilitate the discrimination of the change types. Change direction is measured as the angle of the change vector from pixel measurement at t1 to the corresponding pixel measurement at t2. Since two bands were used in this case the resultant change direction classes can be presented into 4 categories depending on the change directions within pixels in the brightness and greenness bands. Angles measured between 90° and 180° indicate an increase in greenness and a decrease in brightness, representing thus a change that is mainly related to the growth of vegetation biomass. Angles measured between 270° and 360° indicate a decrease in

greenness and an increase in brightness, and changes are strongly related to great losses of vegetation biomass. Angles measured from 0 to 90° indicate an increase in both greenness and brightness and it is mainly related to smaller losses of biomass, such as transformation of sections from forest to grass land. Angles measured from 180° to 270° indicate a decrease in both greenness and brightness and it may relate to vegetation changed to water or a change in the moisture content of bare soils. By combining the change directions with the change and no-change magnitude values the entire study area can be classified into 4 classes of changes, as shown in Table 12, plus one class of unchanged areas. The change map obtained by this classification is shown in Figure 17.

Table 12: Change categories

Class	Brightness	Greenness	Themes
Class 1 (0-90°)	+	+	Biomass loss
Class 2 (90°-180°)	−	+	Biomass gain
Class 3 (180°-270°)	−	−	Greenness loss and with more moisture
Class4 (270°-360°)	+	−	Forest Clearing

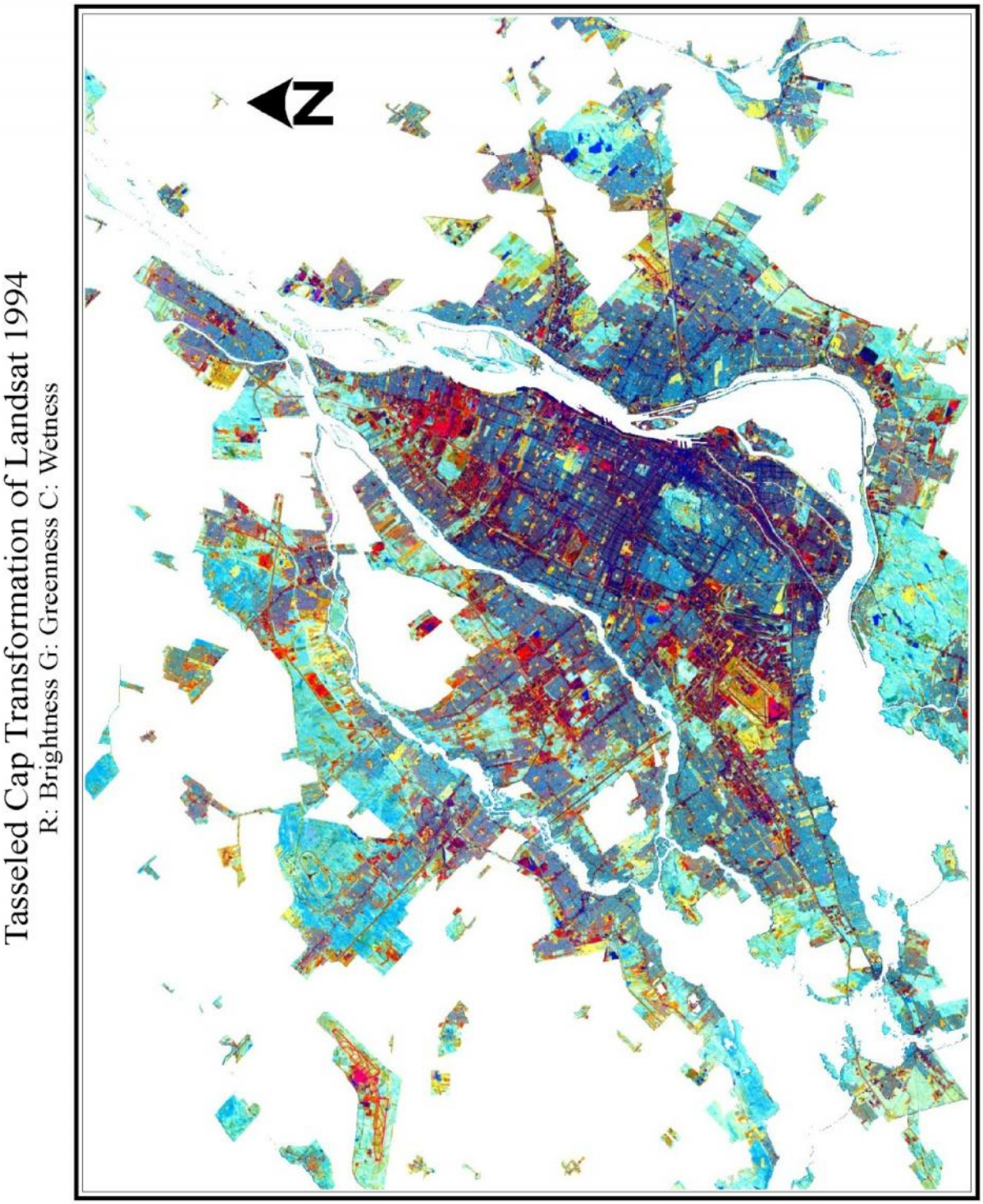

Figure 15: Tasseled Cap Transformation of 1994 LANDSAT data (R: Brightness G: Greenness B: Wetness)

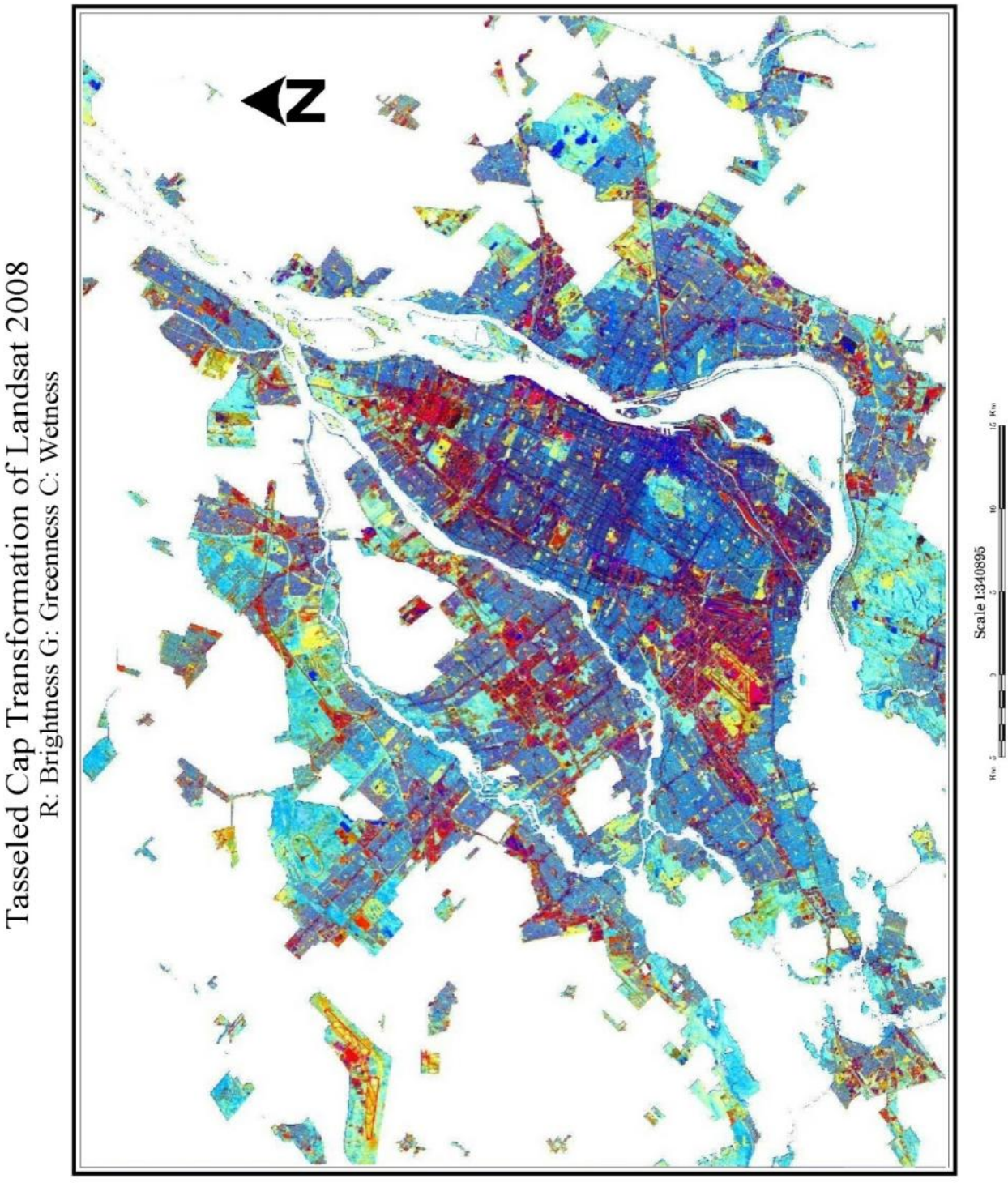

Figure 16: Tasseled Cap Transformation of 2008 LANDSAT data (R: Brightness G: Greenness B: Wetness)

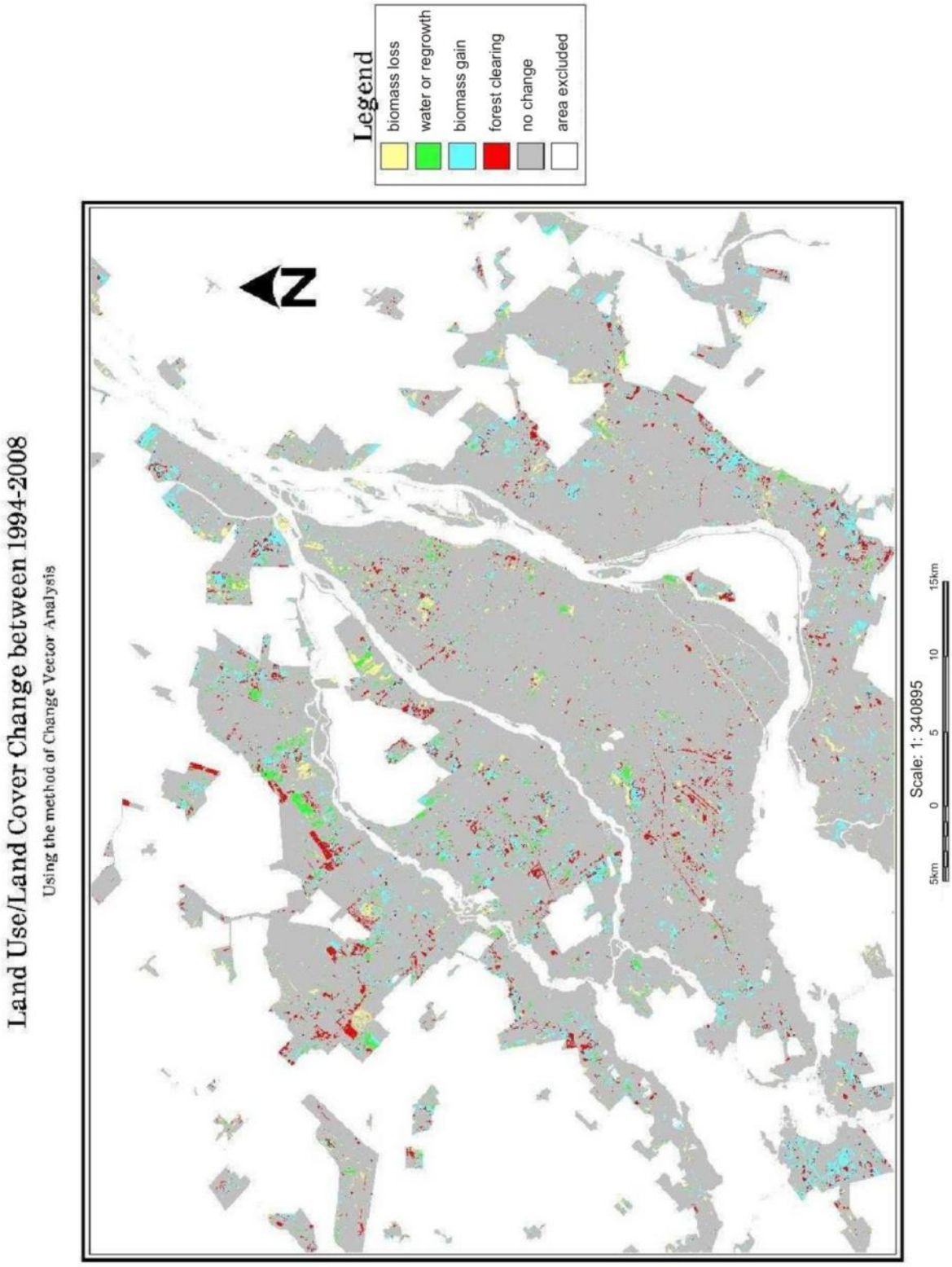

Figure 17: LULC change map between 1994-2008 using the CVA method

From the LCLU change map of figure 17, the derived statistics on the area occupied by each category are shown in Table 13.Based on this table, the total biomass loss is for the 14 year period (1994 -2008): 28.39+75.31+43.43=147.13 km^2. The annual net biomass loss is about 10.5 km^2 per year. This rate is not the same as the one derived from the method of Image Differencing which is 7.59 km^2 per year. These numbers are dissimilar as the classified categories are different. Also, from table 13, forest clearing (class 4) is only 43.43 km^2, however, this number does not refer to the total area of the forest loss because the class 3 (greenness loss with more moisture) occupying 75.31 km^2 may count to the forest loss too.

Table 13: Areas of LULC change in the period 1994-2008

Categories	Area (in km^2)
Biomass loss (class 1)	28.39
Biomass gain (class 2)	23.66
Greenness loss with more moisture (class 3)	75.31
Forest clearing (class 4)	43.43
No change	1322.05
Area excluded	2116.82
Total area	3609.66

5.2.3 Alternative techniques (for location detection)

A different approach to locate changed areas is via the comparison of images representing a spectral index (Cavayas and Baudouin, 2008). One of the most commonly used index is the NDVI (Normalized Difference Vegetation Index) computed by comparing pixel reflectance in the red and NIR spectral bands:

$$NDVI = \frac{\rho_{NIR} - \rho_{RED}}{\rho_{NIR} + \rho_{RED}} \qquad \text{Equation (14)}$$

This index is particularly sensitive to vegetation and less so to building and other land cover. As shown previously, most of the detected changes are related to vegetation cover changes. By taking into account the reflectance in two spectral bands some of the errors eventually present in the case of image differencing can be avoided. In fact, as showed in figure 18, some manmade materials, like asphalt, have low reflectance in the red band similar to vegetation cover. Thus, a change from bare soil to asphalt covered surfaces can be considered as

a vegetation gain and vice versa when the comparison is based solely on the red band. As asphalt has almost the same reflectance in the red and NIR, the NDVI of pixels with asphalt cover takes a near zero value while NDVI for vegetation covers takes high positive values.

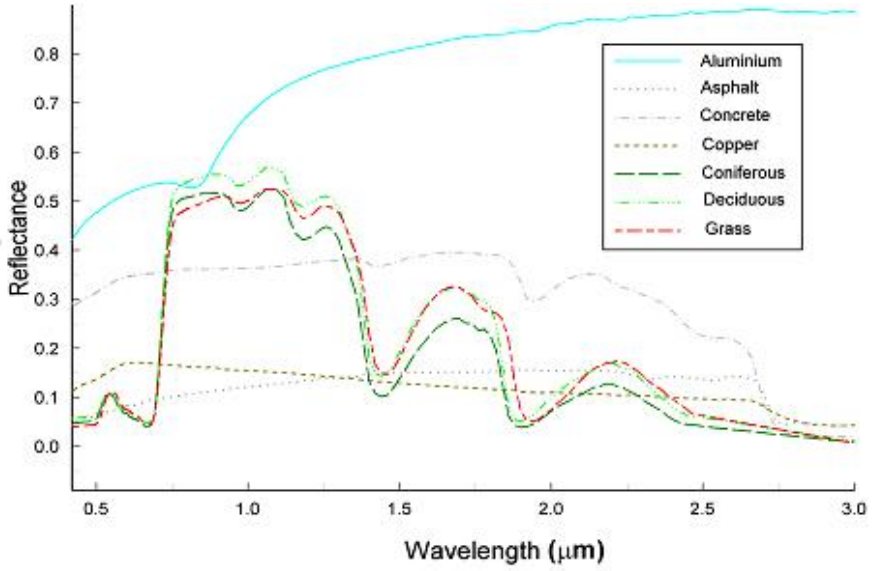

Figure 18: Spectral signatures of common surface materials in urban areas (Source: generated from ASTER Library)

In a publication (Zha *et al*. 2003) proposed a different index. This index was particularly sensitive to built-up materials, the Normalized Difference Built-up Index (NDBI). This index was developed for LANDSAT images to take advantage of the spectral band in the SWIR around 1.6 μm (TM5). It is calculated as

$$NDVI = \frac{\rho_{SWIR} - \rho_{NIR}}{\rho_{SWIR} + \rho_{NIR}} \qquad \text{Equation (15)}$$

As shown in figure 18, in general, built-up materials in this band have higher reflectance in the TM5 band than in the TM4 (NIR) band while the inverse happens for vegetation. So when TM5 band is compared with TM4 band, most of built-up materials give rise to positive values of the NDBI whereas vegetation and water give rise to negative values.

Figure 19 shows the two indexes calculated from LANDSAT images of 1994 and 2008. It is evident that they are highly correlated, with one index almost the negative image of the other.

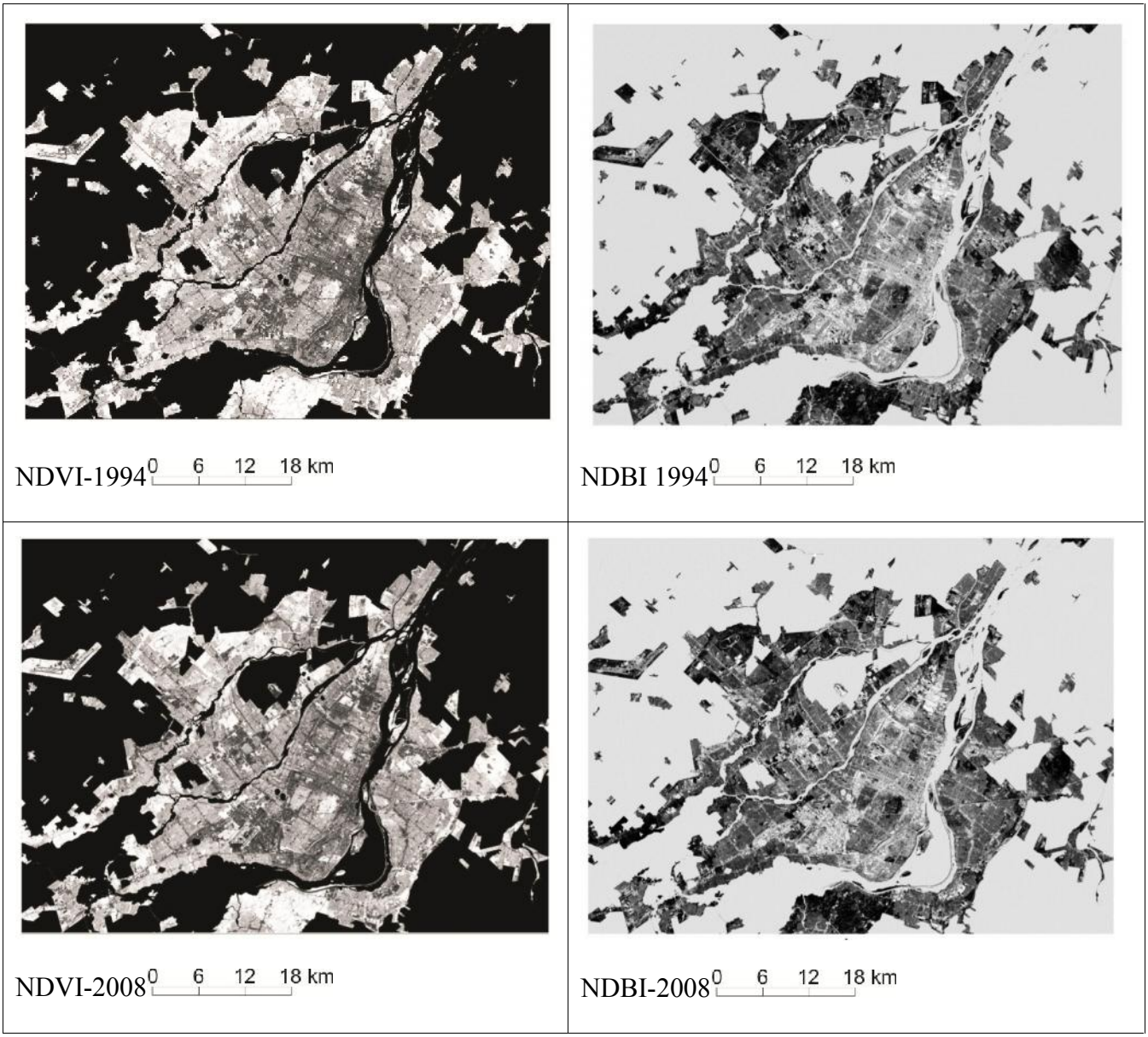

Figure 19: Comparison of the NDVI and NDBI calculated from LANDSAT images of 1994 and 2008

To facilitate the comparison of each index obtained for the two different years, the images were classified. In the case of the NDVI, the following classification is used: (a) absence of vegetation cover to low vegetation cover (NDVI<0.20), (b) low vegetation to relatively high vegetation cover (0.20<NDVI<0.60) and c) relatively high to very high vegetation cover (NDVI>0.60). For simplicity we renamed these three classes as a) no vegetation; (b) sparse vegetation and (c) dense vegetation. Regarding the NDBI, pixels with index value greater than zero is considered as built-up materials (without vegetation cover). The images of the indexes after this classification are shown in figure 20.

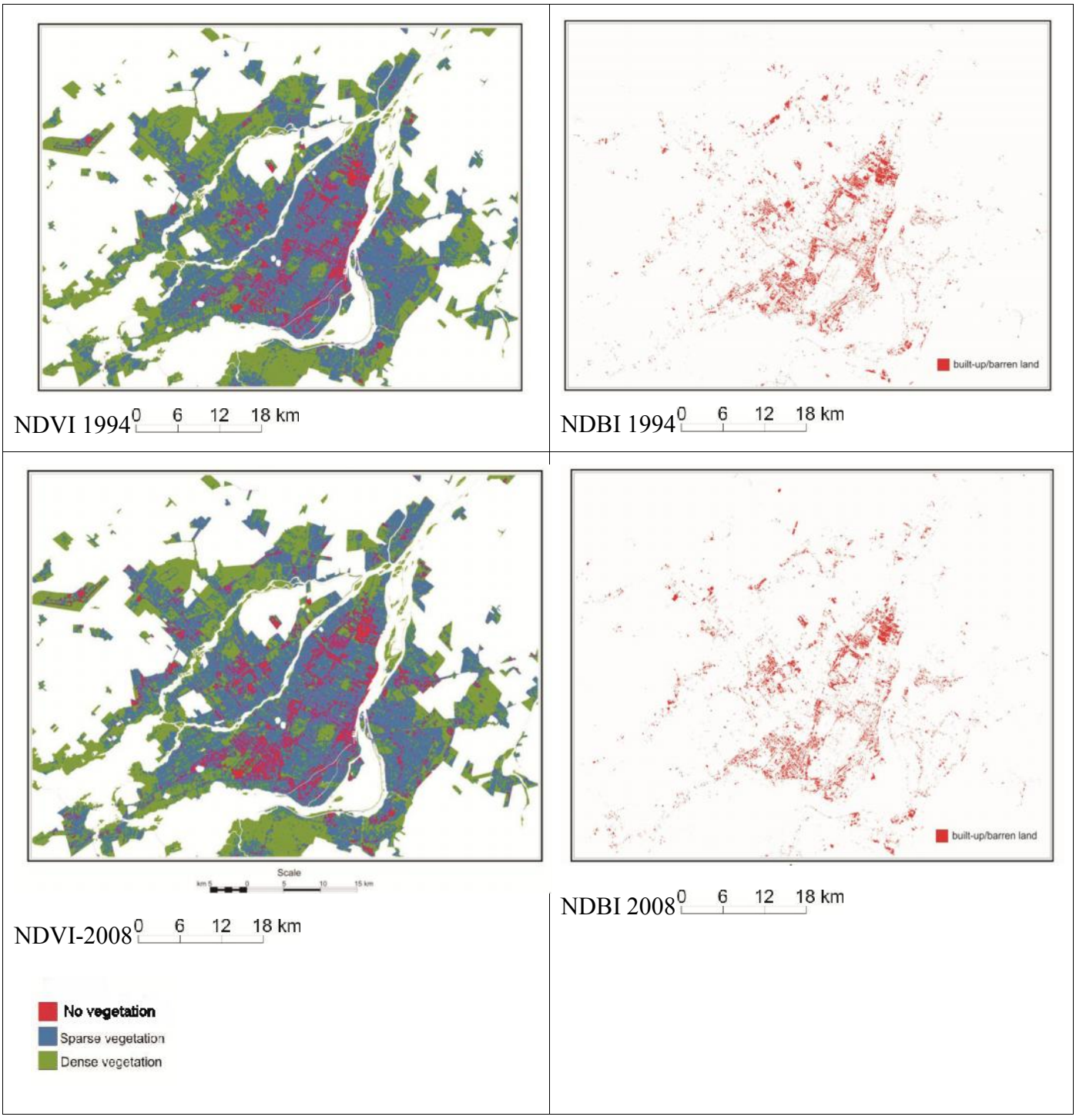

Figure 20: Comparison of the NDVI and NDBI calculated from LANDSAT images of 1994 and 2008 after classification

Figures 21 and figure 22 shows the results of change detection between 1994 and 2008 indexes after classification of each individual image. As in the previous section statistics were computed concerning the changes in vegetation cover (NDVI images) shown in Table 14. Based on this table, the total greenness loss (including the class dense to sparse vegetation) should be for the 14 year period: 36.07+16.85+124.34=147.13 km^2. Thus, the annual greenness loss should be about 12.6 km^2 per year. This rate is relatively close to the one derived from the CVA method which is 10.5 km^2 per year.

Table 14: Change Statistics using the NDVI images

Classes	**Area (km^2)**
No change	1166.81
Sparse vegetation to no vegetation	36.07
Dense vegetation to no vegetation	16.85
No vegetation to sparse vegetation	20.50
Dense vegetation to sparse vegetation	124.34
No vegetation to dense vegetation	1.32
Sparse vegetation to dense vegetation	126.37
Area excluded	2117.41
Total area	3609.66

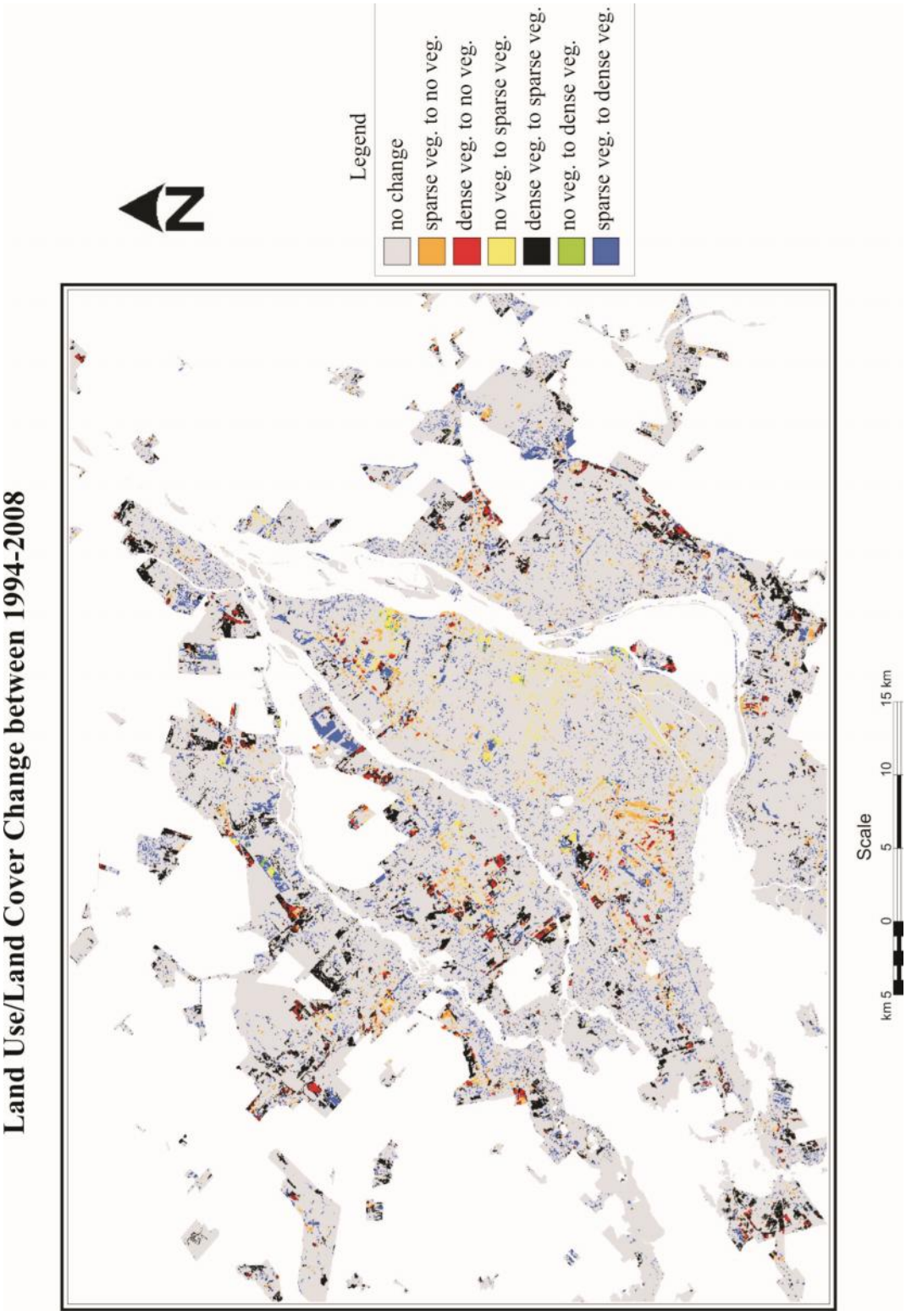

Figure 21: LULC change map between 1994-2008 uisng NDVI method

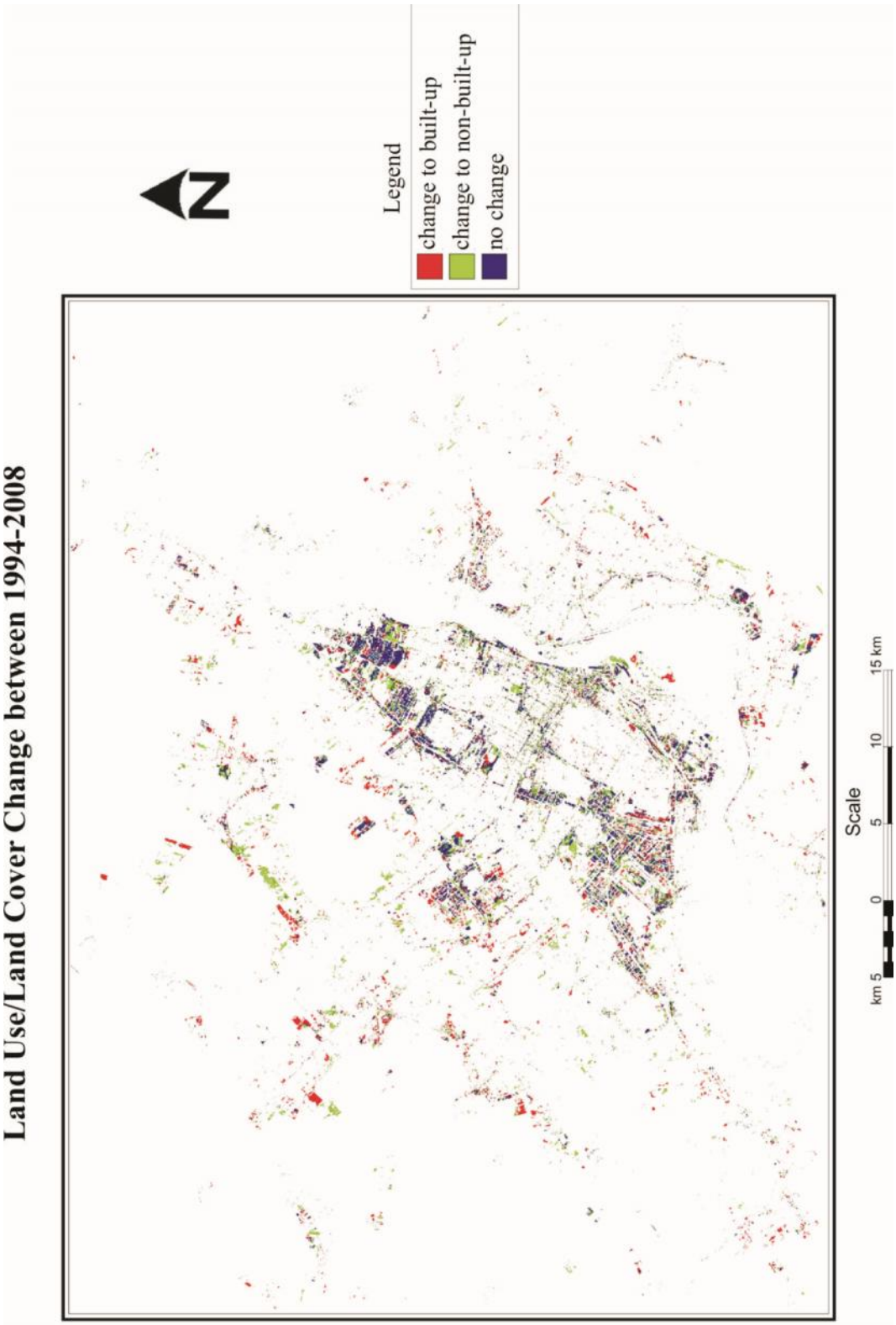

Figure 22: LULC change map between 1994-2008 uisng NDBI method

Equivalent results were obtained using the image differencing and change vector analysis techniques. Figure 23 shows as an example a small portion of the two maps. CVA however is providing more details on the nature of changes in the vegetation cover.

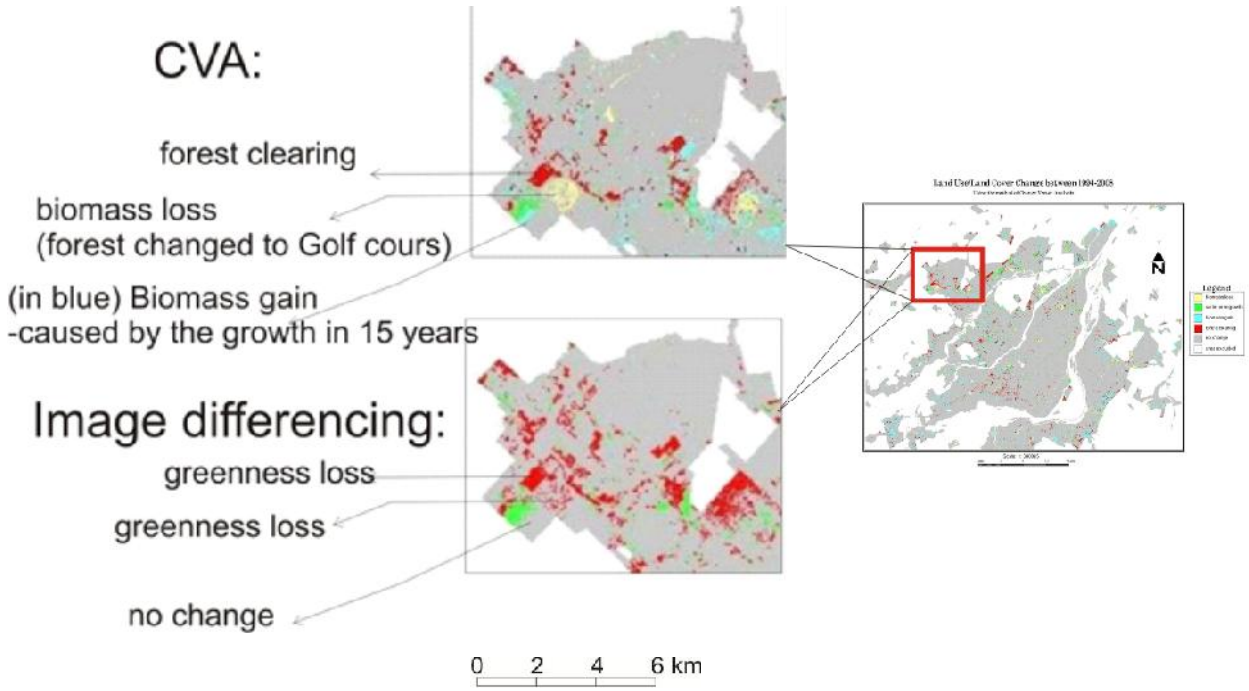

Figure 23: Comparison of the results obtained with the CVA and image differencing techniques

When applying the two indices, we found that the NDBI is not useful for the Montreal region where there are a lot of high mixed areas of vegetation and built-up materials. The NDVI approach is in general comparable to the CVA approach with the latter providing more refined information on vegetation changes.

In summary, image differencing is a simple method to apply providing an adequate picture of the areas of changes.

5.3 Location of changed areas and type of changes

5.3.1 Principal Components Analysis

As applied in this study, the PCA is a three step operation. First, the six bands of the LANDSAT 5 TM image of 1994 and 2008 are combined to generate a new image. Second, the PCA is performed to the combined image. Third, the PCA image is classified using interactive training sites editing. These steps are described in more details in the next paragraphs.

- **Step 1. Creation of a new image**

Two images dated 1994 and 2008can be referred as two pixel vector (1) and vector (2):

$X_{1994}=[X_{1994\text{-}1}, X_{1994\text{-}2}, \ldots X_{1994\text{-}N}]$ vector(1) Equation (16)

and

$X_{2008}=[X_{2008\text{-}1}, X_{2008\text{-}2}, \ldots X_{2008\text{-}N}]$ vector (2) Equation (17)

where

$X_{1994\text{-}1}$ to $X_{1994\text{-}N}$ and $X_{2008\text{-}1}$ to $X_{2008\text{-}N}$ are the reflectance of the pixel X in bands *1* to band N for the year of 1994 and the year *2008* respectively. The first step of this method is to combine the two vectors into one single vector:

$X=[X_{1994\text{-}1}, X_{1994\text{-}2}, \ldots X_{1994\text{-}N}, X_{2008\text{-}1}, X_{2008\text{-}2}, \ldots X_{2008\text{-}N}]$ vector (3) Equation (18)

An image file with a total number of 12 bands is thus generated in the case of TM images.

- **Step 2. PCA transformation**

The PCA transformation was applied to the original images to generate the transformed images using the covariance matrix. The eigen-values and variance explained by each principal component are shown in the Table 15. It can be seen that the first principal component explains most of the variance of the original data set (91.36%). The second principal component describes the largest amount of the variance in the data that is not already explained by the first principal component, and so forth. Indeed, the first 4 components count for over 99.38% of the total variance. The obtained eigen-channels are shown in figure 24. Figure 25 shows a color composition of the first three eigen-channels.

Table 15: Eigenstructure of the multi-temporal LANDSAT TM dataset (1994 and 2008)

Eigen-channel	Eigen-value	Deviation	%Variance
PC1	0.0674	0.2596	91.36%
PC2	0.0046	0.0680	6.26%
PC3	0.0008	0.0274	1.02%
PC4	0.0005	0.0234	0.74%
PC5	0.0003	0.0163	0.36%
PC6	0.0001	0.0097	0.13%
PC7	0.0000	0.0065	0.06%
PC8	0.0000	0.0045	0.03%
PC9	0.0000	0.0036	0.02%
PC10	0.0000	0.0027	0.01%
PC11	0.0000	0.0026	0.01%
PC12	0.0000	0.0023	0.01%

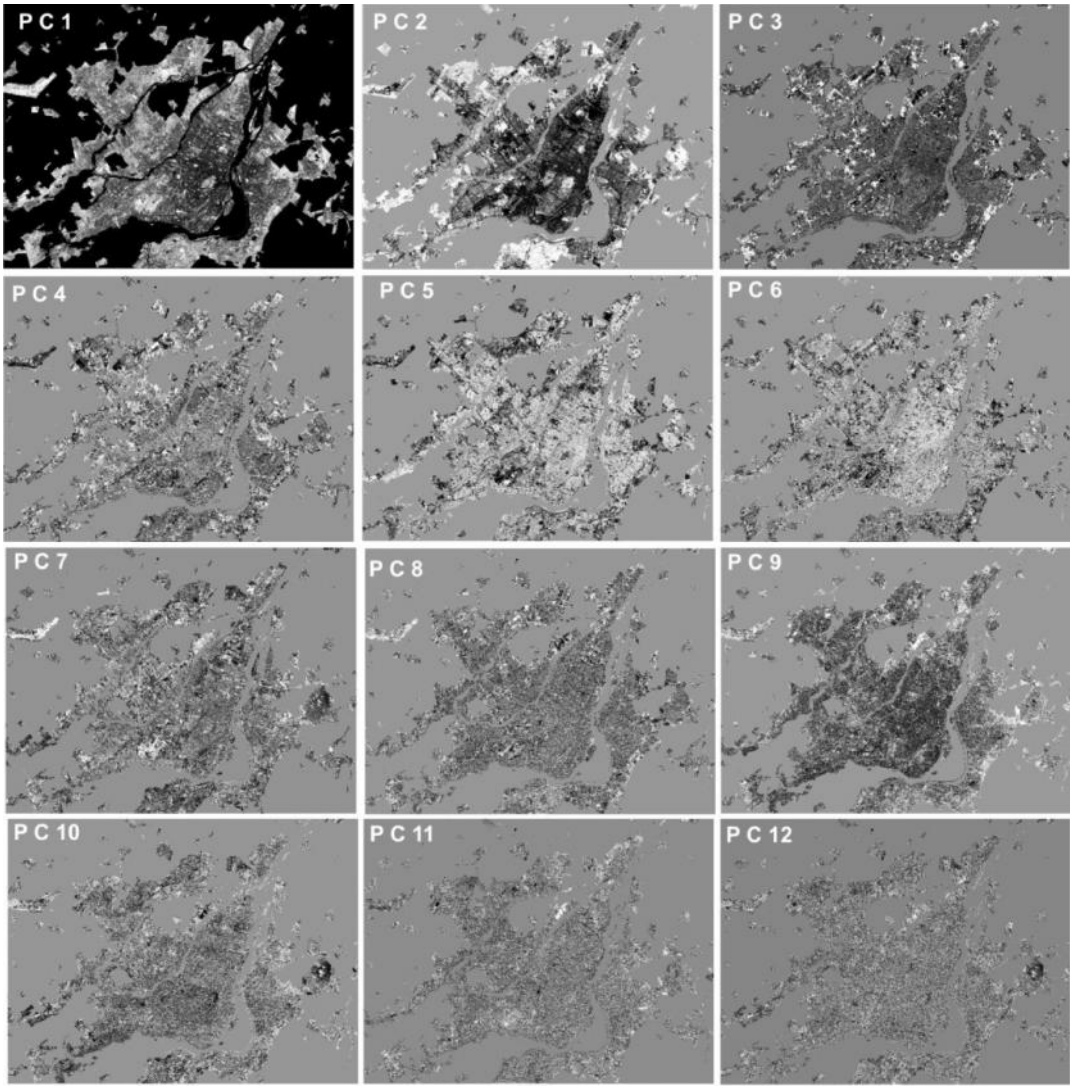

Figure 24: 12 components of composed image created by principal components analysis

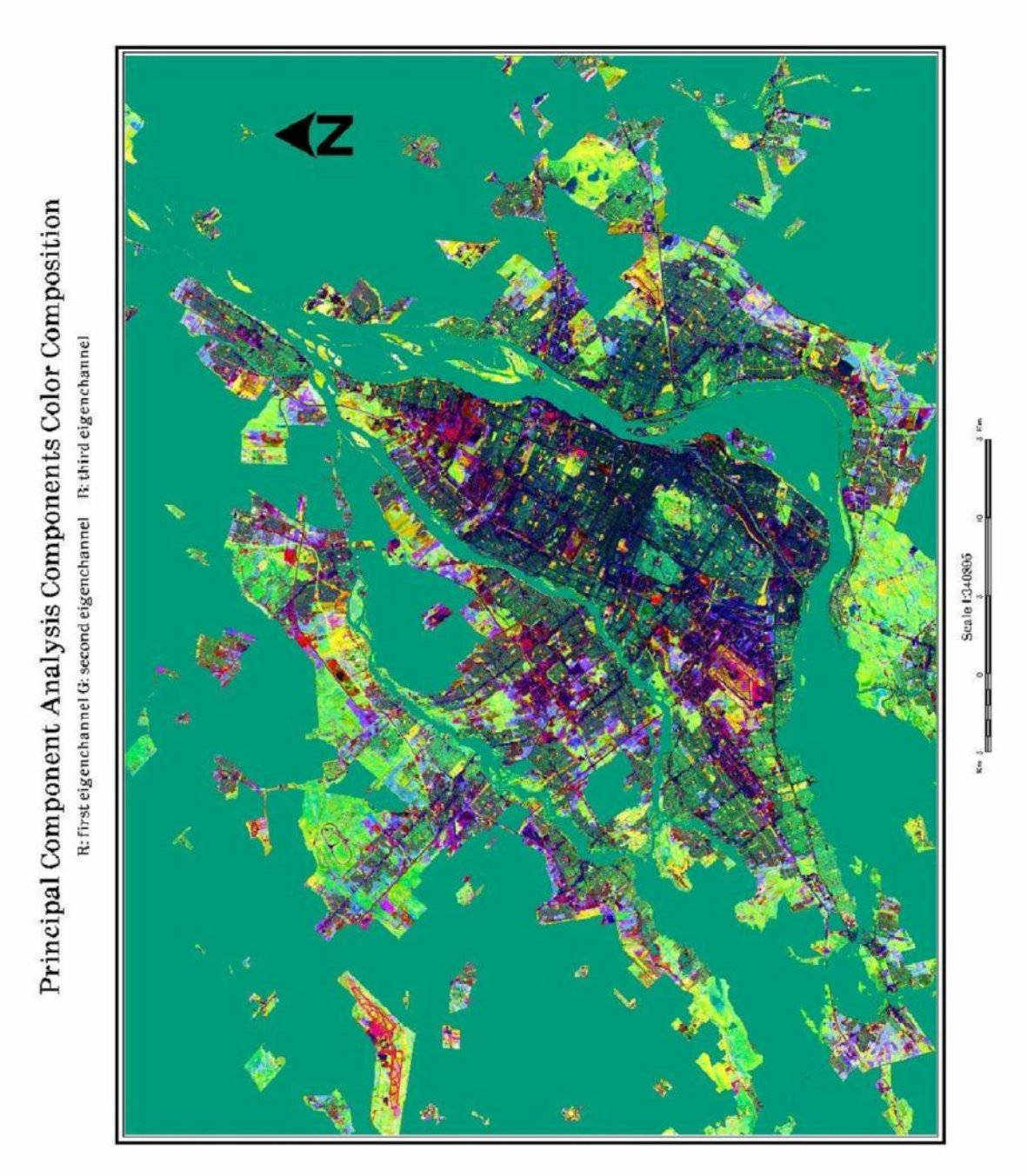

Figure 25: PCA components color composition (R: first Eigenchannel G: second Eigenchannel B: third Eigenchannel)

- **Step 3: Interactive training and classification :**

As the three first principal components contain most of the information of the original images, it is possible to use them for the classification of LULC change. Interactive training of a supervised classifier ("from-to" classes) was carried out on the color composite image created by Principal Components Analysis (Figure 25). 30 training sites were selected on the color composite image by chaining it to the original images and tracing on the screen the contour of the sites as illustrated in figure 26. Also, the aerial photos and the Google Earth image were linked to these 3 images to assist in the identification of training sites. The standard maximum likelihood classifier was then used. The classification result is shown in figure 27.

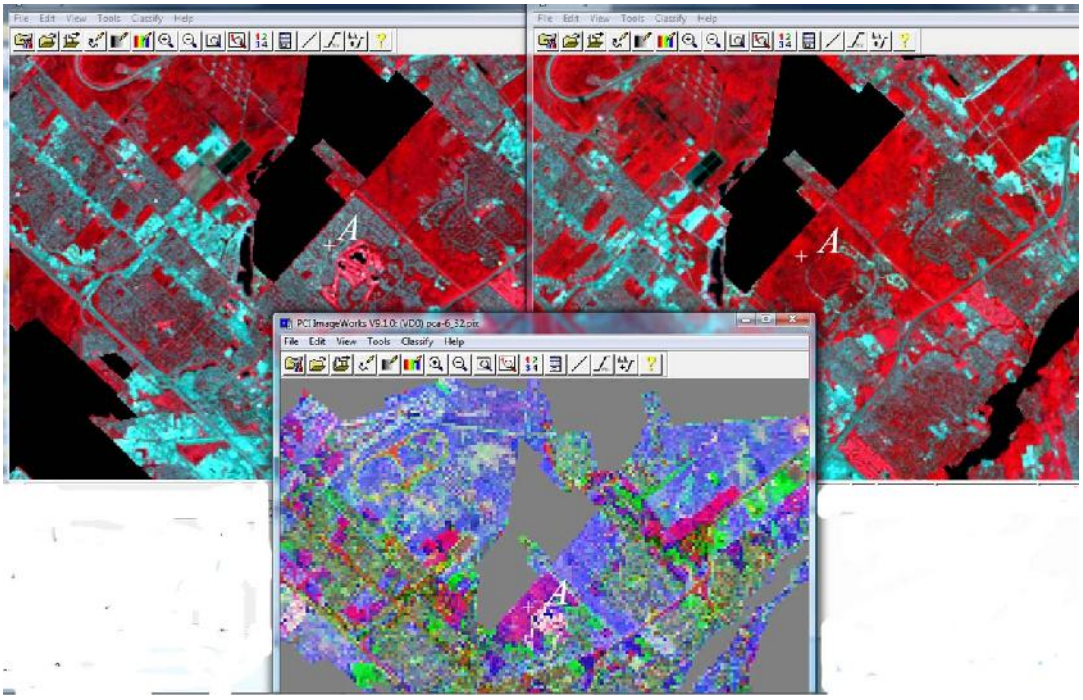

Figure 26: Interactive training for a supervised classification of the first three principal components

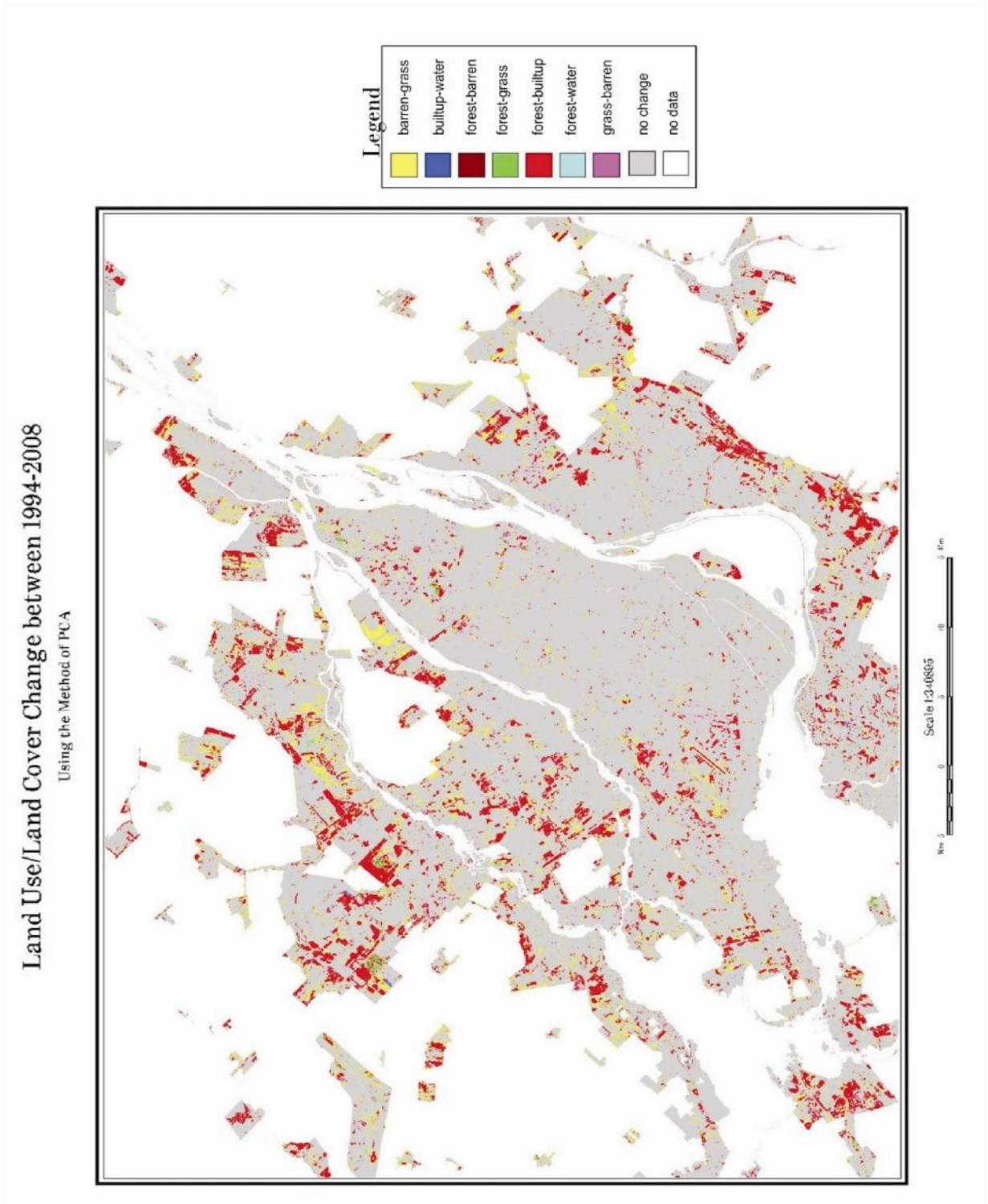

Figure 27: LULC change map between 1994-2008 using the method of PCA

Based on the map of figure 27, the areas occupied by each class are shown in Table 16. In the period from 1994 to 2008, the detected total forest loss (forest to built-up, forest to water, forest to grass and forest to barren land) is 118.36 km^2. The average forest loss of each year is about 8.45 km^2 per year. Meanwhile, the areas converted to built-up are 132.89 km^2 from 1994 to 2008 with a rate of about 9.5 km^2 per year from grass/shrub or forest land.

Table 16: Areas occupied by the classes identified using the PCA approach

Class ("from-to")	**Area_(km^2)**
Grass to barren land	15.41
Barren land to grass	72.73
Forest to built-up	111.86
Grass to built-up	21.03
Forest to water	0.91
Forest to grass	3.43
Built-up to water	0.06
Forest to barren land	2.16
no change	1265.25
Area excluded	2116.82
Total area	3609.66

5.3.2 Post Classification Comparison

In this study, the 1994 and 2008 images were classified separately using a supervised maximum likelihood approach based on 5 classes: water, forest, barren land, grass/golf court, built-up. Training areas were selected from both data sets using the available documents. The classified images are overlaid and analyzed using the GEOMATICS algorithm MAT (Matrix Analysis) to generate the changed classes. 5 LULC classes were classified in each single date image, generating 25 potential types of changed classes. Land use/Land cover map of 1994 and 2008 are presented in the Figure 28 and 29 respectively. The changes between two dates were summarized to 14 major classes and the final LULC change map is shown in figure 30.

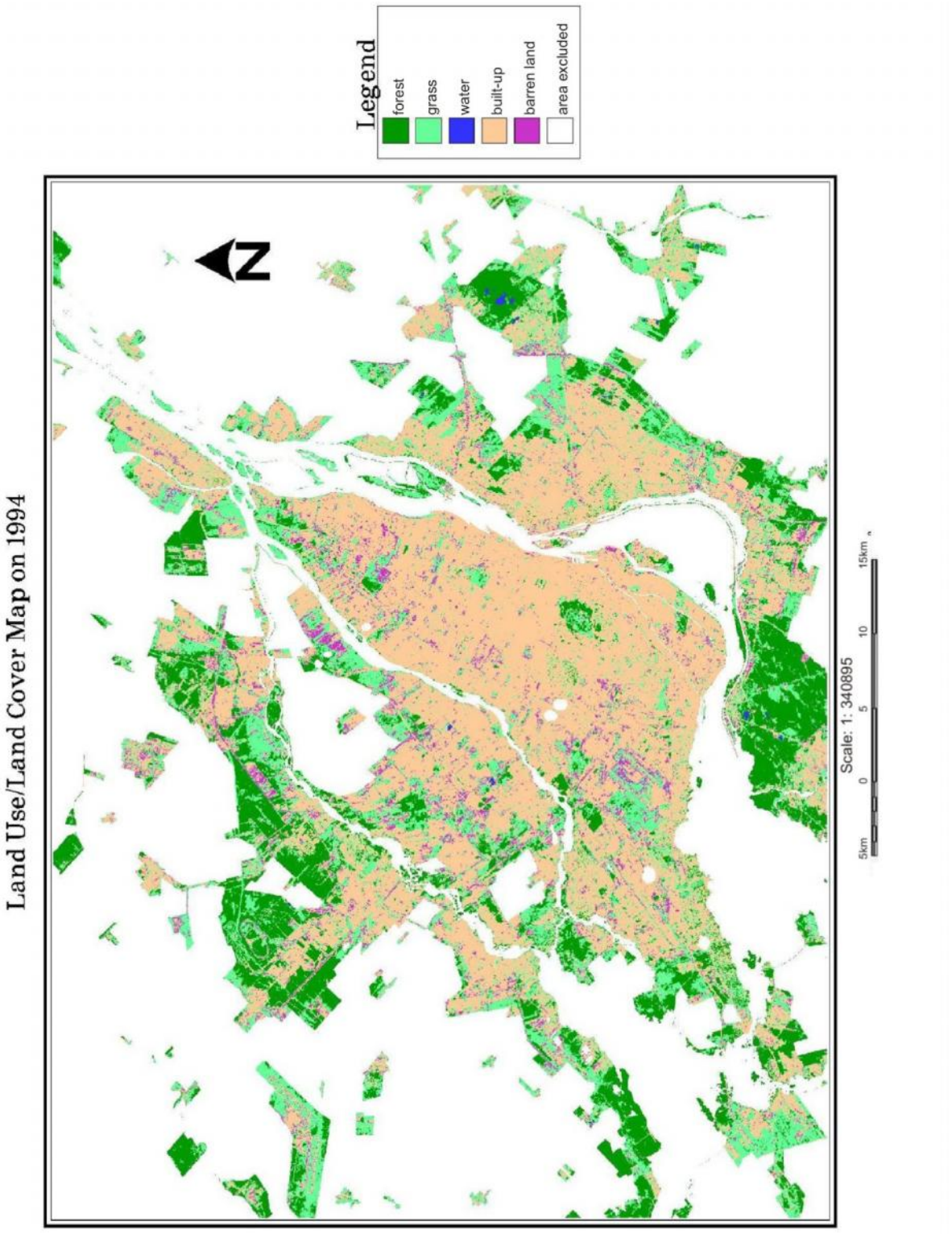

Figure 28: Classification map of LULC on 1994 (in 5 classes: built-up, forest, grass/golf course, water and barren land)

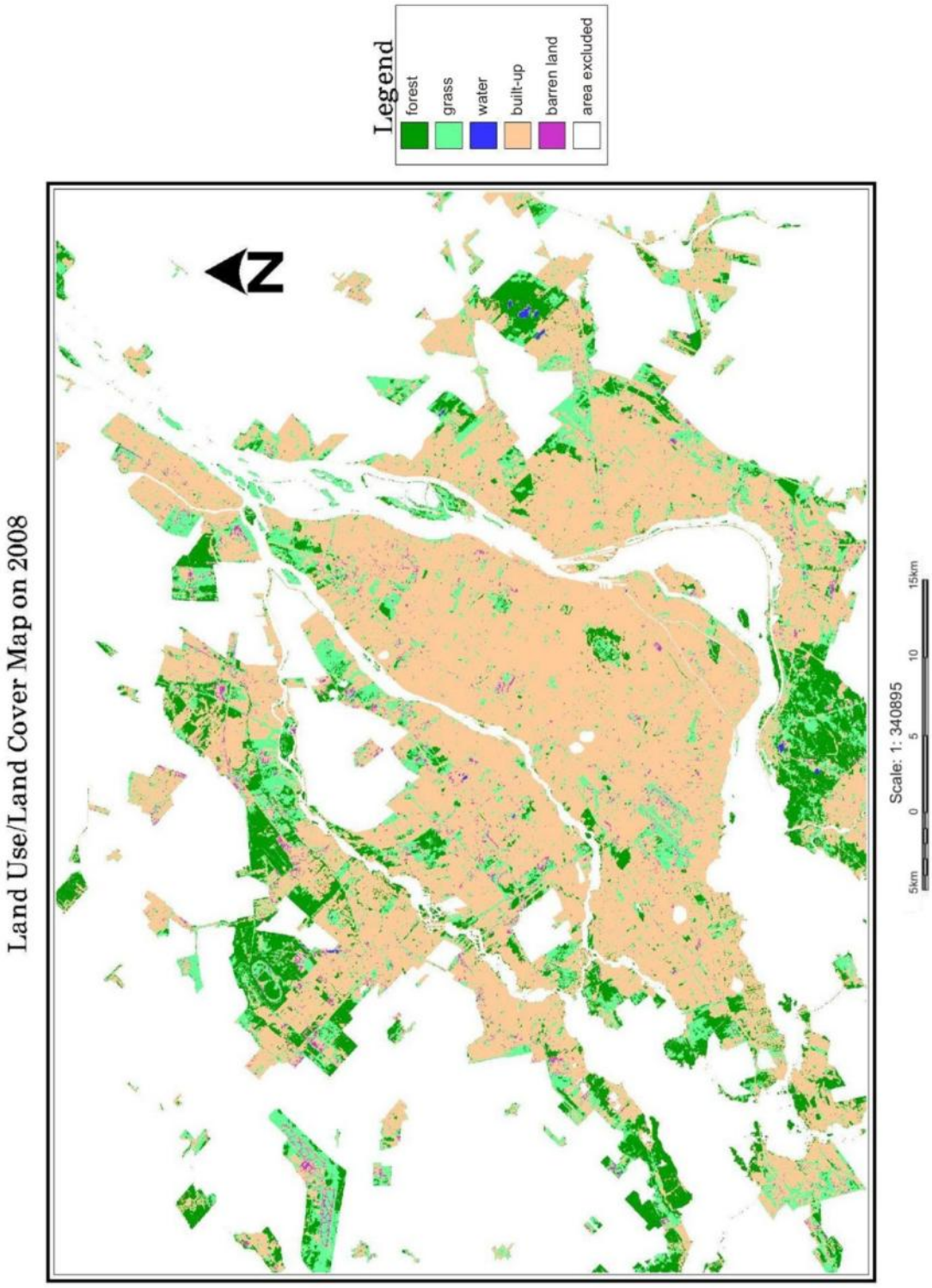

Figure 29: Classification map of LULC on 2008 (in 5 classes: built-up, forest, grass/golf course, water and barren land)

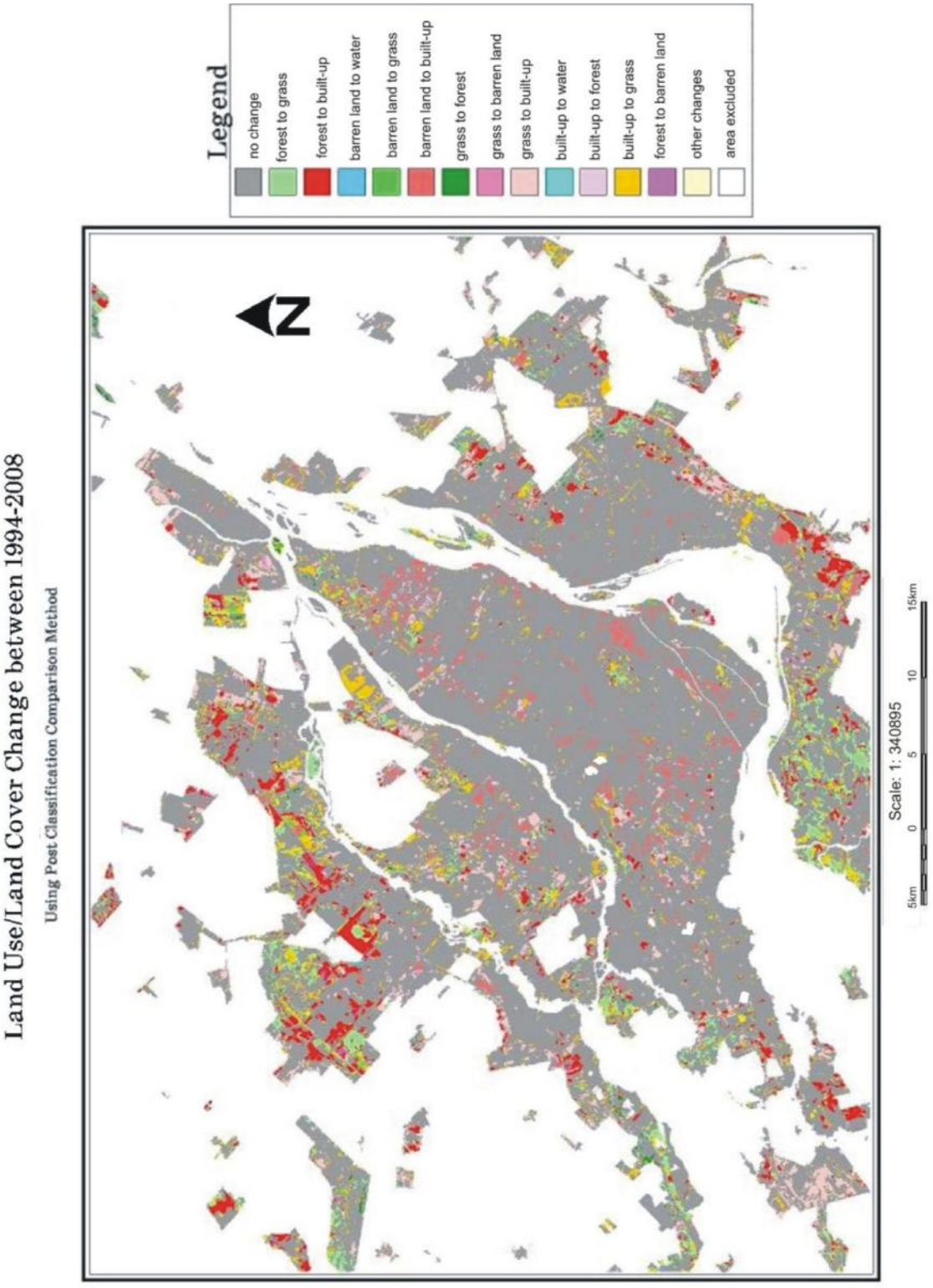

Figure 30: LULC change map between 1994-2008 uisng PCC

From the LULC change map of figure 30, the following transition matrix was generated:

Table 17: Cross tabulation table for 5 classes in 1994 and 2008

2008 \ 1994	water	forest	built-up	barren land	grass	Total area (km^2)
water	1.11	0.21	0.27	0.07	0.07	1.73
forest	0.04	181.09	3.35	0.71	27.83	213.02
built-up	0.43	70.15	718.64	55.14	155.78	1000.14
barren land	0.04	3.2	9.23	6.23	6.49	25.19
grass	0.03	31.28	21.5	19.99	179.39	252.19
Total	1.65	285.93	752.99	82.14	369.56	1492.27

From Table 17 a finer analysis than previously could be done. Thus in the period from 1994 to 2008, the total forest loss should be 104.63 km^2, including 70.15 km^2 to built-up, 31.28 km^2 to grass and 3.20 km^2 to barren land. The annual net forest loss in this period of 14 years is 7.47 km^2 per year. The change rates for each class, computed using Equation (19), are shown in table 18.Positive values present an area increase and negative values, an area decrease.

$$\text{Percentage change} = \frac{\text{area in 2008} - \text{area in1994}}{\text{total area in 1994}} \times 100\% \qquad \text{Equation (19)}$$

Table 18: Change rate of each class in the year of 1994 to 2008

Class	Area_1994 (km^2)	Area_2008 (km^2)	Change (%)
water	1.65	1.73	5.5
forest	285.93	213.02	-25.5
barren land	82.14	25.19	-69.5
grass	369.56	252.19	-31.7
built up	752.99	1000.14	32.9

However, two "from-to" classes seem a bit stranger (Table 17): built-up to forest and grass to forest. The former is of small extent (3.35 km^2). After checking the original image data, we found that the 'built-up to forest' class is due to damage on the 1994 image more easily visible on a color composite (Figure 31-B, the red color). The class from 'grass to forest' is more extended (27.83 km^2) mostly due to changes within some agriculture fields included within the urban perimeter of the Montreal Metropolitan Community and are related to change in crop

density between the years 1994 and 2008 (Figure 32). In fact a high density crop field has similar spectral characteristics as some type of forest cover while a low density crop cover to grass covers.

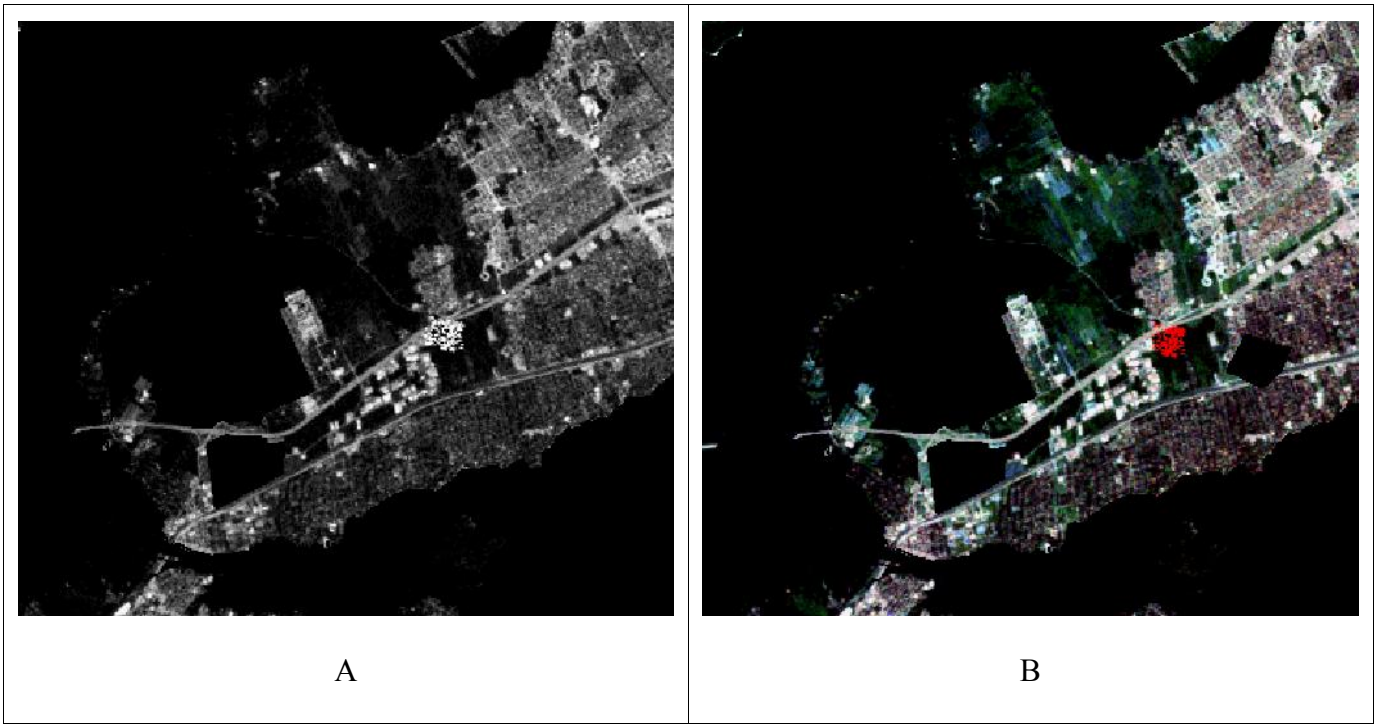

A B

Figure 31: A: band 1 in grayscale B: 3 bands composition image (R - band 1, G - band 2 and B - band 3): the read pixels are the damged pixels

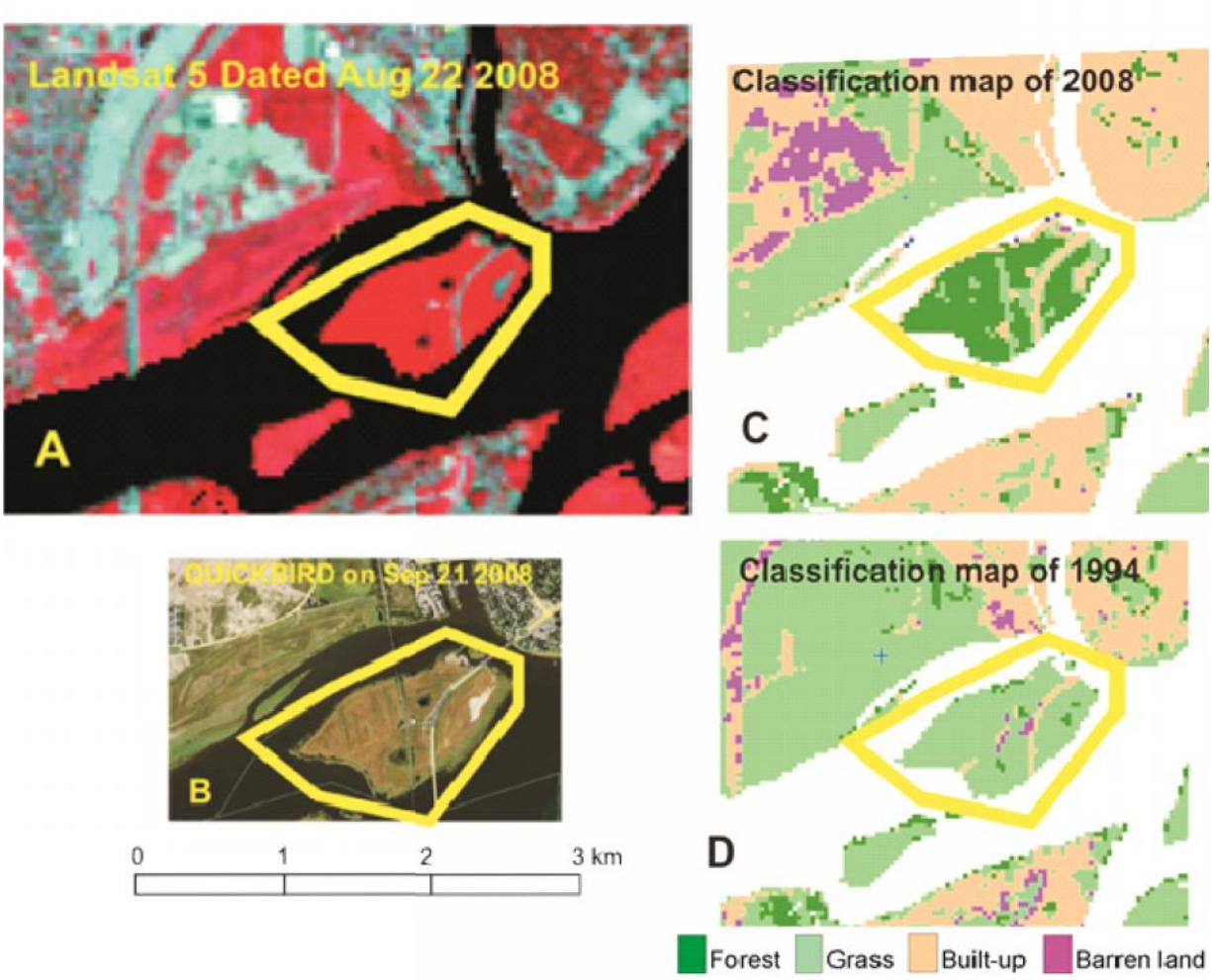

Figure 32: Error analysis for the classification map of 2008 and 1994

5.3.3 Experiment with more classes using LANSAT imagery.

In order to verify if more classes can be identified using LANDSAT imagery, another classification was performed by subdividing the class built-up into 3 classes: (i) low density residential, (ii) high density residential and (iii) commercial/industrial. The results are presented in figure 33 and 34. Both maps, however, indicate that the classification is not accurate because there is a lot of overlapping between these three classes, especially roads classified at one time as commercial and at another time as high or low density residential. This experiment shows that nothing is gained by further subdividing the built-up into more detailed classes using LANDSAT even if there is a relatively accurate picture of the distribution of two residential categories.

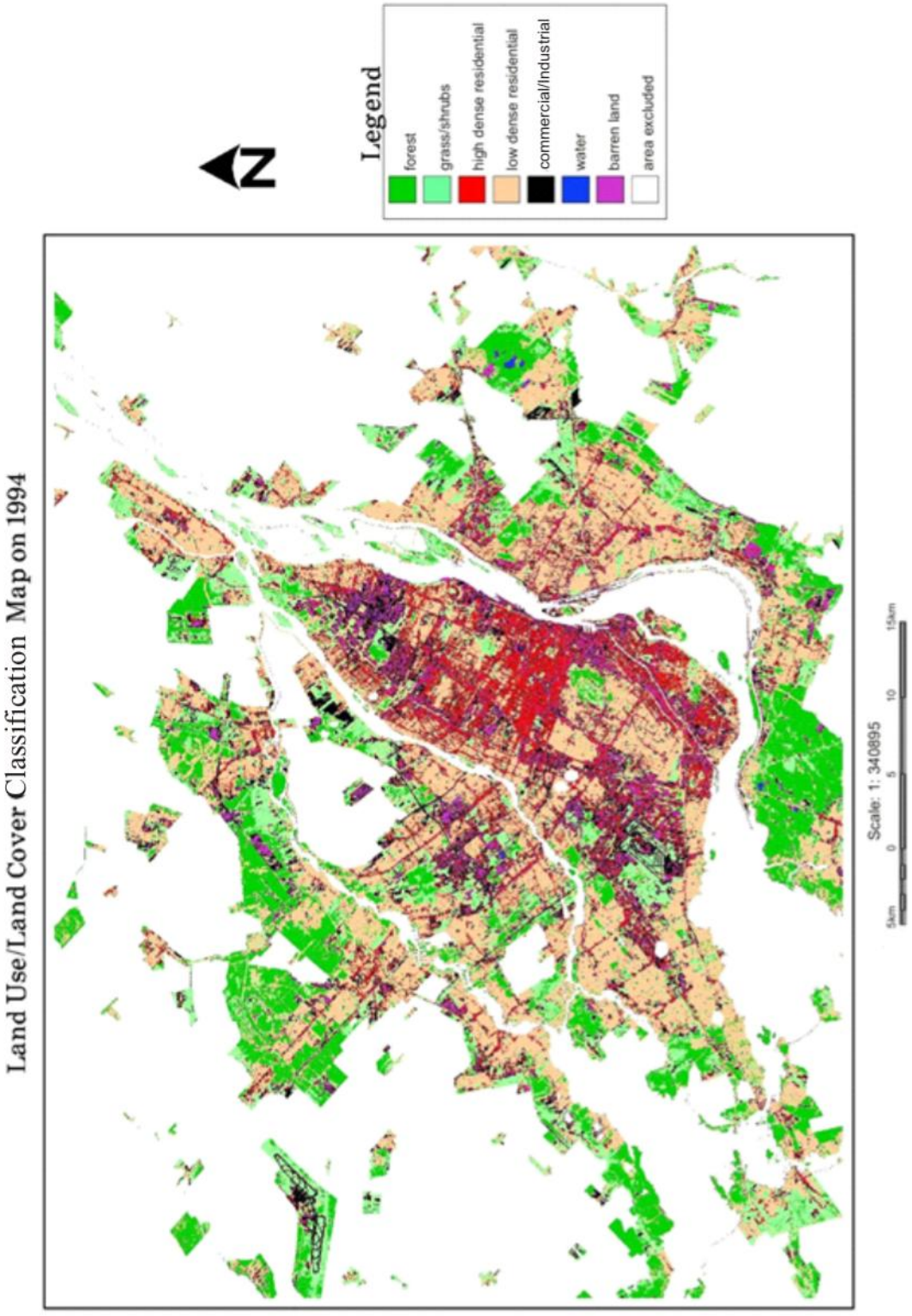

Figure 33: LULC classification map of 1994 image with 7 classes

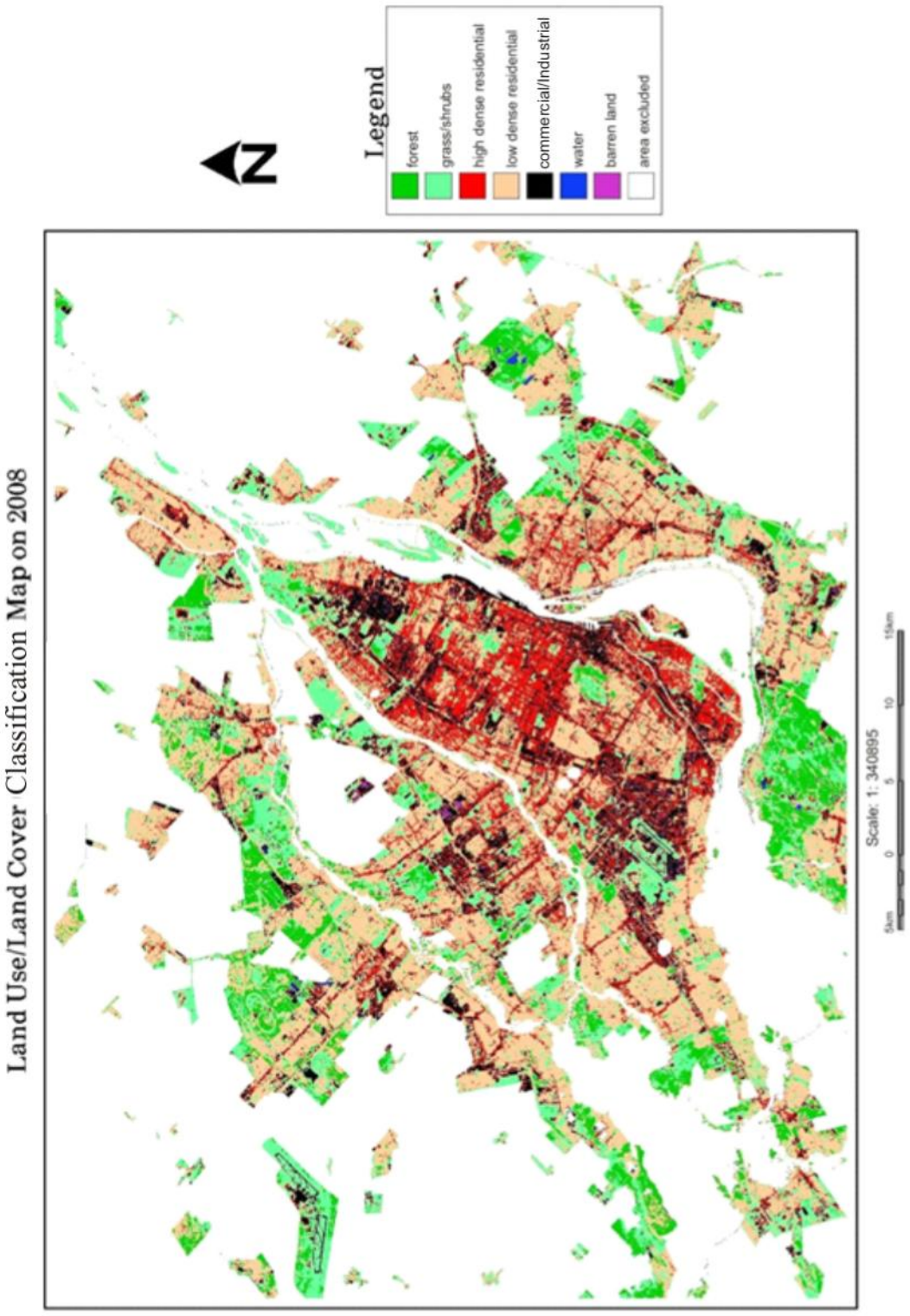

Figure 34: LULC classification map of 2008 image with 7 classes

5.3.3 Accuracy assessment

To assess the accuracy of classifications using either PCC or the PCA methods we used data (1) for 1994 a series of aerial photos at1 m resolution acquired five months before the LANDSAT image (April vs. August, 1994) and (2) for 2008 QUICKBIRD images in 1 m resolution presented on Google Earth acquired the same month and year as the LANDSAT image. A test area was selected as shown in the figures 35and 36 covering 33.97 km^2. The coordinates for the testing area is:

Upper left corner: 73°35'43.7218"W 45°29'51.8704"N

Lower right corner: 73°31'33.2482"W 45o26'30.3987"N

Figure 35: A: 1994 ground truth data, derived from a mosaic of aerial photos acquired in dated April 1994 B: 2008 ground truth data, derived from combining QUICKBIRD images on Google Earth acquired in August 2008

Figure 36 shows the LULC change where the red point located in figure 35. From this figure, the land cover was transferred from forest to built-up.

Google history image dated July 14 2005

Google history image dated Sep. 17 2007

Google history image dated Sep. 21 2008

Google street view image dated May 2009

Figure 36: LULC change from forest to built-up

200 test points were randomly selected for each of the maps mentioned above. They are then processed using the model of accuracy assessment of GEOMATICA software for each tested map. Points falling outside our study area (Saint-Lawrence River) were excluded. The number of remaining points from one test to the other varies slightly from 134 to 139. Land use class for the two years (1994 and 2008) of each point for each tested map was identified by visual interpretation of the ground truth images. In the case where the accuracy of the change detection maps were to be evaluated the comparison of the interpretation results for the two years allowed for identifying the ground-truth “from-to" classes.

The results of this accuracy tests are presented in the following tables as standard confusion matrices. The overall accuracies are as follows:

Supervised classification (the changed areas between 1994-2008) of eigen-channels generated by the PCA method (from-to classes): overall accuracy of 86.6% (see Table 19);

Supervised classification of the 1994 image input to the PCC method: overall accuracy of 90.6% (see Table 20);

Supervised classification of the 2008 image input to the PCC method: overall accuracy of 90.6% (see Table 21);

Test with the final change detection map after the comparison of classified images of 1994 and 2008: overall accuracy of 77% (see Table 22).

Table 19: Error matrix from LULC map from PCA (between 1994-2008)

Classification	Photo-interpretation									
	No-change	Barren to Grass	Forest to Built-up	Forest to Barren	Forest to Grass	Forest to Water	Grass to Built-up	Grass to Barren	Built-up to water	Total
No-change	116	0	2	2	0	0	4	0	0	124
Barren to Grass	1	0	0	0	0	0	0	0	0	1
Forest to Built-up	3	0	0	0	0	0	0	0	0	3
Forest to Barren	0	0	1	0	0	0	0	0	0	1
Forest to Grass	0	0	0	0	0	0	0	0	0	0
Forest to Water	0	0	0	0	0	0	0	0	0	0
Grass to Built-up	1	0	0	3	0	0	0	0	0	4
Grass to Barren	0	0	0	1	0	0	0	0	0	1
Built-up to water	0	0	0	0	0	0	0	0	0	
Total	121	0	3	6	0	0	0			134

Table 20: Error matrix from LULC map of 1994

Classification	Photo-interpretation					
	Built-up	BarrenLand	Forest	Grass	Water	Total
Built-up	103	0	0	4	0	107
Barren Land	0	0	0	2	0	2
Forest	0	0	4	1	0	5
Grass	3	0	8	9	0	20
Water	0	0	0	0	0	0
Total	106	0	12	16	0	134

Table 21: Error matrix from LULC map of 2008

Classification	Photo-interpretation					
	Built-up	BarrenLand	Forest	Grass	Water	Total
Built-up	108	1	1	7	0	117
Barren Land	1	4	0		0	5
Forest	0	0	2	0	0	2
Grass	0	2	1	10	0	13
Water	0	0	0	0	1	1
Total	109	7	4	17	1	138

Table 22: Error matrix for LULC change map (PCC technique)

	no change	forest to barren	forest to grass	forest to builtup	barren to grass	other change	barren to builtup	barren to water	grass to forest	grass to barren	grass to builtup	builtup to water	builtup to forest	builtup to grass	reference class
no change	103	3	1	1		6					4			3	121
forest to barren		1													1
forest to grass															0
forest to built-up				2											2
barren to grass16															0
other change	2	2				1									5
barren to builtup	6														6
barren to water															
grass to forest															
grass to barren land															0
grass to built-up	1														1
builtup to water															
builtup to forest															0
builtup to grass	3														3
classified class	115	6	1	3		7					4			3	139

5.3.4 Summary

The post-classification comparison technique is generally simpler to apply and the results are easily interpreted. In contrast, the classification of the eigen-channels obtained after applying the PCA to multi-temporal LANDSAT images requires the determination of training areas representing both changed and unchanged areas for each combination of LULC classes. This is a very difficult task and requires a good knowledge of the area. In this study, to be able to locate the changed sites, we used the image differencing map as a guide in searching for training sites in the changed areas. Due to this difficulty only 9 "from-to" classes were defined. With the PCC method we were able to derive more "from-to" classes even if we exclude the erroneous 'from to classes' as mentioned in the previous section.

Concerning the quality of the results, PCA gave better results (87%) than the PCC even if the classification accuracy of each image input to the PCC is around 77%. It is to be noted however that these scores are only indicative as the majority of check points represent the class "no-change". Concerning the forest cover changes the two approaches indicated a similar rate, with 7.47 km^2 per year from PCC and 8.45 km^2 per year from PCA.

In general, the results using PCC are not very accurate since the thematic level of detail is very general. However, due to its simplicity we retained the PCC post-classification comparison technique approach to test the potential of the ASTER images in the next chapter.

Chapter 6 Comparison between ASTER and LANDSAT

6.1 Introduction

A total of two ASTER and two LANDSAT scenes were used in this part of the study. By some good fortune one ASTER image and one LANDSAT 7 ETM+ image were collected in 2001 on the same day within 30 minutes of each other. This set of data could minimize the difference caused by atmospheric factors. The data used in this step of the study are listed as following:

1. ASTER images acquired at 11:05am on June 16, 2001 and on September 4, 2007.
2. LANDSAT 7 ETM+ images acquired at 10:34 am on June 15, 2001 and on September 5, 2007.

Using these images various tests were done to study the impacts of the resolution refinement with the ASTER data (section 6.2) as well as the impacts of spectral resolution difference between the two types of images (section 6.3).

6.2 Impact of spatial resolution refinement

Only 5 LULC classes were used in classifying the LANDSAT images: (i) water, (ii) forest (iii) grass, (iv) barren land, and (v) built-up. To examine the impact of spatial resolution refinement with ASTER images two tests were performed by adding in the classification procedure two new classes which were difficult to separate using the LANDSAT images. They are (vi) wetlands and (vii) commercial/industrial. The classification method used was the same as with LANDSAT data, namely the supervised maximum likelihood classification.

Figures37 and 38 illustrate the results of adding a wetland class to the classification. As shown in Figure 37 wetlands are well identified in this lower left portion. However, there is also a large patch of wet land in the middle of the figure which should have been built up areas. This misinterpretation is due to the fact that ASTRA imageries use only three bands. Using more classes actually causes misinterpretation of the classes.

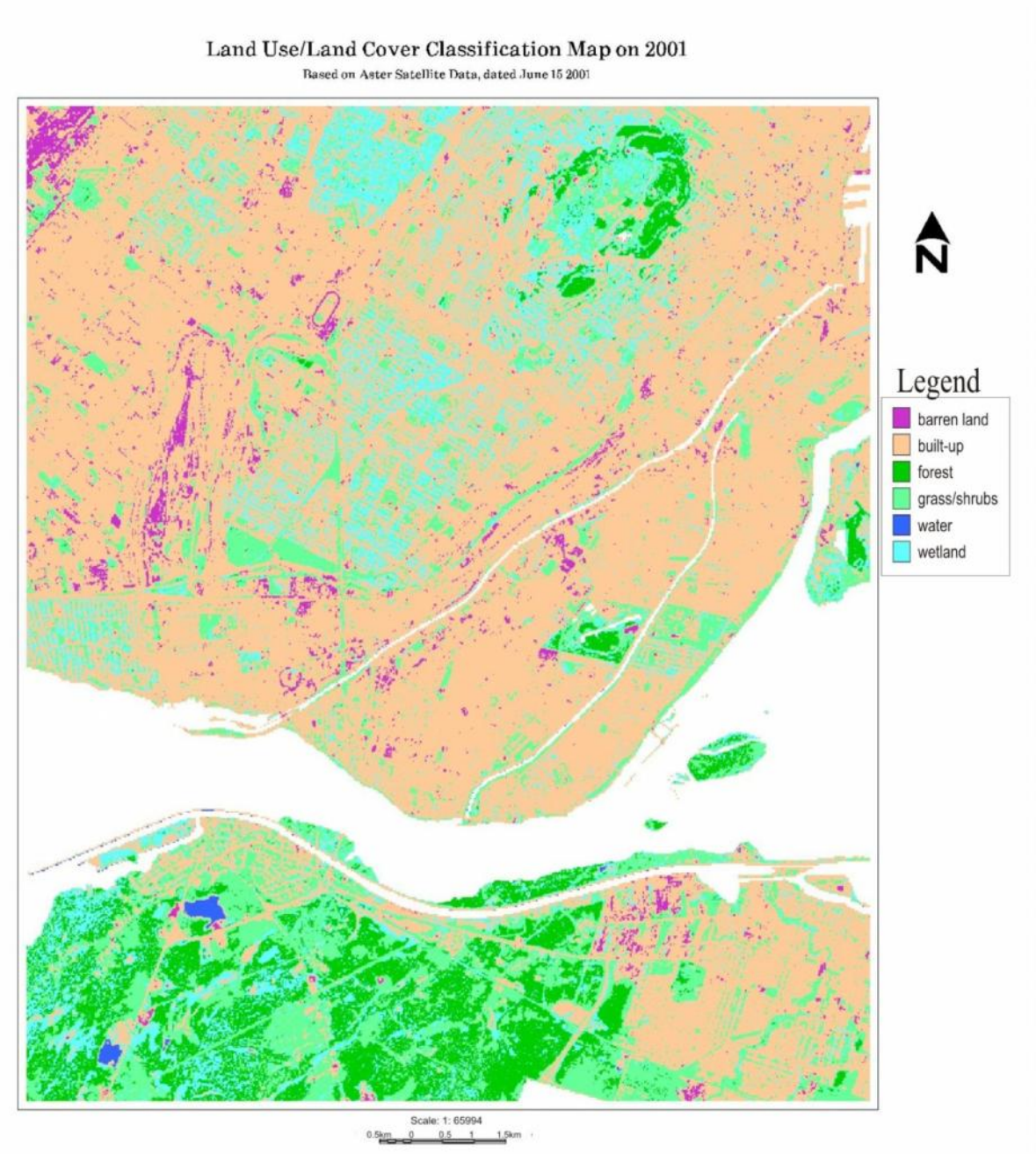

Figure 37: LULC Classification Map on 2001 (with class wetland)

Regarding the commercial/industrial class, it is well identified in the major portion of the image but there are misinterpretations with built-up areas not belonging to that class (high density residential, services, transportation) characterized by low vegetation cover. A typical example is the area near the central business district of the Montreal city in the upper right

portion of Figure 38. Such misinterpretations can be attributed to the similarity of the spectral signatures of man-made materials covering the surfaces.

Based on the results of these two experiments, we decided to compare the ASTER and LANDSAT images on the basis of the same 5 class thematic level: water, forest land, grass/shrubs, barren land, and built-up. The results are presented in the next section.

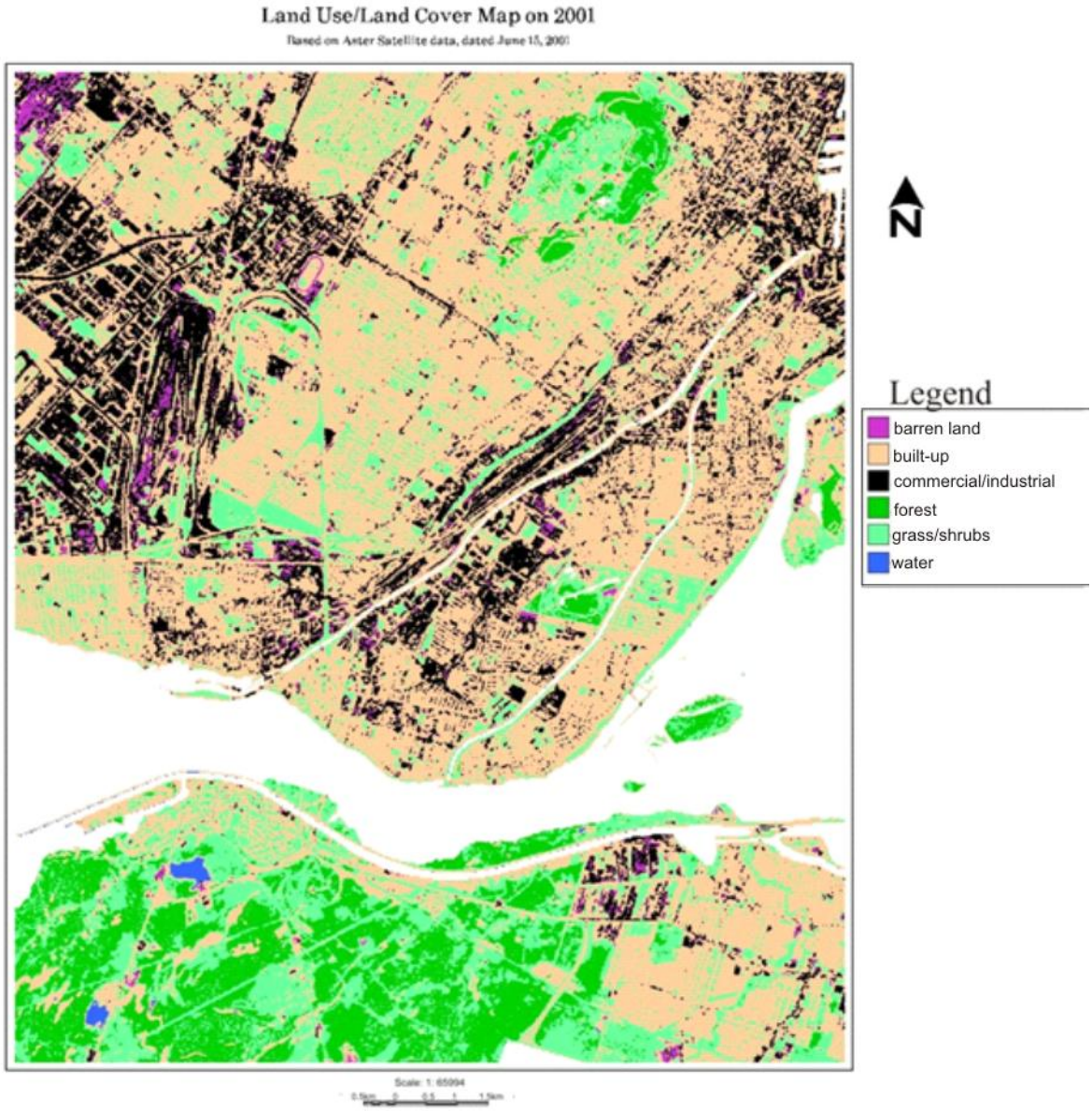

Figure 38: LULC Classification Map on 2001 (with class commercial/industrial)

6.3 Comparing ASTER and LANDSAT

Two classification experiments were performed in order to compare the two image types: (a) only similar to ASTER bands were retained in the case of LANDSAT images; and (b) the six spectral bands of LANDSAT images were used. In order to minimize the incidence of various factors affecting the classification results, the same training sites and classification method- Supervised Maximum Likelihood- were used for both ASTER and LANDSAT data.

Figures 39 and 40 show the classification results for 2001 and 2007 using the ASTER and LANDSAT images (3 bands and 6 bands). Of particular interest in these tests are the 2001 ASTER and LANDSAT images acquired on the same day with less than one hour difference. The classification of the ASTER image reflects better the dominant land cover than the classification of the LANDSAT image with only three bands (figure 41 and 42). In fact residential areas where in the summer time green vegetation is present in abundance are classified as vegetation and there are less confusion between barren land and areas dominated by man-made materials. In the classification of the LANDSAT image, either three or six bands, due to the lower spatial resolution, the built-up class appears more homogeneous. However, this class is over-estimated in the calculated area, especially in the case of the six bands (as shown in table 23 and 24, built up total area is 140 km^2 using LANDSAT 6 bands vs. 113 km^2 using ASTER 3 bands). A typical example is the cemetery in the Mount-Royal area (upper right portion of the image) classified as built-up area. In the case of the 2007 LANDSAT images this over-estimation is still present but to a lesser degree. In the classification of the 2007 ASTER image there is a "transfer" of pixels belonging to the built-up class in 2001 to the barren-land class, while pixels within residential areas, classified as vegetation in 2001 are now classified as built-up. The figures 43 and 44 illustrating the change detection maps obtained with the ASTER and LANDSAT images clearly reflect these inconsistencies in the classification of the two images.

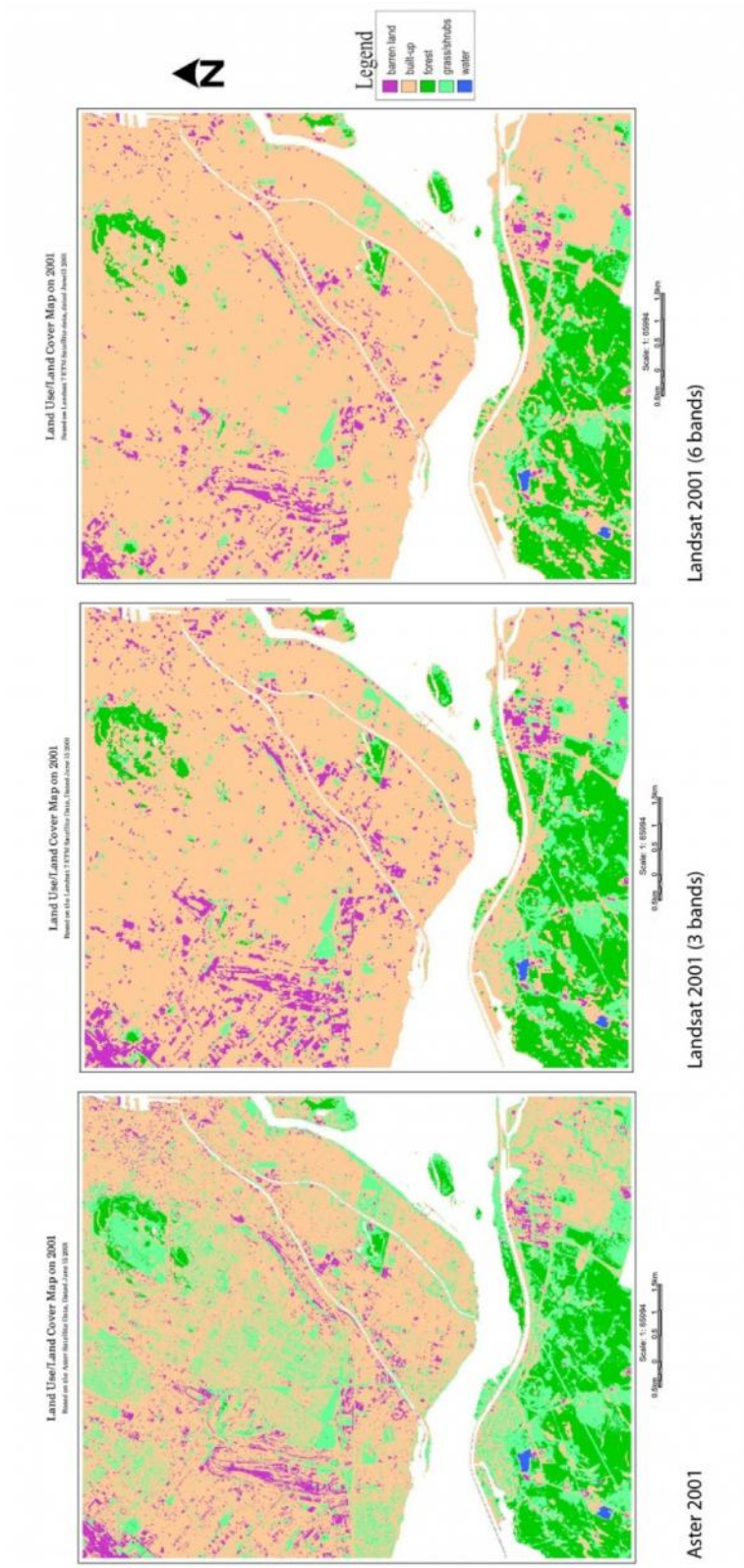

Figure 39: Classification of 2001 ASTER and 2001 LANDSAT images

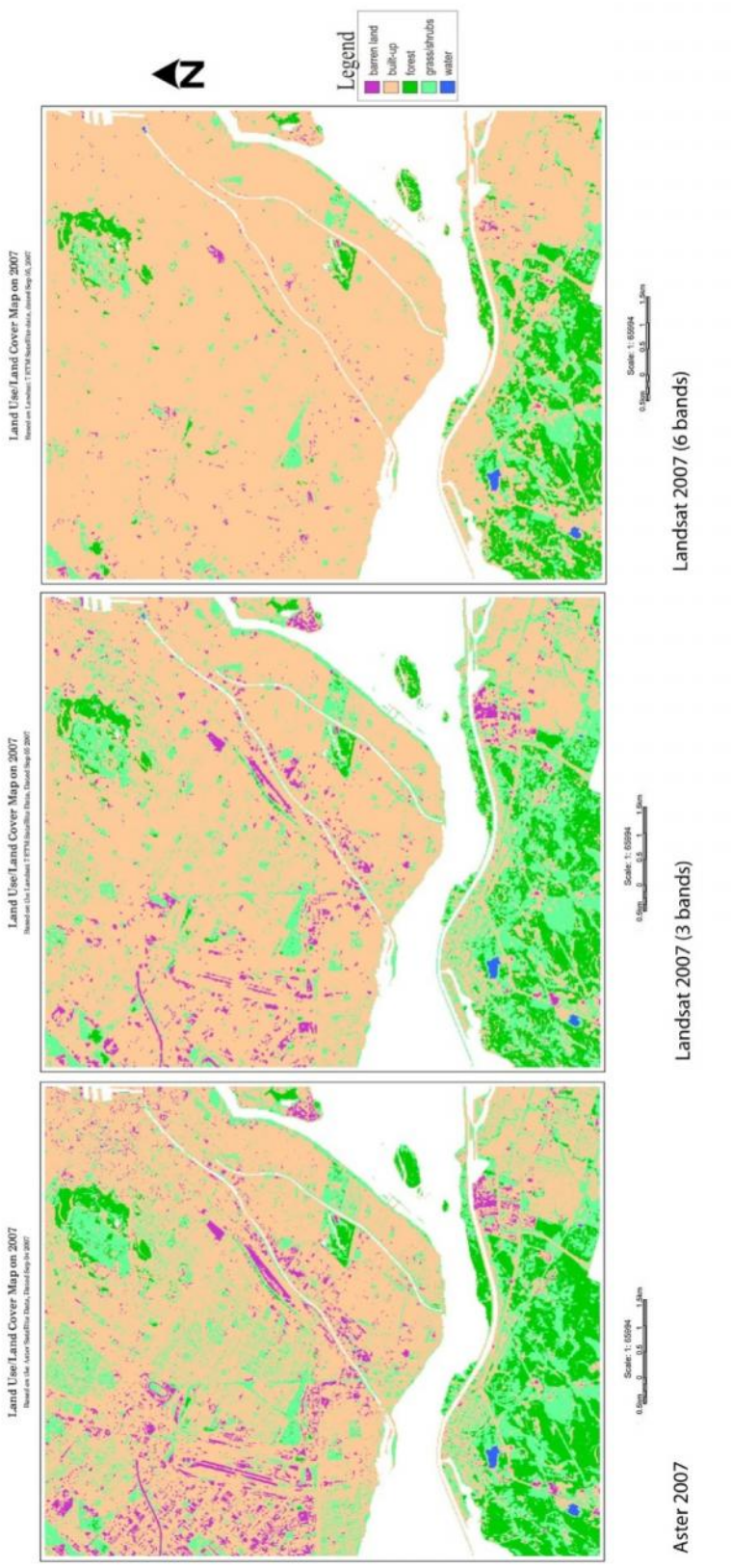

Figure 40: Classification of 2007 ASTER and 2007 LANDSAT images

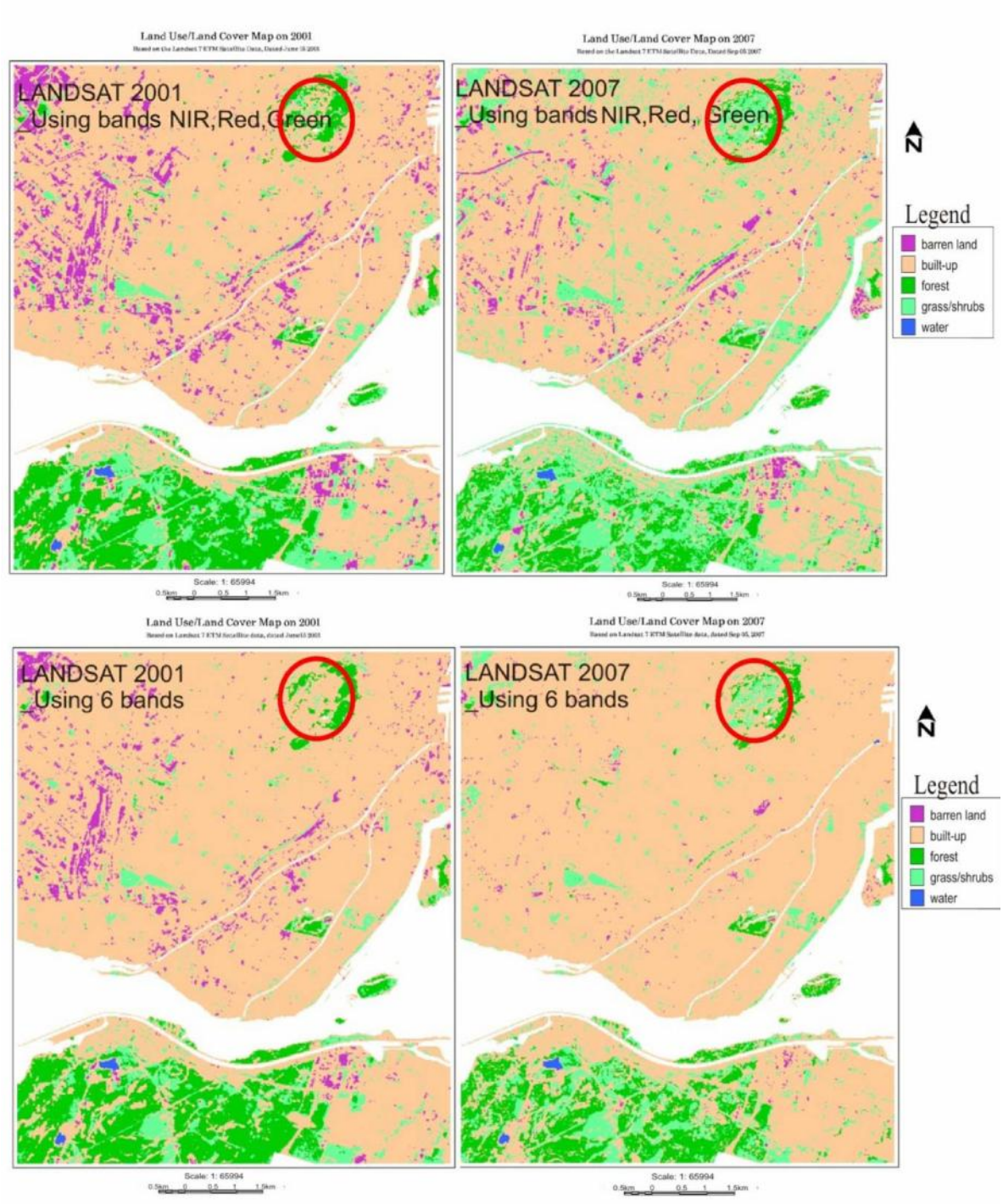

Figure 41: Comparison of LULC Classification Map on 2001 and 2007 from LANDSAT data (using 3 bands and 6 bands)

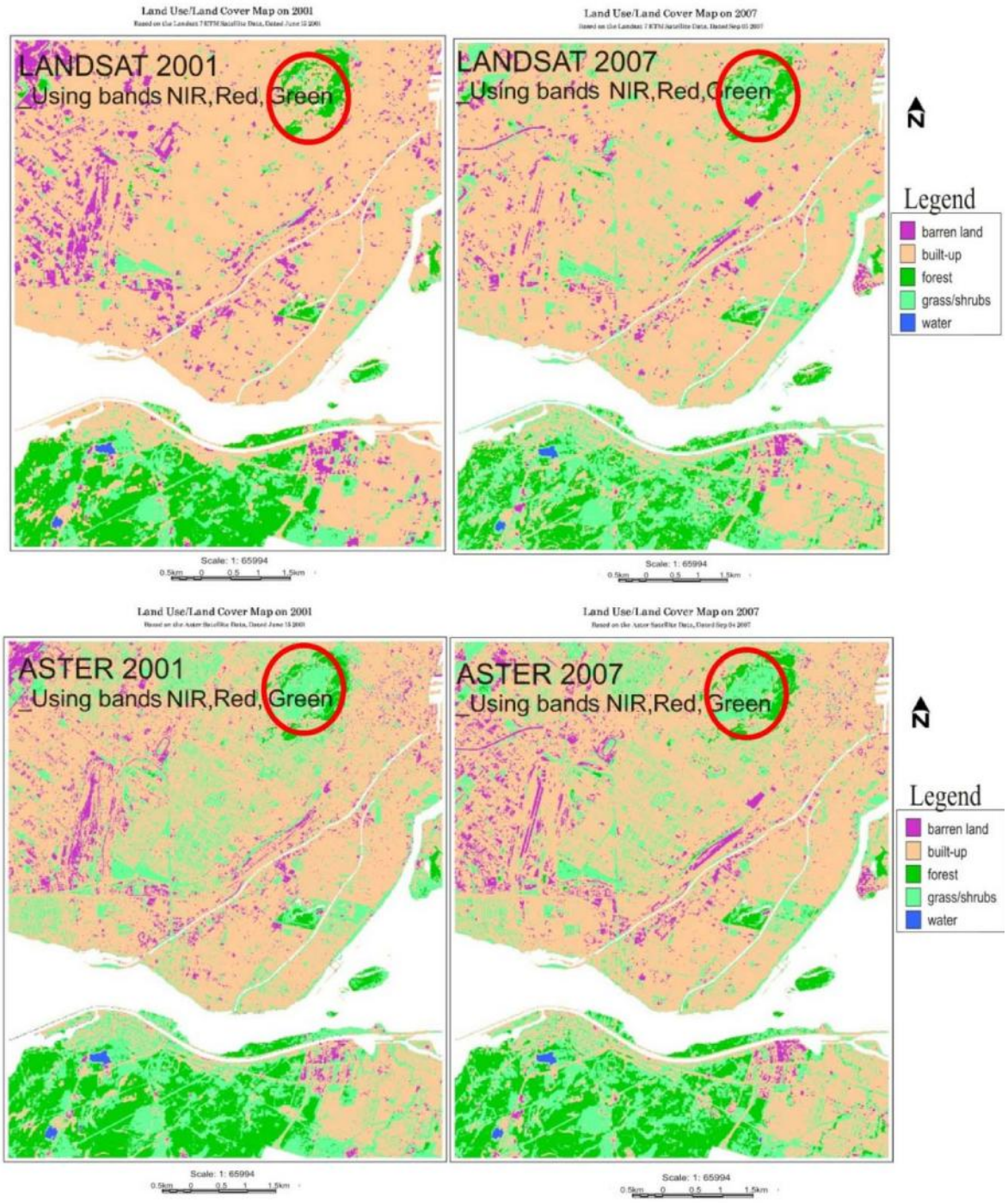

Figure 42: Comparison of LULC Classification Map on 2001 and 2007 from ASTER data and LANDSAT data (ASTER VNIR 3 bands and LANDSAT 3 bands)

.

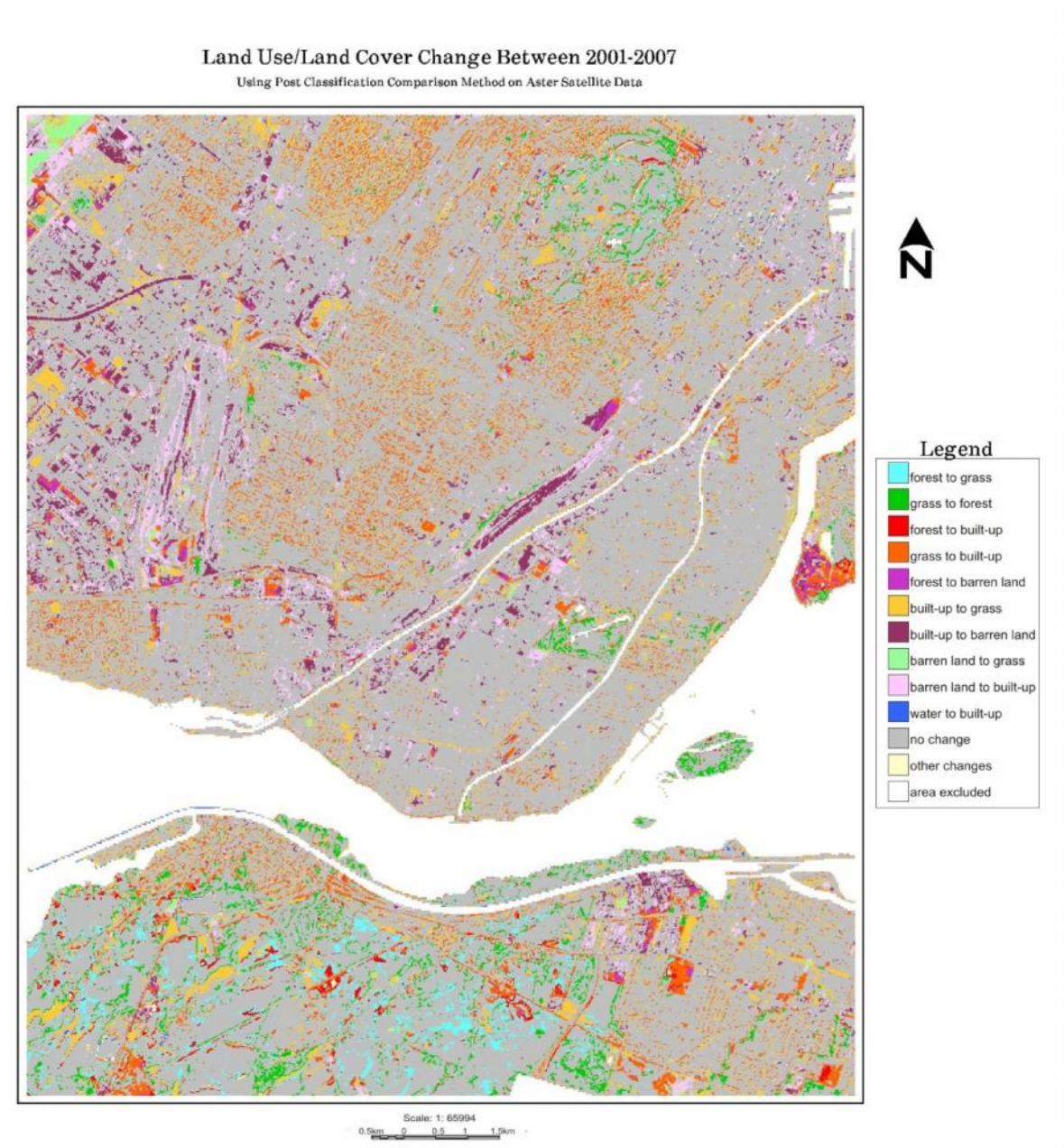

Figure 43: LULC Change Map during 2001-2007 from ASTER data

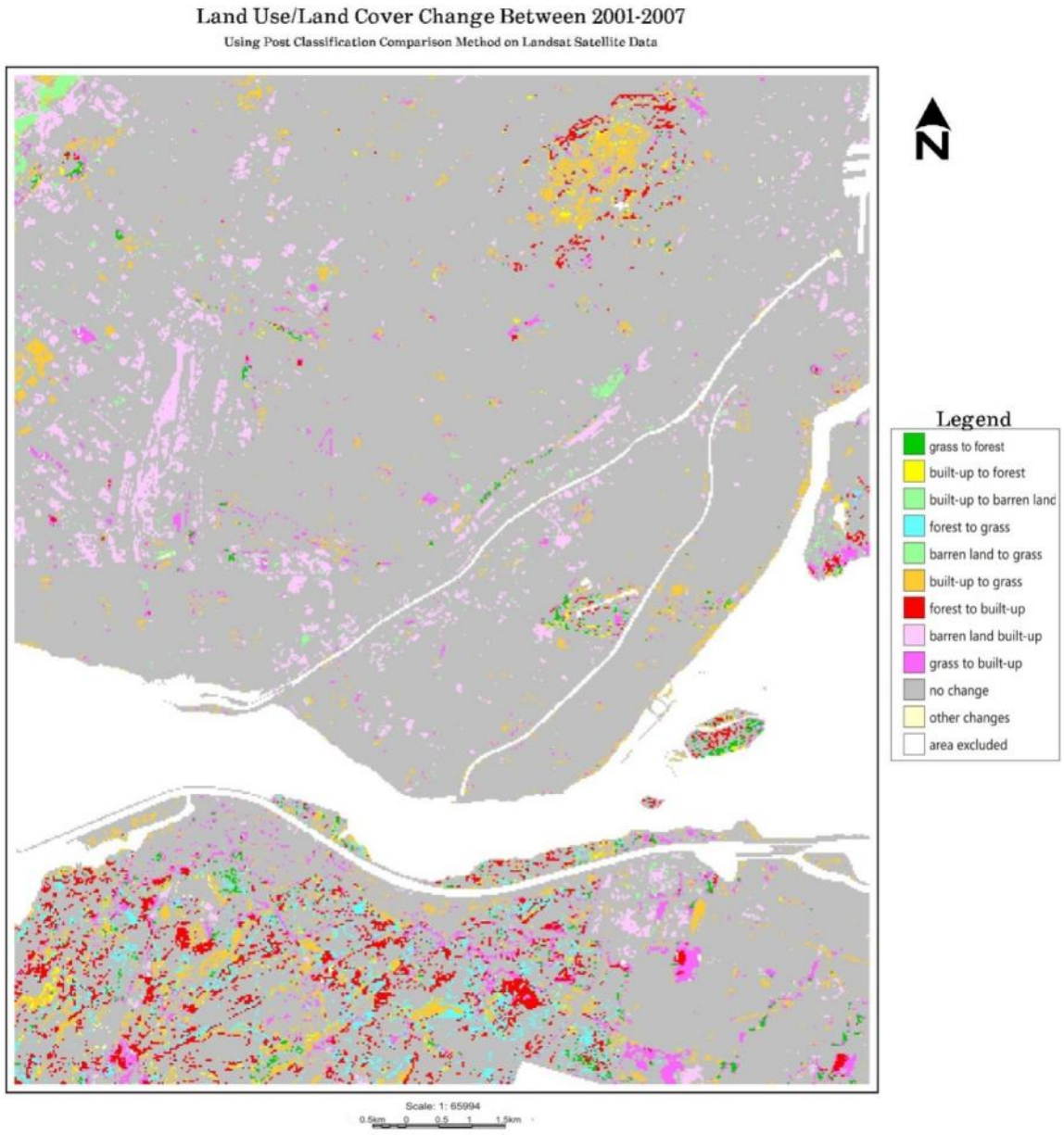

Figure 44: LULC Change Map during 2001-2007 from LANDSAT data (6 bands)

Table 23: LULC change between 2001-2007 from ASTER data (generated from figure 43)

2001 / 2007	forest	grass	built-up	barren land	water	total area(km^2)
forest	14.79	2.56	0.93	0.06	3.71	18.38
grass	3.71	25.56	12.1	0.68	0	42.05
built-up	0.16	9.08	94.43	5.89	0.07	109.63
barren land	0	0.57	5.72	2.68	0	8.97
water	0	0.08	0.23	0	0.26	0.57
Total	18.66	37.89	113.41	9.31	0.33	179.6

Table 24: LULC change between 2001-2007 from LANDSAT data (generated from figure 44)

2001 / 2007	forest	barren land	water	grass	built up	total area(km^2)
forest	13.61	0	0	0.9	0.64	15.15
barren land	0.03	0.46	0	0.07	0.68	1.24
water	0	0	0.23	0	0.04	0.27
grass	2.68	0.28	0	6.43	5.19	14.58
built up	4.01	6.71	0.02	3.66	133.96	148.36
total	20.33	7.45	0.25	11.06	140.51	179.6

6.4 Results of experiments

The main findings drawn for these experiments are as follows:

1. ASTER-VNIR images gave in general better results than LANDSAT images with respect to the dominant land cover such as vegetation, barren land, and man-made materials.
2. Both image types classified using a very general thematic level gave inconsistent results. Classification of the LANDSAT images generalizes better the built-up area in spite of the diversity of the covering materials. However there is clear trend of over-generalization to the detriment of the other LULC classes.
3. Post classification comparison reflects these inconsistencies in individual image classification. Particularly with ASTER images, real changes are mixed with changes in the vegetation cover not related to any LULC class.

Chapter 7 Conclusions and Future Research

In this study, the selected study region was the urban portion (urban perimeter) of the Montreal Metropolitan Community area. Three main objectives for this study were planned: (a) examine the possibility of multi-temporal LANDSAT images to provide information of LULC *changed areas*; (b) examine the possibility of multi-temporal LANDSAT images to provide information on the *type of changes*; and (c) study the impact of spatial resolution improvement on LULC change detection.

To obtain the first objective, LANDSAT images acquired in 1994 and 2008 were compared using image differencing, change vector analysis (CVA), as well as spectral indexes comparison (chapter 5). Image differencing or change vector analysis can provide the information of changed areas in a fast and efficient manner. However, image differencing, based on the red spectral band, can only derive two broad types of change: greenness gain or greenness loss. Change Vector Analysis, using vector magnitude and direction in multi-spectral change space, has the capacity to detect and stratify different types of changes in terms of biomass gain and loss. Regarding the application of the two indices, we conclude that the NDBI is not useful for the Montreal environment where there is a high degree of mixture of vegetation and built-up materials. Misinterpretation thus can be created by a simple densification of the vegetation cover or vegetation growth within the built-up area. The NDVI approach in general is comparable to the CVA approach with the latter providing more refined information on vegetation changes. Thus, except NDBI, all these techniques can be integrated in a continuous monitoring system for a rapid evaluation of changed areas. The produced maps could be helpful to guide the acquisition of high spatial resolution imagery if a detailed identification of the type of changes is required.

To accomplish the second objective, the same LANDSAT images as above were used. Two approaches were examined, the classification of the pooled set of the two LANDSAT images previously transformed using PCA analysis and the standard approach of post-classification comparison (Chapter 5). Both methods could provide a relatively accurate information of “from-to” classes but at a very general thematic level (for example, built-up to green spaces and vice-versa, forest to bare soil and vice-versa, etc.).Even though the Principle Component Analysis method in this study showed that PCA provides more accurate results than the standard approach of post-classification comparison, however, in order to interpret the

physical significance of the principle component images and thus to locate training areas of "from-to" classes, the analyst or interpreter must know the spectral characteristics of the study areas. The knowledge of the studied area could affect greatly the final result. Our hypothesis concerning the low potential of these approaches with medium resolution LANDSAT images to go further away in defining more detailed levels of changed classes is thus verified.

To arrive to the third objective we used ASTER and LANDSAT images acquired over a short time interval both in 2001 and 2007 (Chapter 6). In 2001 the ASTER image was acquired less than one hour after the LANDSAT image while in 2007, the ASTER image was acquired one day before the LANDSAT image. Post-classification comparison was used as the approach of detecting changes. The main conclusion drawn from this experiment is that ASTER images have better spatial resolution but less spectral bands than LANDSAT images did not provide more detailed thematic information (for example forest to commercial or industrial areas). ASTER-VNIR images in general gave better results than LANDSAT images with regard to the dominant land cover such as vegetation, barren land, and man-made materials. Classification of the LANDSAT images generalizes better the built-up area in spite of the diversity of the covering materials. There is clear trend of over-generalization to the detriment of the other LULC classes. The fact that the spatial resolution was improved did not signify necessary an improvement in the results if it was not accompanied by more spectral bands. In that sense the results confirm those obtained by Herold *et al.* (2003) mentioned in Chapter 2.

As a general conclusion of this study, we can notice that medium resolution imagery (about 10-50 m) analyzed by automatic methods and techniques is an efficient tool to monitor changes in an urban environment through changes of the material covers and more particularly of the vegetation cover. A number of techniques examined in this study have been proven efficient. Other techniques, such as spectral un-mixing, neural networks, knowledge based expert systems, and object oriented classification are not examined here but may be necessary to be tested. In those cases, they may be possible to better characterize the types of changes in material covers provided that appropriate spectral signatures from typical material are introduced in the algorithm (asphalt, concrete, bare soils, etc.). Regarding the change detection technique, the use of an existing land cover map with the multi-temporal image set could provide better guidance in understanding the nature of detected changes as demonstrated by the study of Cavayas and

Baudouin (2008). Also, based on the construction permits issued by the government each year may provide a guide to pay attention to monitoring these areas. The methods provided in this study will help to determine if these areas have been modified or not in order to investigate further.

References

Anderson, J. R., Hardy, E. E., Roach, J. T. and Witmer, R. E. (1976). A land use and land cover classification system for use with remote sensor data. Geological Survey Professional Paper, pp. 964. U.S. Geological Survey, Washington, DC.

Bouroubil, M. Y., Vigneault, P., Cavayas, F.&Tremblay, N. (2006). *International Contemporary publishing*, 6 (1), 1-8.

Cavayas F.and Baudouin Y. (2008). Édude des biotopes urbains et périurbains de la CMM : Évolution des occupations du sol, du couvert végétal et des îlots de chaleur sur le territoire de la Communauté métropolitaine de Montréal (1984-2005), *Conseil Régional de l'Environnement de Laval.*

Chen, D. and Stow, D. (2003). Strategies for integrating information from multiple spatial resolutions into land-use/land cover classification routines. *Photogrammetric Engineering & Remote Sensing*, 69 (11),1279-1287.

Civco D. L., Hurb, J. D., Wilson, E. H., Song, M., and Zhang, Z. (2002). A comparison of land use and land cover change detection methods. ASPRS-ACSM Annual Conference and FIG XXII Congress: pp. 2.

Coppin, P.R. and Bauer, M.E. (1996). Digital change detection in forest eco-systems with remote sensing imagery. *Remote Sensing Reviews*, 13, 207-234.

Colwell R. (1983). *Manual of Remote Sensing (2nd Ed.)* American Society of Photogrammetry and Remote Sensing, Falls Church, Va., U.S.A.

Coppin, J., Jonckheere, I., Nackaerts, K. and Muys, B. (2004). Digital change detection methods in ecosystem monitoring: a review. *International Journal of Remote Sensing*, 10, 1565-1596.

Crist, E. P. (1985). A TM tasseled cap equivalent transformation for reflectance factor data, *Remote Sensing of Environment*, 17, 301-306.

Dejardins R. and Cavayas F. (1991). Possibilités et limites des images satellites pour la cartographie des occupations du sol, le cas de Montréal (Québec). *Cahiers de géographie du Québec*, 35 (94) : 137-154.

De Kok, R., Schneider, T. and Ammer, U. (1999). Object based classification and applications in the Alpine forest environment. In Fusion of Sensor Data, Knowledge Sources and Algorithms, Proceedings of the Joint ISPRS/Earsel Workshop, 3–4 June 1999, Valladolid, Spain. *International Archives of Photogrammetry and Remote Sensing*, 32, Part 7-4-3 W6.

Eva, H. and Lambin, E.F. (1998). Burnt area mapping in central Africa using ATSR data. *International Journal of Remote Sensing*, 19, 3473-3497.

Flanders, D., Hall-Bayer, M. and Perverzoff, J. (2003). Preliminary evaluation of eCognition object-based software for cut block delineation and feature extraction. *Canadian Journal of Remote Sensing*, 29, 441–452.

Foody, G. M. (2001). Monitoring the magnitude of land-cover change around the southern limits of the Sahara. *Photogrammetric Engineering and Remote Sensing*, 67, 841–847.

Fung, T. and LeDrew, E. (1987). The application of principal component analysis to change detection. *Photogrammetric Engineering and Remote Sensing,* 53*,* 1649-1658.

Fung, T. (1990).An assessment of TM imagery for land-cover change detection. *IEEE Transactions on Geoscience and Remote Sensing*, 28, 681–684.

Green, K., Kempka, D. and Lackey, L. (1994). Using remote sensing to detect and monitor land cover and land use change, *Photogrammetric Engineering & Remote Sensing*, 60, 331-337.

Herold, M., Gardner, M. E. and Roberts, D. A. (2003). Spectral resolution requirements for mapping urban areas. *IEEE Transactions on Geoscience and Remote Sensing*, 41, 1907-1919.

Jensen, J. R. and Toll, D. L. (1982). Detecting residential and use development at the urban fringe. *Photogrammetric Engineering and Remote Sensing,* 48, 629-643.

Jensen, J. R. (2005). *Introductory digital image processing: A remote sensing perspective*, (*3rd Ed.*). Pearson Prentice Hall. Upper Saddle River, U.S.A.

Jensen, J.R., Cowen, D., Narumalani, S. and Hall, J. (1997). *Principles of change detection using digital remote sensor data.* Cambridge University Press. Cambridge, United Kingdom.

Jensen, J. R. (2007). *Remote Sensing of the Environment (2nd Ed.).* Pearson Prentice Hall. Upper Saddle River, U.S.A.

Lambin, E. F. and Strahler, A. H. (1994). Change-vector analysis in multi-temporal space: a tool to detect and categorize land-cover change processes using high temporal resolution satellite data. *Remote Sensing of Environment*, 48, 231–244.

Li, X. and Yeh, A. G.O. (1998). Principal component analysis of stacked multi-temporal images for the monitoring of rapid urban expansion in the Pearl River Delta. *International Journal of Remote Sensing*, 19 (8), 1501–1518.

Lillesand, T., Kiefer, R. and Chipman, J. (2004). *Remote Sensing and Image Interpretation*(*5th ed*.) John Wiley and Sons, New York. U.S.A.

Lu, D., Mausel, P., Brondizio, E. and Moran, E. (2003). Change detection techniques. *International Journal of Remote Sensing*, 25(12), 2365-2407.

Lunetta, R.S. and Elvidge, C. D. (1998). *Remote sensing change detection: environmental monitoring methods and applications.* Ann Arbor Press. Chelsea, MI, U.S.A.

Mas, J. F. (1997). Monitoring land-cover changes in the Terminos Lagoon Region, Mexico: a comparison of change detection techniques. Proceedings of the IV International. Conference on Remote Sensing for Marine and Coastal Environments, Orlando, FL, U.S.A. (Amsterdam: National Aerospace Laboratory), 159–167.

Michalek, J., Wager, T., Luczkovich, J. and Stoffle, R. (1993). Multispectral change vector analysis for monitoring coastal marine environments. *Photogrammetric Engineering and Remote Sensing*, 59, 381–384.

Millward, A. A., Piwowar, J. M. and Howarth, P. J. (2006). Time-series analysis of medium-resolution, multi-sensor satellite data for identifying landscape change. *Photogrammetric Engineering and Remote Sensing.* 72 (6), 653-663.

Olthof, I., Latifovic, R. and Pouliot, D. (2009). Development of a circa 2000 land cover map of Northern Canada at 30 m resolution from LANDSAT. *Canadian Journal of Remote Sensing,* 35(2), 152-165.

Petit, C., Scudder, T. and Lamin, E.(2001). Quantifying processes of land-cover change by remote sensing: resettlement and rapid land-cover change in southeastern Zambia. *International Journal of Remote Sensing*, 22, 3435–3456.

Rencz, Andrew N. and Ryerson, Robert A. (1999), eds. *Manual of Remote Sensing for the Earth Science.* J. Wiley and Sons, New-York, U.S.A.

Singh, A. (1989). Digital change detection techniques using remotely sensed data. *International Journal of Remote Sensing*, 10, 989–1003.

The act to preserve agriculture land and agricultural activities. Retrieved Feb 12 2012, from http://www.cptaq.gouv.qc.ca/fileadmin/en/publications/guides/Summary.pdf

Vermote, E.F., Tanre, D., Deuze, J.L., Herman, M. and Morcrette, J.J., 1997, Second simulation of the satellite signal in the solar spectrum, 6S: An overview. *IEEE Transactions on Geoscience and Remote Sensing*. 35(3):675-686.

Waler, J. S. and Blaschke, T. (2007) Object-based land-cover classification for the Phoenix metropolitan area: optimization vs. transportability. *International Journal of Remote Sensing*, 29(7), 2021-2040.

Welch, R. (1985). Cartographic Potential of SPOT Image Data. *Photogrammetric Engineering*

and Remote Sensing, 51 (8), 1085-1091.

Yuan, F., Sawaya K.E, Loeffelholz, B.C. and Bauer, M. E.(2005). Land cover classification and change analysis of the Twin Cities (Minnesota) Metropolitan Area by multi-temporal LANDSAT remote sensing. *Remote Sensing of Environment,* 98, 317 – 328.

Zha, Y., Gao, J. and Ni, S. (2003). Use of normalized difference built-up index in automatically mapping urban areas from TM imagery. *International Journal of Remote Sensing,* 24(3), 583-594.